Charles University in Prague
Faculty of Mathematics and Physics

Doctoral Thesis

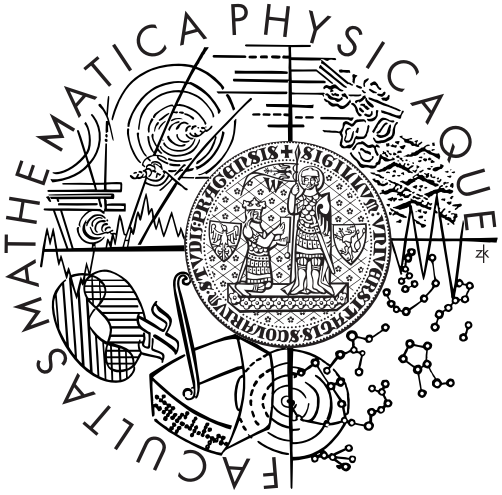

Jiří Kosinka

Algorithms for Minkowski Pythagorean Hodograph Curves

Department of Mathematics Education

Supervisor: *Prof. RNDr. Adolf Karger, DrSc.*

Field of Study: *General Problems of Mathematics and Computer Science*

Acknowledgements

I would like to thank Prof. Adolf Karger, my supervisor, for his suggestions and constant support during this research. I am also thankful to Prof. Bert Jüttler for his guidance through my short term attachment at Johannes Kepler University in Linz, Austria, which was crucial to the successful completion of this thesis.

I would also like to thank the Austrian Science Fund for partially supporting this research through project P17387-N12.

Of course, I am grateful to my parents and my girlfriend Gabriela for their patience and love. Without them this work would never have come into existence (literally).

I hereby certify that I have written this thesis myself without using any sources other than cited.

In Prague, March 14, 2006 Jiří Kosinka

Abstract

As observed by Choi et al. (1999), curves in Minkowski space $\mathbb{R}^{2,1}$ are very well suited to describe the medial axis transform (MAT) of a planar domain, and Minkowski Pythagorean hodograph (MPH) curves correspond to domains, where both the boundaries and their offsets are rational curves (Moon, 1999).

In this thesis, we focus mainly on MPH cubics. We show that any MPH cubic (including the case of light–like tangents) is a cubic helix in Minkowski space. With the help of tangent indicatrices of MPH curves, we derive a complete classification of planar and spatial MPH cubics.

Based on these results, we give a thorough discussion of G^1 Hermite interpolation by MPH cubics, focusing on solvability and approximation order. Among other results, it is shown that any space–like C^∞ curve without isolated Minkowski inflections can be approximately converted into a G^1 spline curve composed of MPH cubics with the approximation order being equal to four. The theoretical results are illustrated by several examples. In addition, we show how the curvature of a curve in Minkowski space is related to the boundaries of the associated planar domain.

Keywords

Minkowski Pythagorean hodograph curve, helix, Minkowski space, Hermite interpolation, space–like vector, Taylor expansion.

Contents

1 Introduction

Offsets of planar curves are needed for various applications. For example, they are used as the tool paths of computer–numerical–control (CNC) machines. Since the accuracy and efficiency of the representation of curves and surfaces is one of the basic issues in computer aided geometric design (CAGD), curves with polynomial or rational offsets have been thoroughly investigated. In particular, Pythagorean hodograph (PH) curves, which were introduced by Farouki & Sakkalis (1990), are polynomial curves with rational offsets. Many related references can be found in the excellent survey of Farouki (2002).

In order to use the offset to a given curve as a tool path or for other applications, the so–called trimming procedure has to be applied. This procedure trims off the unwanted pieces and gives the true offset. Depending on the geometry and the offset distance, the trimming procedure can be time–consuming and computationally difficult.

An elegant approach to this problem was formulated by Moon (1999) and Choi et al. (1999). It is based on the medial axis transform (MAT) of a planar domain (see Pottmann and Peternell (1998) and Degen (2004), and the references cited therein), which identifies the domain with a (system of) space curve(s). Recall that the medial axis of a planar domain consists of the centers of all inscribed circles, which touch the boundary in at least two points. The MAT is then the system of space curves obtained by lifting the points of the medial axis of the domain into xyr–space, using the radius of the corresponding circle as the additional coordinate, see Fig. 1 and Fig. 2.

Motivated by the offset formula for the boundaries of a planar domain, Moon defined MPH curves as polynomial speed curves in Minkowski (or pseudo–Euclidean) space with respect to Minkowski inner product. If the MAT is a (piecewise) MPH curve, the δ–offset curves of the corresponding boundary

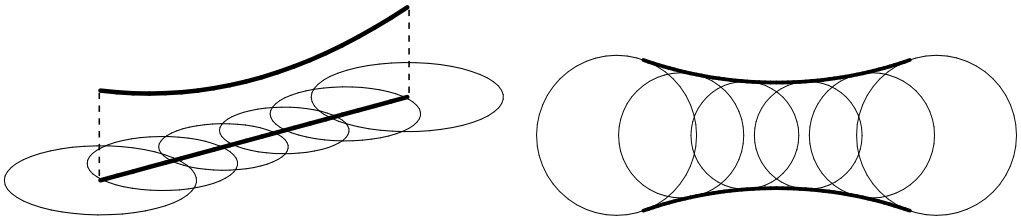

Figure 1: Left: The medial axis transform in xyr–space and the corresponding circles in the xy–plane. Right: The envelope of the circles defines the boundary of the planar domain.

domain are rational. Moreover, the trimming procedure for the inner offsets becomes simpler, see Fig. 3 (cf. Pottmann and Peternell, 1998). The parts of the MAT, where the corresponding circle radius r is less than δ, have to be trimmed.

Based on so called domain decomposition technique, Choi et al. (1999) have designed an interpolation scheme for interpolating the MAT of a planar domain by MPH cubics. Recently, Kim & Ahn (2003) addressed the problem of C^1 Hermite interpolation using MPH quartics and introduced a new concept, $C^{1/2}$ interpolation. MPH curves in higher dimensions have recently been analyzed by Cho et al. (2004).

The approximation of the MAT by pseudo–Euclidean arc splines and by parabolic arcs has been outlined by Pottmann and Peternell (1998).

Cubic curves with constant slope in Euclidean space have thoroughly been investigated by Wunderlich (1973). For any given slope α, there exists exactly one cubic curve in three–dimensional Euclidean space – which is called the cubic helix – for which the ratio of curvature to torsion equals α. Its normal

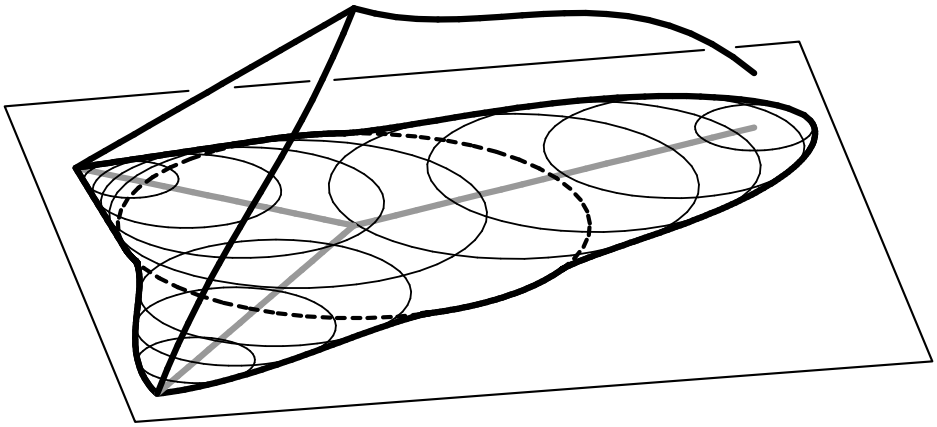

Figure 2: The medial axis transform in xyr–space consisting of three curves and the boundary of the corresponding planar domain. The medial axis is shown in grey.

form for $\alpha = \pi/4$ is given by

$$\mathbf{c}(t) = (3t^2, t - 3t^3, t + 3t^3)^\top. \tag{1}$$

Cubic helices for other slopes α are obtained by a uniform scaling of the z–coordinate, see Fig. 4. According to Wagner and Ravani (1997), the cubic helix is also the only cubic which is equipped with a rational Frenet–Serret motion. More precisely, the unit tangent, normal and binormal of the curve can be described by rational functions.

While the only planar PH cubic is the so–called Tschirnhausen cubic, Farouki and Sakkalis (1994) proved later that spatial PH cubics are helices, i.e. curves of constant slope. A classification of PH cubics in Euclidean space can be obtained by combining these results: any PH cubic can be constructed as a helix with any given slope "above" the Tschirnhausen cubic.

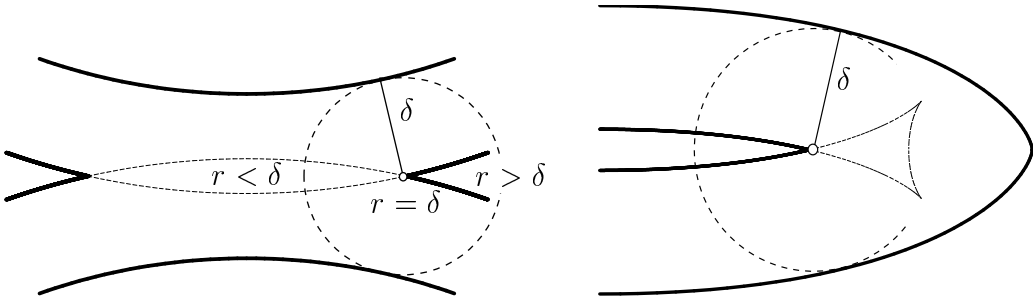

Figure 3: Trimming procedure using medial axis transform.

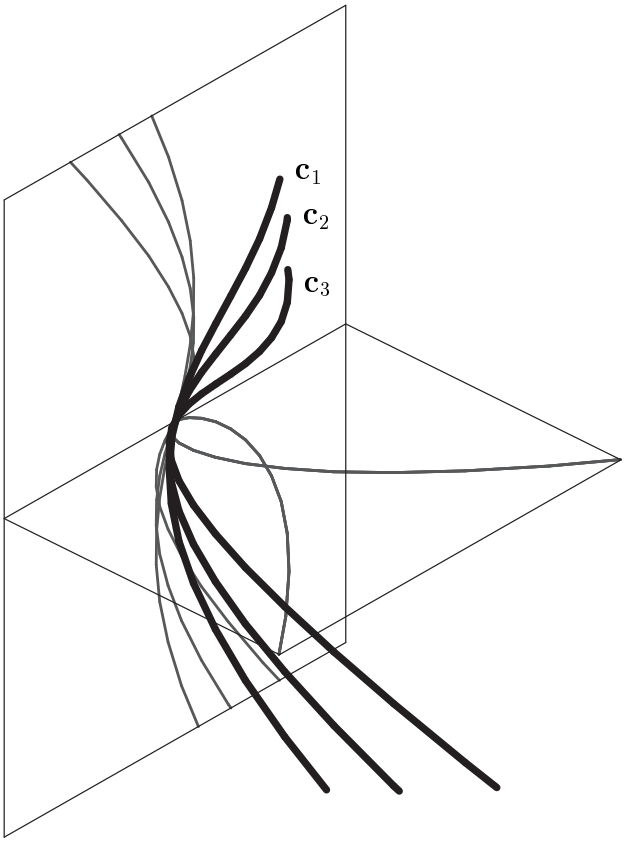

Figure 4: Three examples of the cubic helix $\mathbf{c}_1$, $\mathbf{c}_2$ and $\mathbf{c}_3$ (black) and their projections to coordinates planes (grey).

In its first part, this thesis analyzes some geometric properties of MPH cubics. As the main result, it is shown that these curves are again helices and can be classified, similarly to the Euclidean case, cf. Kosinka and Jüttler (2006).

Starting from the results of Choi et al. (1999), the second part of this thesis addresses the problem of G^1 Hermite interpolation by MPH cubics. Based on the mutual position of the given end tangent vectors, we formulate an algorithm for computing the interpolants in Bernstein–Bézier form. Lorentz transforms are used to map the given Hermite data to one among five canonical positions, which significantly simplify the analysis. In the 'regular' case the problem has four solutions, which can be computed by solving two quadratic equations.

Based on canonical positions of the input data and the causal character of the difference of the end tangent vectors we derive sufficient and necessary conditions for interpolants to exist. In fact, the difference of the endpoints has to lie inside certain quadratic cones depending solely on the end tangent vectors. Singular cases are also discussed.

In order to analyze the convergence order of the interpolants, an asymptotic approach by means of Taylor expansions and Frenet formulas in Minkowski space is introduced. As a result, we give conditions for converting curves into MPH cubic splines. It turns out that any space–like C^∞ curve can be approximately converted into a G^1 MPH cubic spline. The approximation order is four, provided that the curve has no isolated Minkowski inflections. Otherwise the approximation order drops to two, cf. Kosinka and Jüttler (2006).

In addition to these results on MPH cubics, we provide a geometric interpretation of the Minkowski curvature and Minkowski inflections in terms of the geometry of the associated planar domain.

The remainder of this thesis is organized as follows. Section 2 summarizes some basic notions and facts concerning three–dimensional Minkowski geometry, Bézier, PH and MPH curves, differential geometry of curves in Minkowski space and helices in Minkowski space.

Section 3 focuses on properties of MPH cubics. In particular, we study MPH cubics in the context of cubic helices in Minkowski space resulting in a complete classification of planar and spatial MPH cubics.

Section 4 discusses a Hermite interpolation of G^1 boundary data via MPH cubics. Based on canonical positions of boundary tangent vectors and with the help of Taylor expansions we give a thorough analysis of existence and number of MPH cubic interpolants to given G^1 data. Moreover, the theoretical results are illustrated by several numerical examples. Finally we conclude the thesis.

2 Preliminaries

This section summarizes some basic concepts and some results concerning Minkowski space, polynomial Bézier curves, PH and MPH curves and differential geometry of curves in Minkowski space.

2.1 Minkowski space

The three–dimensional Minkowski space $\mathbb{R}^{2,1}$ is a real vector space with an indefinite inner product given by the matrix $G = \mathrm{diag}(1, 1, -1)$. The inner product of two vectors $\mathbf{u} = (u_1, u_2, u_3)^\top$, $\mathbf{v} = (v_1, v_2, v_3)^\top$, $\mathbf{u}, \mathbf{v} \in \mathbb{R}^{2,1}$ is defined as

$$\langle \mathbf{u}, \mathbf{v} \rangle = \mathbf{u}^\top G \mathbf{v} = u_1 v_1 + u_2 v_2 - u_3 v_3. \tag{2}$$

The three axes spanned by the vectors $\mathbf{e}_1 = (1, 0, 0)^\top$, $\mathbf{e}_2 = (0, 1, 0)^\top$ and $\mathbf{e}_3 = (0, 0, 1)^\top$ will be denoted as the x–, y– and r–axis, respectively.

Since the quadratic form defined by G is not positive definite as in the Euclidean case, the square norm of $\mathbf{u}$ defined by $||\mathbf{u}||^2 = \langle \mathbf{u}, \mathbf{u} \rangle$ may be positive, negative or zero. Motivated by the theory of relativity we distinguish three so–called 'causal characters' of vectors. A vector $\mathbf{u}$ is called space–like if $||\mathbf{u}||^2 > 0$, time–like if $||\mathbf{u}||^2 < 0$, and light–like (or isotropic) if $||\mathbf{u}||^2 = 0$.

All light–like vectors form a cone in $\mathbb{R}^{2,1}$, the so called light cone. We denote a light cone with the vertex at a point $\mathbf{w}$ by $\mathcal{C}_\mathbf{w}$ (see Fig. 5).

Two vectors $\mathbf{u}, \mathbf{v} \in \mathbb{R}^{2,1}$ are said to be orthogonal if $\langle \mathbf{u}, \mathbf{v} \rangle = 0$. Therefore a normal vector of a plane given by $ax + by + cz = 0$ has the coordinates $\mathbf{n} = (a, b, -c)^\top$. The cross–product in the Minkowski space can be defined analogously to the Euclidean case as

$$\mathbf{w} = \mathbf{u} \bowtie \mathbf{v} = (u_2 v_3 - u_3 v_2, u_3 v_1 - u_1 v_3, -u_1 v_2 + u_2 v_1)^\top. \tag{3}$$

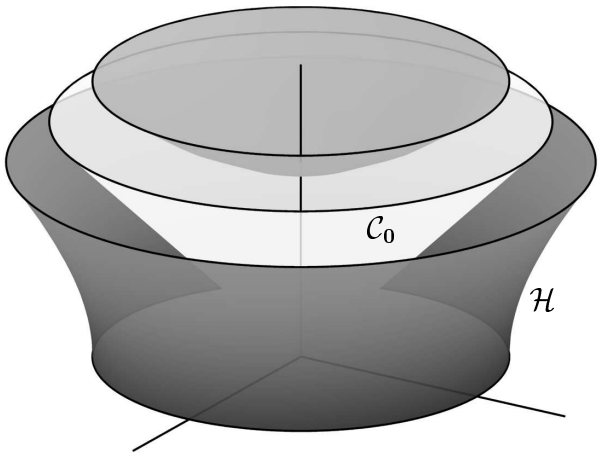

Figure 5: The unit hyperboloid $\mathcal{H}$ and the light cone $\mathcal{C}_0$.

Clearly, $\langle \mathbf{u}, \mathbf{u} \ltimes \mathbf{v} \rangle = 0$ for all $\mathbf{u}, \mathbf{v} \in \mathbb{R}^{2,1}$.

A vector $\mathbf{u} \in \mathbb{R}^{2,1}$ is called a unit vector if $||\mathbf{u}||^2 = \pm 1$. When $\mathbf{u}$ is a space–like vector, it can be normalized to $||\mathbf{u}||^2 = 1$, in the time–like case to $||\mathbf{u}||^2 = -1$. The hyperboloid of one sheet given by $x^2 + y^2 - r^2 = 1$ spanned by the endpoints of all unit space–like vectors will be called the unit hyperboloid $\mathcal{H}$ (see Fig. 5).

Let u, v and w be three vectors in $\mathbb{R}^{2,1}$. A scalar triple product of u, v and w is defined as

$$[u, v, w] = \langle u, v \ltimes w \rangle. \tag{4}$$

The scalar triple product in Minkowski space is the same as in Euclidean space, since the sign changes in Minkowski inner and cross–product cancel out. Therefore $[u, v, w] = \det(u, v, w)$.

A plane in Minkowski space is called space–, time– or light–like if the restriction of the quadratic form defined by G on this plane is positive definite, indefinite nondegenerate or degenerate, respectively. The type of a plane ρ

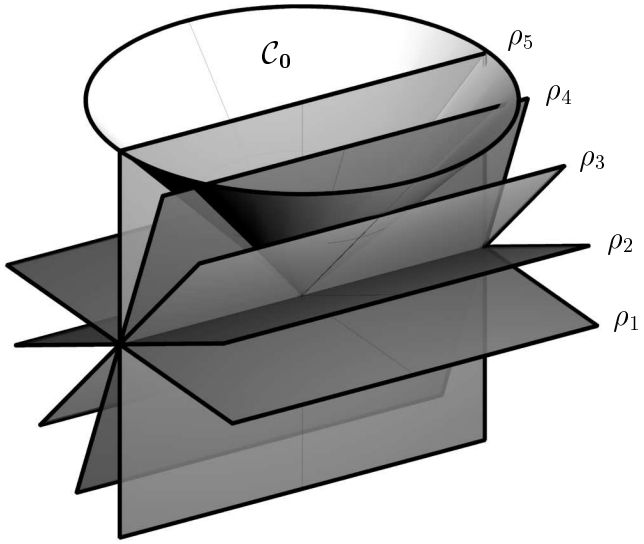

Figure 6: Space–like planes ρ_1 and ρ_2, light–like plane ρ_3, time–like planes ρ_4 and ρ_5 and the light cone $\mathcal{C}_\mathbf{0}$.

can be characterized by the Euclidean angle α included between ρ and the xy plane. For light–like planes, $\alpha = \frac{\pi}{4}$.

Figure 6 shows five planes along with the light cone $\mathcal{C}_\mathbf{0}$. Planes ρ_1 and ρ_2 are space–like, plane ρ_3 is light–like (tangent to $\mathcal{C}_\mathbf{0}$) and planes ρ_4 and ρ_5 are time–like. Moreover, planes ρ_1, ρ_5 are mutually perpendicular as well as planes ρ_2, ρ_4. The light–like plane ρ_3 is perpendicular to itself.

Remark 1 In this thesis, we define the Minkowski space as a real linear space equipped with an indefinite inner product, following Choi et al. (1999), Moon (1999). Alternatively, one may also define it as a special affine space, see Kriele (1999).

2.2 Lorentz transforms

A linear transform $L : \mathbb{R}^{2,1} \to \mathbb{R}^{2,1}$ is called a Lorentz transform if it maintains the Minkowski inner product, i.e. $\langle \mathbf{u}, \mathbf{v} \rangle = \langle L\mathbf{u}, L\mathbf{v} \rangle$ for all $\mathbf{u}, \mathbf{v} \in \mathbb{R}^{2,1}$. The group of all Lorentz transforms $\mathcal{L} = O(2,1)$ is called the Lorentz group.

Let $K = (k_{i,j})_{i,j=1,2,3}$ be a Lorentz transform. Then the column vectors $\mathbf{k}_1$, $\mathbf{k}_2$ and $\mathbf{k}_3$ satisfy $\langle \mathbf{k}_i, \mathbf{k}_j \rangle = G_{i,j}$, $i, j \in \{1, 2, 3\}$, i.e. they form an orthonormal basis of $\mathbb{R}^{2,1}$.

From $\langle \mathbf{k}_3, \mathbf{k}_3 \rangle = G_{3,3} = -1$ one obtains $k_{33}^2 \geq 1$. A transform K is said to be *orthochronous* if $k_{33} \geq 1$. The determinant of any Lorentz transform K equals to ± 1, and special ones are characterized by $\det(K) = 1$.

The Lorentz group $\mathcal{L}$ consists of four components. The special orthochronous Lorentz transforms form a subgroup $SO_+(2,1)$ of $\mathcal{L}$. The other components are $T_1 \cdot SO_+(2,1)$, $T_2 \cdot SO_+(2,1)$ and $T_1 \cdot T_2 \cdot SO_+(2,1)$, where $T_1 = \mathrm{diag}(1, 1, -1)$ and $T_2 = \mathrm{diag}(1, -1, 1)$. Let

$$R(\alpha) = \begin{pmatrix} \cos\alpha & -\sin\alpha & 0 \\ \sin\alpha & \cos\alpha & 0 \\ 0 & 0 & 1 \end{pmatrix} \quad \text{and} \quad H(\beta) = \begin{pmatrix} 1 & 0 & 0 \\ 0 & \cosh\beta & \sinh\beta \\ 0 & \sinh\beta & \cosh\beta \end{pmatrix} \tag{5}$$

be a rotation of the spatial coordinates x, y, and a hyperbolic rotation with a hyperbolic angle β, respectively. Any special orthochronous Lorentz transform $L \in SO_+(2,1)$ can be represented as $L = R(\alpha_1)H(\beta)R(\alpha_2)$, see Fig. 7.

The restriction of the hyperbolic rotation to the time–like yr–plane (i.e. to Minkowski space $\mathbb{R}^{1,1}$) is given by

$$h(\beta) = \begin{pmatrix} \cosh\beta & \sinh\beta \\ \sinh\beta & \cosh\beta \end{pmatrix}. \tag{6}$$

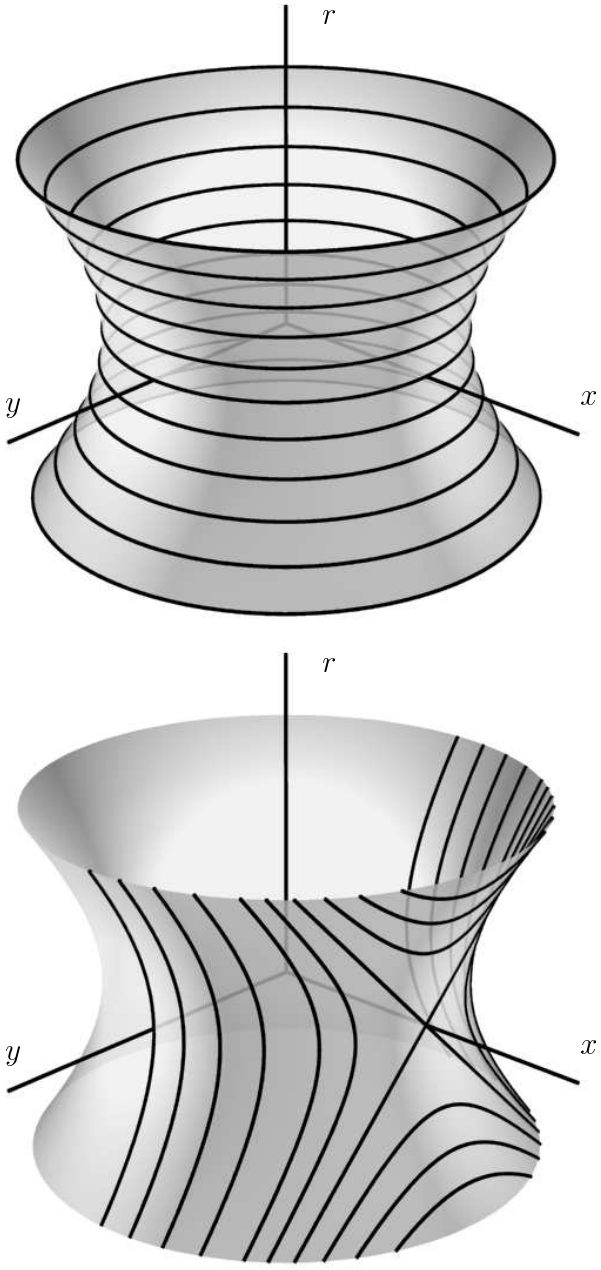

Figure 7: A representation of special orthochronous Lorentz transforms. Top: trajectories of the rotation $R(\alpha)$, bottom: trajectories of the hyperbolic rotation $H(\beta)$.

2.3 Free form curves

The two most common methods for representing curves in geometric modeling are implicit equations and parametric equations.

The implicit equation of a curve lying in the xy plane has the form

$$f(x, y) = 0, \tag{7}$$

where f is a sufficiently smooth function of x and y. This equation describes an implicit relationship between the x and y coordinates of the points lying on the curve. The equation for a given curve is unique up to a multiplicative constant. A well known example is the unit circle centered at the origin given by the equation $x^2 + y^2 - 1 = 0$.

In the parametric case, each coordinate of a curve point is represented separately as an explicit (sufficiently smooth) function of an independent parameter, i.e.

$$\mathbf{c}(t) = (x(t), y(t))^\top, \ t \in [a, b]. \tag{8}$$

The interval $[a, b]$ can be arbitrary, but it is usually normalized to $[0, 1]$. The first quadrant of the unit circle centered at the origin has the parametric form

$$x(t) = \cos(t), \ y(t) = \sin(t), \ t \in [0, \frac{\pi}{2}]. \tag{9}$$

By a substitution $u = \tan \frac{t}{2}$ we obtain an alternate representation

$$x(u) = \frac{1 - u^2}{1 + u^2}, \ y(u) = \frac{2u}{1 + u^2}, \ u \in [0, 1]. \tag{10}$$

Obviously, the parametric representation is not unique (see Fig. 8).

It is quite instructive to think of a parametric curve $\mathbf{c}(t)$ as of the path traced out by a particle moving in a plane, where t is time. The first and second derivative of $\mathbf{c}(t)$ are the velocity and the acceleration of the particle, respectively.

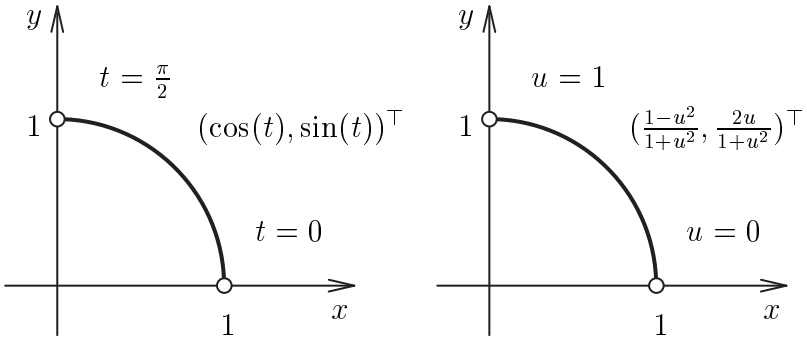

Figure 8: Different parametric representations of a circle segment.

Both the implicit and the parametric form have their advantages and disadvantages. We give a brief comparison of the two methods: (pluses denote advantages and minuses disadvantages of the parametric form)

+ by adding a third coordinate, the parametric form is easily extended to represent curves in three dimensional space: $\mathbf{c}(t) = (x(t), y(t), z(t))^\top$. The implicit form does not allow this generalization;

+ it is quite difficult to represent bounded or trimmed curve segments by the implicit form. On the other hand, one can easily select the desired part of a given parametric curve by choosing the parameter interval;

+ parametric curves possess a natural direction of their course, i.e. from $\mathbf{c}(a)$ to $\mathbf{c}(b)$, when $a < b$. Therefore, it is easy to generate ordered sequences of points along the curve;

+ compute a point on the curve – difficult in the implicit form, easy in the parametric form;

– given a point, determine whether the point lies on the curve or not – difficult in the parametric form, easy in the implicit form;

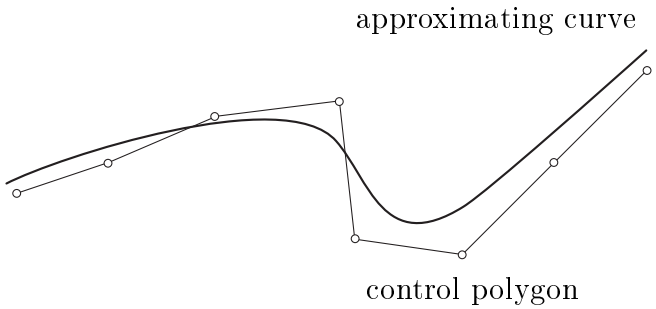

Figure 9: Curve fitting via approximation: the approximating curve follows the given control polygon.

– when using the parametric form, one must sometimes deal with parametric anomalies, which are not related to true geometry, e.g. the point $(0,0)^\top$ of the curve $(t,t^3)^\top$.

For the remainder of this thesis, we are concerned with the parametric representation only, as it dominates in computer design.

A fundamental problem in geometric design is the so–called curve fitting: given a set of points, find a "nice" curve, which passes through these points. This method is called interpolation. However, it is not our concern in this thesis.

An alternate method is referred to as approximation: given a set of (control) points, find a curve, which "nicely" follows the control polygon formed by the control points, see Fig. 9.

Clearly, by allowing the coordinate functions $x(t)$ and $y(t)$ to be arbitrary, we obtain a great variety of curves. However, there are trade–offs when implementing a geometric modeling system. Therefore, we restrict ourselves

to a class of functions, which are capable of representing precisely all the curves we want to use and are easily and efficiently processed in a computer. A widely used class of functions are the polynomials.

There are to methods for representing polynomial parametric curves: power basis and Bézier method. Although mathematically equivalent, the Bézier method is far better suited for representing polynomial parametric curves.

2.3.1 Polynomial Bézier curves

A Bézier curve of degree $n \in \mathbb{N}$ is defined by (cf. Piegl and Tiller (1995))

$$\mathbf{b}(t) = \sum_{i=0}^{n} B_{i,n}(t)\mathbf{p}_i, \ t \in [0,1], \tag{11}$$

where the basis (blending) functions are the classical nth degree Bernstein polynomials given by

$$B_{i,n}(t) = \frac{n!}{i!(n-i)!} t^i (1-t)^{n-i}. \tag{12}$$

Coefficients $\mathbf{p}_i$ are called control points.

Figure 10 shows several examples of Bézier cubics ($n = 3$) with different control polygons. The corresponding Bernstein polynomials

$$B_{0,3}(t) = (1-t)^3, \tag{13}$$
$$B_{1,3}(t) = 3t(1-t)^2, \tag{14}$$
$$B_{2,3}(t) = 3t^2(1-t), \tag{15}$$
$$B_{3,3}(t) = t^3 \tag{16}$$

are shown in Fig. 11.

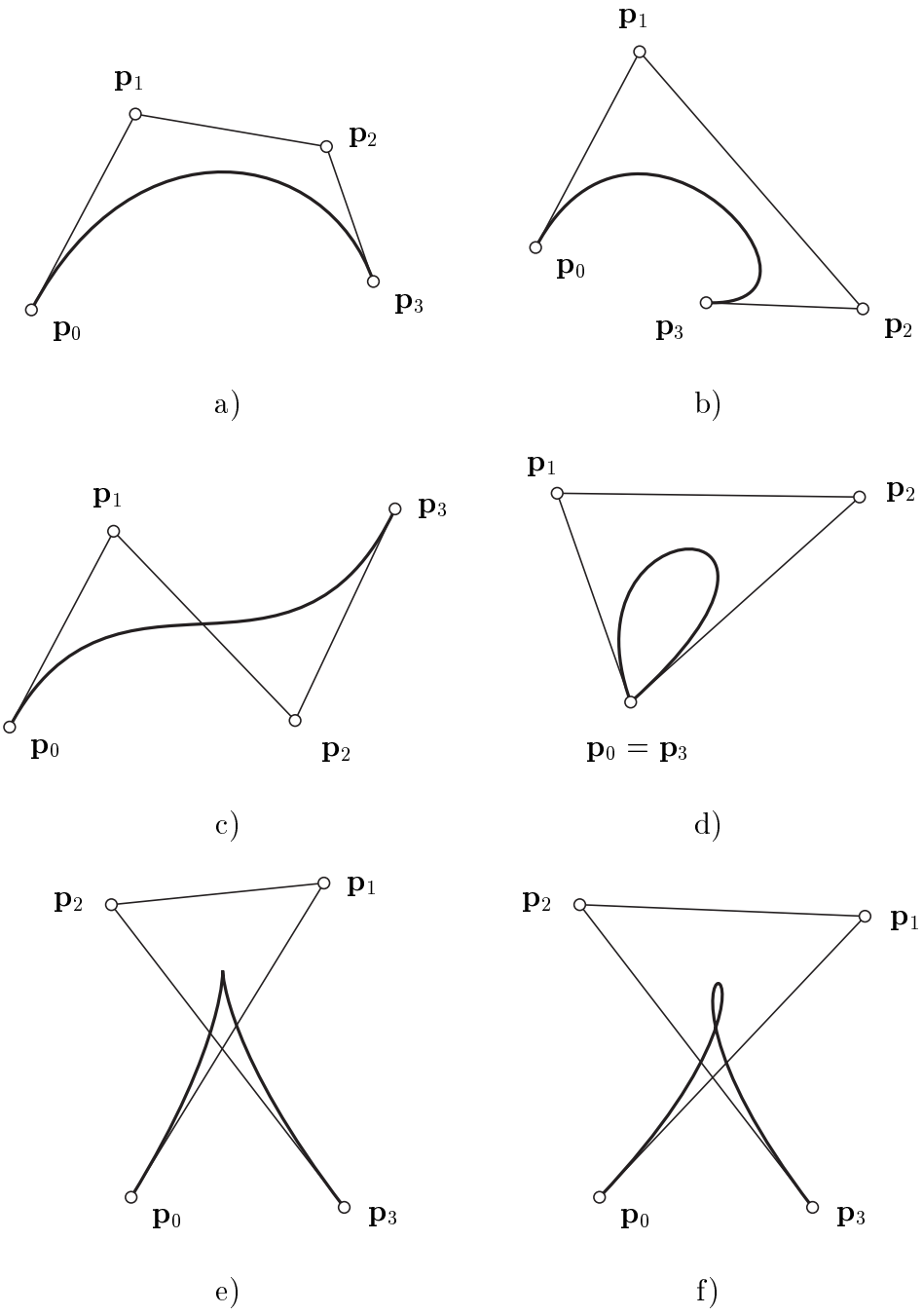

Figure 10: Examples of Bézier cubics: c) cubic with an inflection point, d) closed cubic, e) cubic with a cusp and f) cubic with a loop.

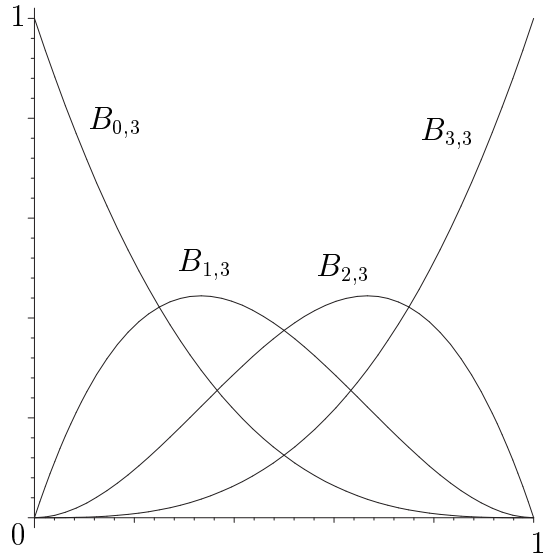

Figure 11: Bernstein basis polynomials of degree three.

Properties of Bézier curves: Let us take a closer look at properties of Bernstein polynomials, which can be easily derived from their definition:

1. nonnegativity: $B_{i,n}(t) \geq 0$ for all i, n and $t \in [0,1]$;
2. partition of unity: $\sum_{i=0}^{n} B_{i,n}(t) = 1$ for all $t \in [0,1]$;
3. $B_{0,n}(0) = B_{n,n}(1) = 1$;
4. $B_{i,n}(t)$ attains exactly one maximum on the interval $[0,1]$ for $t = \frac{i}{n}$;
5. symmetry: for any n, the set of polynomials $\{B_{i,n}(t)\}$ is symmetric with respect to $t = \frac{1}{2}$;
6. recursive definition: $B_{i,n}(t) = (1-t)B_{i,n-1}(t) + tB_{i-1,n-1}(t)$, where by definition $B_{i,n}(t) \equiv 0$ for $i < 0$ or $i > n$;

7. derivative:
$$B'_{i,n}(t) = n(B_{i-1,n-1}(t) - B_{i,n-1}(t)), \tag{17}$$
where $B_{-1,n-1}(t) \equiv B_{n,n-1}(t) \equiv 0$.

These properties of Bernstein polynomials and the definition (11) yield the following properties of Bézier curves.

1. end points interpolation: $\mathbf{b}(0) = \mathbf{p}_0$ and $\mathbf{b}(1) = \mathbf{p}_n$;
2. end tangent vectors: $\mathbf{b}'(0) = n(\mathbf{p}_1 - \mathbf{p}_0)$ and $\mathbf{b}'(1) = n(\mathbf{p}_n - \mathbf{p}_{n-1})$;
3. convex hull property: any Bézier curve is contained in the convex hull of its defining control polygon;
4. variation diminishing property: no straight line (plane in 3D case) intersects a Bézier curve more times than it intersects the curve's control polygon. This expresses the property that a Bézier curve follows its control polygon rather nicely and does not wiggle more than its control polygon (see Fig. 10);
5. Bézier curves are invariant under affine mappings, i.e. (loosely speaking) one applies the transformation to the curve by applying it to the control polygon.

The deCasteljau Algorithm: Let $n = 2$ and $\mathbf{b}(t) = \sum_{i=0}^{2} B_{i,2}(t)\mathbf{p}_i,\ t \in [0,1]$. Then

$$\begin{aligned} \mathbf{b}(t) &= (1-t)^2\mathbf{p}_0 + 2t(1-t)\mathbf{p}_1 + t^2\mathbf{p}_2 && (18)\\ &= (1-t)(\underbrace{(1-t)\mathbf{p}_0 + t\mathbf{p}_1}_{linear}) + t(\underbrace{(1-t)\mathbf{p}_1 + t\mathbf{p}_2}_{linear}). && (19) \end{aligned}$$

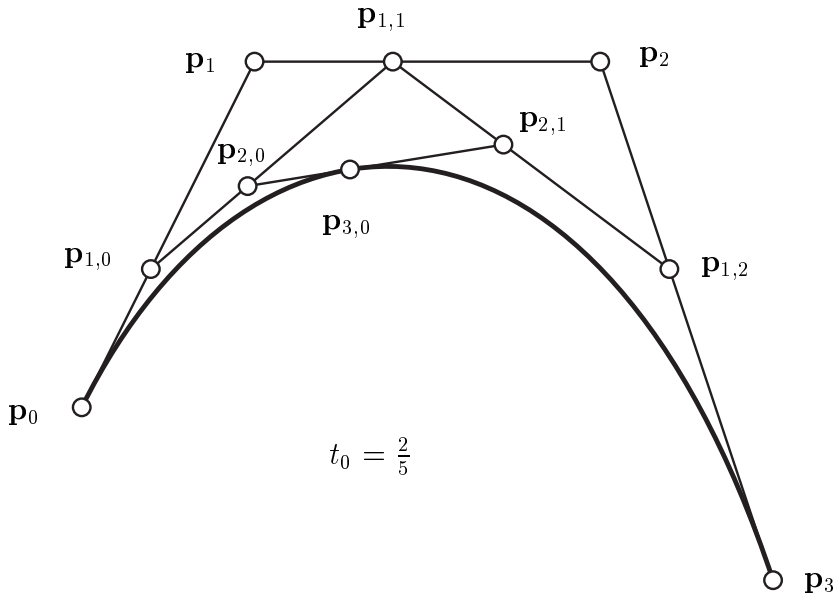

Figure 12: The deCasteljau algorithm: a construction of a point on a Bézier curve by repeated linear interpolation.

We can see that $\mathbf{b}(t)$ is obtained as a linear interpolation of two first–degree Bézier curves. In particular, any point on $\mathbf{b}(t)$ is obtained by three linear interpolations.

Let us consider a fixed value $t = t_0$ and let

$$\mathbf{p}_{1,0} = (1 - t_0)\mathbf{p}_0 + t_0\mathbf{p}_1, \tag{20}$$

$$\mathbf{p}_{1,1} = (1 - t_0)\mathbf{p}_1 + t_0\mathbf{p}_2, \tag{21}$$

$$\mathbf{p}_{2,0} = (1 - t_0)\mathbf{p}_{1,0} + t_0\mathbf{p}_{1,1}. \tag{22}$$

It follows that $\mathbf{b}(t_0) = \mathbf{p}_{2,0}$. An example for a cubic case is shown in Figure 12.

Denoting a general nth degree Bézier curve given by the set of control points

$\mathbf{p}_0$					
	$\mathbf{p}_{1,0}$				
$\mathbf{p}_1$		$\mathbf{p}_{2,0}$			
	$\mathbf{p}_{1,1}$				
$\mathbf{p}_2$		$\vdots$			
$\vdots$	$\vdots$	$\vdots$		$\mathbf{p}_{n-1,0}$	
$\vdots$	$\vdots$	$\vdots$	$\cdots$		$\mathbf{p}_{n,0} = \mathbf{b}(t_0)$
$\vdots$	$\vdots$	$\vdots$		$\mathbf{p}_{n-1,1}$	
$\mathbf{p}_{n-2}$		$\vdots$			
	$\mathbf{p}_{1,n-2}$				
$\mathbf{p}_{n-1}$		$\mathbf{p}_{2,n-2}$			
	$\mathbf{p}_{1,n-1}$				
$\mathbf{p}_n$					

Table 1: Points generated by the deCasteljau algorithm.

$\{\mathbf{p}_0, \ldots, \mathbf{p}_n\}$ by $\mathbf{b}_n(\mathbf{p}_0, \ldots, \mathbf{p}_n)$, we have

$$\mathbf{b}_n(\mathbf{p}_0, \ldots, \mathbf{p}_n) = (1-t)\mathbf{b}_{n-1}(\mathbf{p}_0, \ldots, \mathbf{p}_{n-1}) + t\mathbf{b}_{n-1}(\mathbf{p}_1, \ldots, \mathbf{p}_n). \tag{23}$$

This follows from the recursive definition of the Bernstein basis functions (see property 6). Fixing $t = t_0$ and denoting $\mathbf{p}_i$ by $\mathbf{p}_{0,i}$, equation (23) yields a recursive algorithm for computing the point $\mathbf{b}(t_0) = \mathbf{p}_{n,0}(t_0)$ on an nth degree Bézier curve:

$$\mathbf{p}_{k,i}(t_0) = (1-t_0)\mathbf{p}_{k-1,i}(t_0) + t_0\mathbf{p}_{k-1,i+1}(t_0), \tag{24}$$

where $k = 1, 2, \ldots, n$ and $i = 0, 1, \ldots, n-k$. Equation (24) is called the deCasteljau algorithm. It is a corner cutting process (cf. Fig. 12), which yields the triangular table of points shown in Table 1.

We conclude this section with several remarks. Clearly, the Bézier curves are very well suited for interactive curve design. The control polygon gives

the designer an intuitive handle of the curve shape, which is ensured by the convex hull and variation diminishing property of Bézier curves. However, among conic sections only a parabola can be exactly represented by a polynomial Bézier curve. Although, rational Bézier curves remedy this shortcoming, they fall beyond the scope of the present thesis.

2.4 Pythagorean hodograph curves

Let us consider a planar polynomial curve $\mathbf{c}(t) = (x(t), y(t))^\top$. Despite all the attractive features described in the previous section, polynomial parametric curves have certain limitations that degrade their overall utility in practical design applications.

Before proceeding, let us be more specific about some of the shortcomings of polynomial curves. When such a curve is to be evaluated at a uniform sequence of parameter values $\{t_i\}$, the resulting geometric points $\{\mathbf{p}_i\}$ are not uniformly distributed along the curve, since its "parameter flow" is necessarily uneven if it is not a straight line. To compensate this, it requires a determination of the functional relation between the arc length s along the curve and the parameter t. In general, the arc length function

$$s(t) = \int \sqrt{x'(t)^2 + y'(t)^2}\, \mathrm{d}t \tag{25}$$

is an integral that cannot be resolved in terms of elementary functions of t. Thus, turning to a numerical quadrature to approximate $s(t)$ involves inefficient and potentially error–prone computations.

Another problem arises with regard to offset curves. In applications (such as computer–numerical–control (CNC) machining, tolerance analysis and path

planing), one is interested in the curves

$$\mathbf{o}_\delta(t) = \left(x(t) \pm \delta \frac{y'(t)}{\sqrt{x'(t)^2 + y'(t)^2}}, y(t) \mp \delta \frac{x'(t)}{\sqrt{x'(t)^2 + y'(t)^2}} \right)^\top \tag{26}$$

at a fixed distance δ from $\mathbf{c}(t) = (x(t), y(t))^\top$ in the direction (or in the opposite direction) of its unit normal vector. The offset $\mathbf{o}_\delta(t)$ is not, in general, a polynomial or rational curve.

As observed by Farouki & Sakkalis (1990), the so–called Pythagorean hodograph (PH) curves overcome the deficiencies mentioned above. The distinguishing feature of a polynomial PH curve $\mathbf{c}(t)$ is that the components of its hodograph $\mathbf{c}'(t)$ satisfy a Pythagorean condition, i.e. the sum of their squares is equal to the square of a polynomial $\sigma(t)$. The fulfilment of this condition entails rather different approaches in the context of planar and spatial PH curves.

2.4.1 Planar Pythagorean hodograph curves

Let $\mathbf{c}(t) = (x(t), y(t))^\top$ be a planar polynomial curve. The hodograph $\mathbf{c}'(t)$ must satisfy

$$x'(t)^2 + y'(t)^2 = \sigma^2(t), \tag{27}$$

where $\sigma(t)$ is a polynomial. This condition is equivalent (see Kubota (1972)) to the requirement that, in terms of polynomials $u(t)$, $v(t)$ and $w(t)$, the hodograph $\mathbf{c}'(t)$ has the form

$$\begin{aligned} x'(t) &= w(t)(u(t)^2 - v(t)^2), \\ y'(t) &= w(t)(2u(t)v(t)), \\ \sigma(t) &= w(t)(u(t)^2 + v(t)^2). \end{aligned} \tag{28}$$

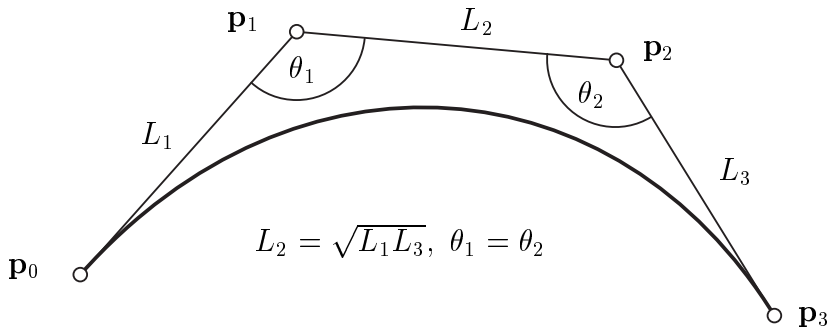

Figure 13: Control polygon of a planar PH cubic.

Taking $w(t) = 1$ and $u(t)$, $v(t)$ such that $\gcd(u(t), v(t)) = 1$ gives a primitive Pythagorean hodograph defining a regular PH curve (i.e. $\gcd(x'(t), y'(t)) = 1$) of an odd degree.

A direct consequence of (27) is that, for a PH curve, the arc length function (25) is just a (possibly piecewise) polynomial (rather than an irreducible integral). Moreover, the offsets (26) of PH curves admit exact (possibly piecewise) rational representations (eliminating the need for approximation schemes). The exact arc length and offset properties of PH curves are extremely useful in the context of CNC machining.

Taking constants for $u(t)$, $v(t)$ and $w(t)$ reveals a trivial fact that straight lines are PH curves. The first non–trivial examples are cubics, defined by $w(t) = 1$ and linear polynomials $u(t)$, $v(t)$ in (28). PH cubics can be characterized geometrically in terms of their Bézier control polygons formed by the set of control points $\{\mathbf{p}_0, \mathbf{p}_1, \mathbf{p}_2, \mathbf{p}_3\}$. Namely, if $L_k = |\mathbf{p}_k - \mathbf{p}_{k-1}|$, $k = 1, 2, 3$, are the lengths of the corresponding control polygon legs, and θ_1, θ_2 are the angles at the interior points $\mathbf{p}_1$, $\mathbf{p}_2$, the conditions

$$L_2 = \sqrt{L_1 L_3} \text{ and } \theta_1 = \theta_2 \tag{29}$$

are sufficient and necessary for a PH cubic (cf. Farouki & Sakkalis (1990),

Fig. 13). The simplicity of this characterization reveals that modulo rigid body motions, scalings and linear reparameterizations, all planar PH cubics are segments of a unique curve, the Tschirnhausen cubic, see Fig. 20. Since it has no inflections, this curve is of limited value in design applications.

For shape flexibility similar to that of "ordinary" cubics, we must appeal to PH quintics, defined by $w(t) = 1$ and quadratic polynomials $u(t)$, $v(t)$ in (28). The PH quintics can inflect and can interpolate arbitrary C^1 Hermite data.

2.4.2 Spatial Pythagorean hodograph curves

Analogously to the planar case, a spatial PH curve $\mathbf{c}(t) = (x(t), y(t), z(t))^\top$ satisfies

$$x'(t)^2 + y'(t)^2 + z'(t)^2 = \sigma^2(t), \tag{30}$$

for some polynomial $\sigma(t)$. These curves were introduced by Farouki and Sakkalis (1994), however, a sufficient and necessary characterization of polynomial solutions to (30) was given by Dietz et al. (1993) in terms of four polynomials $u(t)$, $v(t)$, $p(t)$ and $q(t)$:

$$\begin{aligned} x'(t) &= u(t)^2 + v(t)^2 - p(t)^2 - q(t)^2, \\ y'(t) &= 2(u(t)q(t) + v(t)p(t)), \\ z'(t) &= 2(v(t)q(t) - u(t)p(t)), \\ \sigma(t) &= u(t)^2 + v(t)^2 + p(t)^2 + q(t)^2, \end{aligned} \tag{31}$$

which defines a regular spatial PH curve with $\gcd(x'(t), y'(t), z'(t)) = 1$ whenever $u(t)$, $v(t)$, $p(t)$ and $q(t)$ have no common factor.

As in the case of planar PH curves, the twisted PH cubics can be characterized by geometrical constraints on their Bézier control polygons. In fact,

spatial PH cubics are all segments of (non–circular) helices, i.e. their tangents maintain a constant angle with a given axis, and they exhibit a constant ratio of curvature to torsion.

The arc length function $s(t)$ of spatial PH curves is obtained by a trivial extension of the methods given above for planar PH curves. The spatial analogy to an offset is the so–called canal surface with a given spatial curve as its spine, i.e. the envelope of a one parameter family of spheres with a fixed radius centered at the spine curve. Since PH curves admit orthogonal frames (cf. Wagner and Ravani (1997)) dependent rationally on t, the canal surfaces with PH spine curves can be rationally parameterized (see Farouki and Sakkalis (1994)).

Now, we leave the theory and applications of PH curves and turn our attention to Pythagorean hodograph curves in Minkowski space.

2.5 Minkowski Pythagorean hodograph curves and the MAT

Recall that a polynomial curve in Euclidean space is said to be a Pythagorean hodograph (PH) curve, if the norm of its first derivative (or hodograph) is a (possibly piecewise) polynomial. Following Moon (1999), MPH curves are defined similarly, but with respect to the norm induced by the Minkowski inner product. More precisely, a polynomial curve $\mathbf{c}(t) \in \mathbb{R}^{2,1}$, $\mathbf{c}(t) = (x(t), y(t), r(t))^\top$ is called an MPH curve if a polynomial $\sigma(t)$ exists such that

$$x'(t)^2 + y'(t)^2 - r'(t)^2 = \sigma(t)^2. \tag{32}$$

Moon has shown that a sufficient and necessary condition for the satisfaction of equation (32) is given in terms of four polynomials $u(t)$, $v(t)$, $p(t)$ and $q(t)$:

$$\begin{aligned} x'(t) &= u(t)^2 - v(t)^2 - p(t)^2 + q(t)^2, \\ y'(t) &= -2(u(t)v(t) + p(t)q(t)), \\ r'(t) &= 2(u(t)q(t) + v(t)p(t)), \\ \sigma(t) &= u(t)^2 + v(t)^2 - p(t)^2 - q(t)^2. \end{aligned} \tag{33}$$

We recall the motivation that led Moon (1999) to the definition of MPH curves. Consider a domain $\Omega \in \mathbb{R}^2$. The medial axis (MA) of Ω is the locus of all the centers of maximal disks touching the boundary $\partial\Omega$ in at least two points, which are inscribed into the domain Ω. Let $(x(t), y(t))^\top$ be a parameterization of a part of the medial axis of Ω and let $r(t)$ be a radius function, which specifies the radii of the maximal disks with centers at $(x(t), y(t))$. The corresponding part of the medial axis transform (MAT) is then a spatial curve $(x(t), y(t), r(t))^\top$ (cf. Fig. 14).

On the other hand, given a segment $\mathbf{g}(t) = (x(t), y(t), r(t))^\top$, $t \in I$, of the MAT, we can recover the original domain by forming the union of the disks,

$$\Omega = \bigcup_{t \in I} D_{r(t)}(x(t), y(t)), \tag{34}$$

where $D_r(x, y)$ is the disk with center (x, y) and radius r. Its boundary $\partial\Omega$ is obtained as the envelope of the medial axis circles. The envelopes determined by a C^1 segment $\mathbf{g}(t) = (x(t), y(t), r(t))^\top$ of the MAT (see Choi et al., 1997) are

$$\mathbf{b}^{(\pm)}(t) = \begin{pmatrix} x \\ y \end{pmatrix} - \frac{r}{x'^2 + y'^2} \left[r' \begin{pmatrix} x' \\ y' \end{pmatrix} \pm \sqrt{x'^2 + y'^2 - r'^2} \begin{pmatrix} -y' \\ x' \end{pmatrix} \right], \tag{35}$$

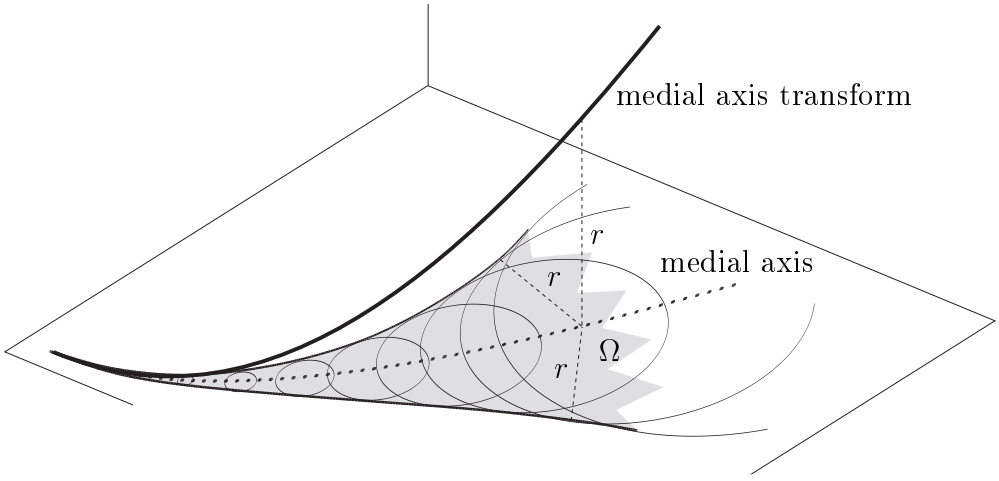

Figure 14: A medial axis transform and the corresponding planar domain Ω.

provided that $r > 0$. Moreover, δ–offsets of $\partial\Omega$ may be computed the same way by lifting the MAT to $(x(t), y(t), r(t) \pm \delta)^\top$, see Fig. 15. As observed by Moon (1999) and Choi et al. (1999), if the corresponding MAT is an MPH curve, then the coordinate functions of the corresponding boundary curves and their offsets are (possibly piecewise) rational.

A curve segment $\mathbf{c}(t) \in \mathbb{R}^{2,1}$, $t \in [a, b]$ is called space–, time– or light–like if its tangent vector $\mathbf{c}'(t)$, $t \in [a, b]$ is space–, time– or light–like, respectively.

Remark 2 As an immediate consequence of the definition, the tangent vector $\mathbf{c}'(t)$ of an MPH curve cannot be time–like. Also, light–like tangent vectors $\mathbf{c}'(t)$ correspond to roots of the polynomial w in (32). In the remainder of this thesis we consider curves with space–like tangent vectors, i.e. space–like curves. Note that the MAT of a planar domain is a (collection of) space curve(s) with space–like or light–like tangent vectors, where the latter ones appear only at isolated points, typically at vertices (points with extremal curvature) of the boundaries.

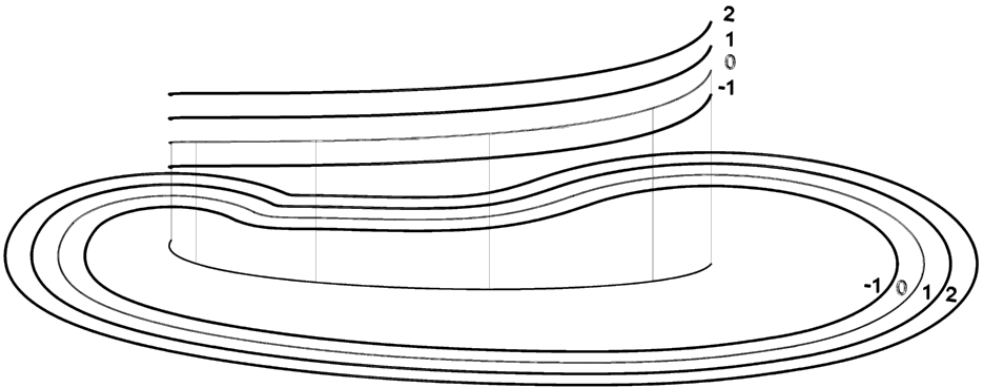

Figure 15: Offsets of a domain boundary can be obtained by lifting the corresponding MAT in the direction of its third coordinate.

2.6 Frenet formulas in Minkowski space

This section introduces several facts from the differential geometry of curves in the Minkowski space, cf. Blaschke (1929); Ekmekci & Ilarslan (1998); Walrave (1995).

Remark 3 If not stated otherwise, all curves are supposed to be three times continuously differentiable (C^3) for the remainder of this thesis. As we are mainly interested in cubics, this is essentially no restriction.

We consider a curve segment $\mathbf{c}(t) \in \mathbb{R}^{2,1}$. In order to rule out straight line and inflections, we suppose that the first two derivative vectors $\mathbf{c}'(t)$ and $\mathbf{c}''(t)$ are linearly independent. More precisely, points with linearly dependent vectors $\mathbf{c}'(t)$ and $\mathbf{c}''(t)$ correspond to inflections in the sense of affine differential geometry, which will be excluded.

We distinguish three different cases:

Case 1: Consider a space–like curve $\mathbf{c}(s) \in \mathbb{R}^{2,1}$, i.e. $||\mathbf{c}'(s)|| > 0$. We may assume that the curve is parameterized by its arc length, i.e. $||\mathbf{c}'(s)|| = 1$. Then we define a (space–like) unit tangent vector $\mathbf{T} = \mathbf{c}'(s)$ of $\mathbf{c}(s)$.

Subcase 1.1: If the vector $\mathbf{T}'$ is space–like or time–like on some parameter interval, the Frenet formulas take the form

$$\begin{aligned} \mathbf{T}' &= \kappa\mathbf{N}, \\ \mathbf{N}' &= -\langle\mathbf{N},\mathbf{N}\rangle\,\kappa\mathbf{T} + \tau\mathbf{B}, \\ \mathbf{B}' &= \tau\mathbf{N}. \end{aligned}$$

The unit vectors $\mathbf{N}$ and $\mathbf{B}$ are the unit normal and binormal vector, $\kappa > 0$ and τ are the Minkowski curvature and torsion of $\mathbf{c}(s)$, respectively. The three vectors $\mathbf{T}$, $\mathbf{N}$ and $\mathbf{B}$ form an orthonormal basis.

Subcase 1.2: The vector $\mathbf{T}'$ of a space–like curve may be light–like at an isolated point, or within an entire interval. The two cases will be called *Minkowski inflections* and *inflected segments*, respectively. The Frenet formulas of a space–like curve within an inflected segment take the form

$$\begin{aligned} \mathbf{T}' &= \mathbf{N}, \\ \mathbf{N}' &= \tau\mathbf{N}, \\ \mathbf{B}' &= -\mathbf{T} - \tau\mathbf{B}, \end{aligned}$$

where $\langle\mathbf{T},\mathbf{N}\rangle = \langle\mathbf{T},\mathbf{B}\rangle = 0$, $\langle\mathbf{N},\mathbf{N}\rangle = \langle\mathbf{B},\mathbf{B}\rangle = 0$ and $\langle\mathbf{N},\mathbf{B}\rangle = 1$. In this situation, the Minkowski curvature evaluates to $\kappa = 1$. The three vectors $\mathbf{T}$, $\mathbf{N}$ and $\mathbf{B}$ form a so–called pseudo–orthonormal basis (see Fig. 16).

Case 2: Consider a light–like curve $\mathbf{c}(s) \in \mathbb{R}^{2,1}$, i.e. $\langle\mathbf{c}'(s),\mathbf{c}'(s)\rangle = 0$. It follows that $\langle\mathbf{c}'(s),\mathbf{c}''(s)\rangle = 0$ and thus $\mathbf{c}''(s)$ lies in a light–like plane.

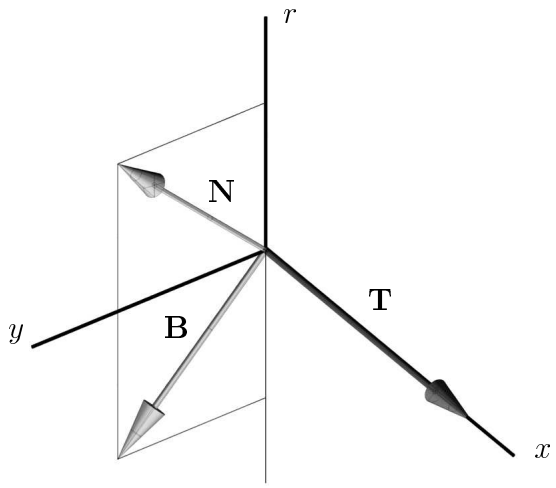

Figure 16: Vectors $\mathbf{T} = (1,0,0)^\top$, $\mathbf{N} = (0, \frac{\sqrt{2}}{2}, \frac{\sqrt{2}}{2})^\top$ and $\mathbf{B} = (0, \frac{\sqrt{2}}{2}, -\frac{\sqrt{2}}{2})^\top$ forming a pseudo–basis in Minkowski space.

Therefore $\mathbf{c}''(s)$ is space–like (light–like vector $\mathbf{c}''(s)$ leads to an inflection). We may assume that the curve is parameterized by its so called pseudo arc length, i.e. $||\mathbf{c}''(s)|| = 1$. Then we have

$$\begin{aligned} \mathbf{T}' &= \mathbf{N}, \\ \mathbf{N}' &= \tau\mathbf{T} - \mathbf{B}, \\ \mathbf{B}' &= -\tau\mathbf{N}, \end{aligned}$$

where $\langle \mathbf{N}, \mathbf{T} \rangle = \langle \mathbf{N}, \mathbf{B} \rangle = 0$, $\langle \mathbf{T}, \mathbf{T} \rangle = \langle \mathbf{B}, \mathbf{B} \rangle = 0$ and $\langle \mathbf{T}, \mathbf{B} \rangle = 1$. Again, the Minkowski curvature evaluates to $\kappa = 1$.

Case 3: Let us consider a time–like curve $\mathbf{c}(s) \in \mathbb{R}^{2,1}$ parameterized by its arc length, i.e. $||\mathbf{c}'(s)|| = -1$. Then we define a (time–like) unit tangent vector $\mathbf{T} = \mathbf{c}'(s)$. As $\langle \mathbf{T}, \mathbf{T}' \rangle = 0$, the vector $\mathbf{T}'$ lies in a space–like plane.

Therefore, $\mathbf{T}'$ is always space–like. The Frenet formulas take the form

$$\begin{aligned} \mathbf{T}' &= \kappa\mathbf{N}, \\ \mathbf{N}' &= \kappa\mathbf{T} + \tau\mathbf{B}, \\ \mathbf{B}' &= -\tau\mathbf{N}, \end{aligned}$$

where $\mathbf{N}$ and $\mathbf{B}$ are the unit normal and binormal vector, $\kappa > 0$ and τ are the Minkowski curvature and torsion of $\mathbf{c}(s)$, respectively. The three vectors $\mathbf{T}$, $\mathbf{N}$ and $\mathbf{B}$ form an orthonormal basis.

Remark 4 For the remainder of the thesis the notion inflection also includes Minkowski inflections.

2.6.1 Minkowski curvature, torsion and inflections

Proposition 1 *Let $\mathbf{c}(t) \in \mathbb{R}^{2,1}$ be a space–like curve without inflections. Then the curvature $\kappa(t)$ and torsion $\tau(t)$ of $\mathbf{c}(t)$ are given by*

$$\kappa(t) = \frac{\sqrt{|\langle \mathbf{c}'(t) \rtimes \mathbf{c}''(t), \mathbf{c}'(t) \rtimes \mathbf{c}''(t) \rangle|}}{||\mathbf{c}'(t)||^3} \tag{40}$$

and

$$\tau(t) = \frac{[\mathbf{c}'(t), \mathbf{c}''(t), \mathbf{c}'''(t)]}{|\langle \mathbf{c}'(t) \rtimes \mathbf{c}''(t), \mathbf{c}'(t) \rtimes \mathbf{c}''(t) \rangle|}. \tag{41}$$

Proof: Let us consider a space–like curve $\mathbf{c}(t) \in \mathbb{R}^{2,1}$ without inflections. Let $t = t(s)$ be a reparameterization of $\mathbf{c}(t)$ such that $\mathbf{c}(t(s))$ is parameterized by the arc length and let $\mathbf{T}(s)$, $\mathbf{N}(s)$ and $\mathbf{B}(s)$ be the tangent, normal and binormal vector and $\kappa(s)$ and $\tau(s)$ the curvature and torsion of $\mathbf{c}(t)$. We

denote by $\mathbf{c}'$ and $\dot{\mathbf{c}}$ the first derivative of $\mathbf{c}$ with respect to t and s, respectively. For the sake of brevity we omit the dependence on s. Then we have

$$\mathbf{T} = \mathbf{c}'(t)\frac{\mathrm{d}t}{\mathrm{d}s}. \tag{42}$$

Two consecutive differentiations of (42) with respect to s and simplifications using Frenet formulas yield

$$\kappa\mathbf{N} = \mathbf{c}''(t)\left(\frac{\mathrm{d}t}{\mathrm{d}s}\right)^2 + \mathbf{c}'(t)\frac{\mathrm{d}^2t}{\mathrm{d}s^2}, \tag{43}$$

$$\dot{\kappa}\mathbf{N} + \kappa(-\langle\mathbf{N},\mathbf{N}\rangle\kappa\mathbf{T} + \tau\mathbf{B}) = \mathbf{c}'''(t)\left(\frac{\mathrm{d}t}{\mathrm{d}s}\right)^3 + \mathbf{c}''(t)A + \mathbf{c}'(t)B, \tag{44}$$

where $A = 3\frac{\mathrm{d}t}{\mathrm{d}s}\frac{\mathrm{d}^2t}{\mathrm{d}s^2}$ and $B = \frac{\mathrm{d}^3t}{\mathrm{d}s^3}$.

Let us consider the cross–product $\mathbf{T} \bowtie \kappa\mathbf{N}$. Using (42) and (43) we obtain

$$\kappa(\mathbf{T} \bowtie \mathbf{N}) = \left(\frac{\mathrm{d}t}{\mathrm{d}s}\right)^3 (\mathbf{c}'(t) \bowtie \mathbf{c}''(t)). \tag{45}$$

Since $||\mathbf{c}'(t)|| = 1/\frac{\mathrm{d}t}{\mathrm{d}s}$, considering a square norm of (45) we have

$$\kappa^2 = \frac{||\mathbf{c}'(t) \bowtie \mathbf{c}''(t)||^2}{||\mathbf{c}'(t)||^6||\mathbf{T} \bowtie \mathbf{N}||^2}. \tag{46}$$

As $\kappa > 0$ and $\mathbf{T}$, $\mathbf{N}$ are unit vectors in this case, we can conclude that

$$\kappa(t) = \frac{\sqrt{|\langle\mathbf{c}'(t) \bowtie \mathbf{c}''(t), \mathbf{c}'(t) \bowtie \mathbf{c}''(t)\rangle|}}{||\mathbf{c}'(t)||^3}. \tag{47}$$

Now, let us form the scalar triple product $[\mathbf{T}, \kappa\mathbf{N}, \dot{\kappa}\mathbf{N}+\kappa(-\langle\mathbf{N},\mathbf{N}\rangle\kappa\mathbf{T}+\tau\mathbf{B})]$. Using (42), (43) and (44), we get

$$\tau\kappa^2[T, N, B] = \left(\frac{\mathrm{d}t}{\mathrm{d}s}\right)^6 [\mathbf{c}'(t), \mathbf{c}''(t), \mathbf{c}'''(t)]. \tag{48}$$

The identity $[T, N, B] = 1$ and (46) thus give

$$\tau(t) = \frac{[\mathbf{c}'(t), \mathbf{c}''(t), \mathbf{c}'''(t)]}{|\langle \mathbf{c}'(t) \bowtie \mathbf{c}''(t), \mathbf{c}'(t) \bowtie \mathbf{c}''(t) \rangle|}. \tag{49}$$

□

The next result characterizes inflections.

Proposition 2 *Let $\mathbf{c}(t) \in \mathbb{R}^{2,1}$ be a space–like curve. Then $\mathbf{c}(t)$ has an inflection corresponding to t_0 if and only if $||\mathbf{c}'(t_0) \bowtie \mathbf{c}''(t_0)||^2 = 0$.*

Proof: For the sake of brevity, we will omit the dependence on the parameter t. Let $\mathbf{T}$ and κ be the unit tangent vector and the curvature of $\mathbf{c}$. The Frenet formulas imply, cf. (46):

$$||\mathbf{c}' \bowtie \mathbf{c}''||^2 = ||\mathbf{c}'||^6 ||\mathbf{T} \bowtie \mathbf{T}'||^2. \tag{50}$$

Firstly, let $\mathbf{c}$ have an inflection. Then $\mathbf{T}'$ is a light–like vector. As $\langle \mathbf{T}, \mathbf{T} \rangle = 1$, by differentiating we obtain $\langle \mathbf{T}, \mathbf{T}' \rangle = 0$. One can easily check that $\langle \mathbf{T}, \mathbf{T}' \rangle = 0$ implies $||\mathbf{T} \bowtie \mathbf{T}'||^2 = 0$ (the geometric argument is that the vectors $\mathbf{T}$, $\mathbf{T}'$ define a light–like plane). Finally, (50) yields that $||\mathbf{c}' \bowtie \mathbf{c}''||^2 = 0$.

Secondly, let $||\mathbf{c}' \bowtie \mathbf{c}''||^2 = 0$. From (50) we get that $||\mathbf{T} \bowtie \mathbf{T}'||^2 = 0$ has to hold. Again, since $\langle \mathbf{T}, \mathbf{T}' \rangle = 0$, we can conclude that the vector $\mathbf{T}'$ is light–like. □

2.7 An interpretation of the Minkowski curvature

We discuss the relationship between the Minkowski curvature of a space–like curve in $\mathbb{R}^{2,1}$ and the curvatures of the boundaries of the associated planar domain. The results lead to an interpretation of Minkowski inflections and of inflected segments.

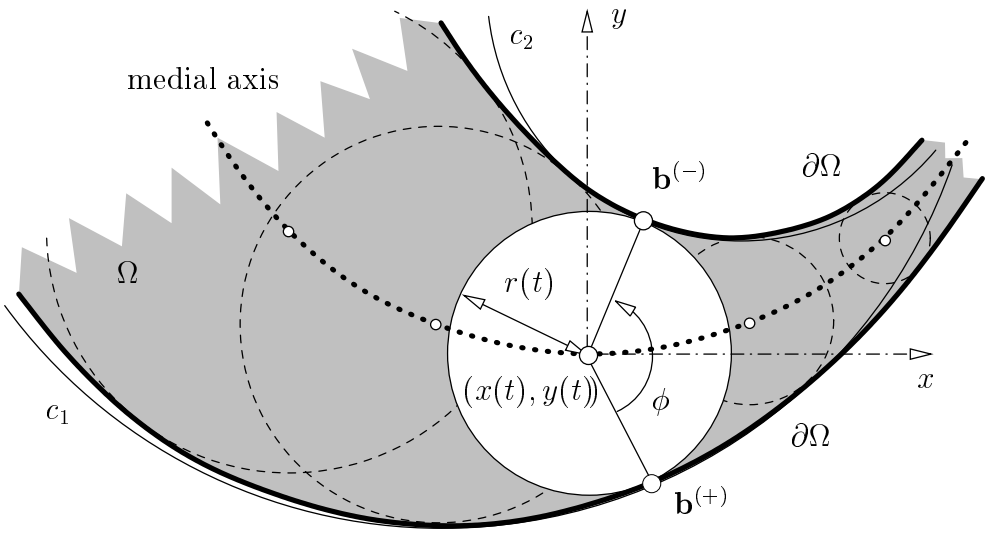

Figure 17: A planar domain, its medial axis (dotted), an inscribed circle, and the curvatures of the boundaries (visualized by the osculating circles c_1 and c_2).

Proposition 3 *Let* $\mathbf{p} = (x(t), y(t), r(t))^\top$ *be a space–like curve in* $\mathbb{R}^{2,1}$. *Then*

$$\langle \mathbf{T}', \mathbf{T}' \rangle = \frac{1}{(\rho_1 - r)(\rho_2 + r)\sin^2\frac{\phi}{2}} = \frac{k_1 k_2}{(1 - rk_1)(1 + rk_2)\sin^2\frac{\phi}{2}}, \tag{51}$$

where $\mathbf{T}'$ *denotes the derivative of the unit tangent vector of* $\mathbf{p}$ *with respect to the Minkowski arc length,* $k_1 = \frac{1}{\rho_1}, k_2 = \frac{1}{\rho_2}$ *are the oriented curvatures according to the parameterization* (35) *of the boundaries of the associated planar domain* Ω *(see* (34)*), and the angle* ϕ *equals* $\phi = \angle(\mathbf{b}^{(+)}, (x, y), \mathbf{b}^{(-)})$, *cf. Figure 17.*

Proof: We choose the coordinates such that the origin is located at $x(0), y(0)$, while the derivative $x'(0), y'(0)$ is aligned with the x–axis, see Figure 17. Then $\mathbf{b}^{(\pm)} = r(c, \mp s)$, where $c = \cos\frac{\phi}{2}$, $s = \sin\frac{\phi}{2}$. We replace the two boundary curves by their osculating circles c_1, c_2 at $\mathbf{b}^{(\pm)}$ with the radii ρ_i. The two

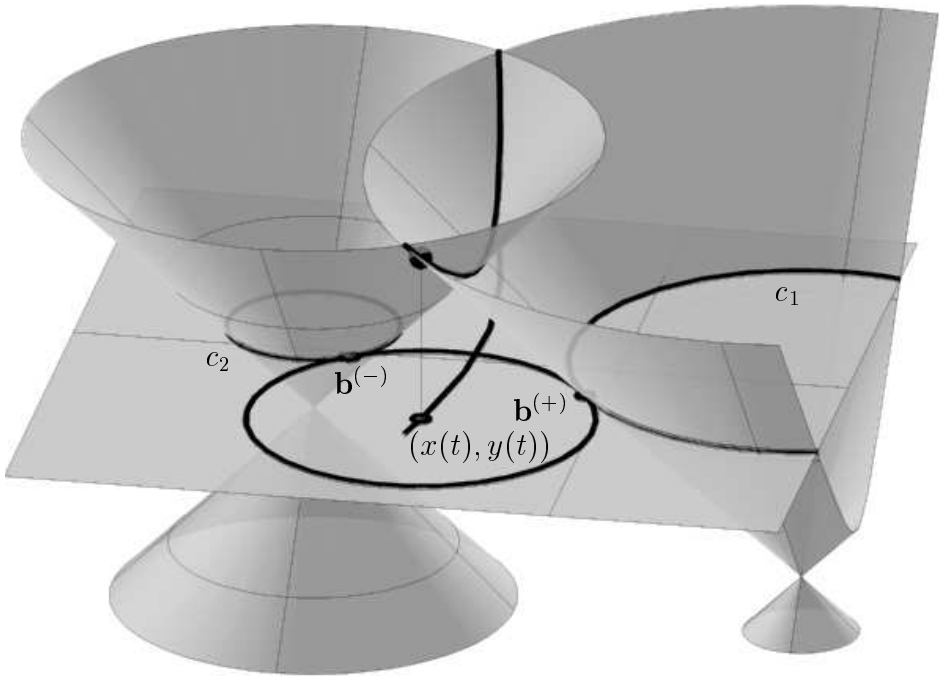

Figure 18: Illustration of the proof of Proposition 3 via intersection of two circular cones. The conic and its projection into the xy plane are shown.

circles define two light cones in $\mathbb{R}^{2,1}$ with apexes at

$$\mathbf{a}_1 = ((r-\rho_1)c, -(r-\rho_1)s, \rho_1)^\top \text{ and } \mathbf{a}_2 = ((r+\rho_2)c, (r+\rho_2)s, -\rho_2)^\top.$$

Each of them has a second order contact with the developable surface of constant slope $\pi/4$ through the corresponding boundary along the generating line through $\mathbf{b}^{(\pm)}$. The developable surfaces of constant slope are the graph surfaces of the oriented distance functions associated with the boundaries.

One branch of the intersection curve of the light cones is a conic section (see Fig. 18), which has a contact of second order with the MAT $(x(t), y(t), r(t))^\top$

at the point $(0,0,r(0))^\top$. It has the quadratic Taylor approximant

$$\mathbf{m}_2(\sigma) = \begin{pmatrix} 0 \\ 0 \\ r \end{pmatrix} + \frac{\sigma}{s} \begin{pmatrix} 1 \\ 0 \\ -c \end{pmatrix} + \frac{\sigma^2}{2}\mathbf{T}'(0) \tag{52}$$

with respect to the Minkowski arc length σ, where

$$\mathbf{T}'(0) = \frac{1}{2(\rho_1 - r)(\rho_2 + r)s^2} \begin{pmatrix} (2r - \rho_1 + \rho_2)c \\ (\rho_1 + \rho_2)s \\ -2r + \rho_1 - \rho_2 \end{pmatrix}. \tag{53}$$

Indeed, the quadratic Taylor approximant $\mathbf{m}_2(\sigma)$ satisfies approximately the equations of the light cones, $\|\mathbf{a}_i - \mathbf{m}_2(\sigma)\|^2 = \mathcal{O}(\sigma^3)$, and it also approximately satisfies the equations of the Minkowski arc length parameterization, $\|\mathbf{m}_2'(\sigma)\|^2 = 1 + \mathcal{O}(\sigma^2)$. Eq. (51) follows directly from (53). □

Corollary 1 *If $\langle \mathbf{T}', \mathbf{T}' \rangle \neq 0$, then $\kappa = \sqrt{|\langle \mathbf{T}', \mathbf{T}' \rangle|}$. Consequently, Minkowski inflections correspond to inflections of at least one of the boundaries, and inflected segments correspond to planar domains where at least one of the boundaries is locally a straight line. Otherwise $\kappa = 0$ or $\kappa = 1$, see Section 2.6.*

2.8 Curves of zero curvature or torsion

Let us take a closer look at curves in Minkowski space with curvature or torsion identically equal to zero. As a direct consequence of the Frenet formulas one can easily verify that a curve $\mathbf{c}(t)$ in Euclidean or Minkowski space has

the curvature identically equal to zero if and only if it is a part of a straight line.

Definition 1 *A curve in* $\mathbb{R}^3$ *or* $\mathbb{R}^{2,1}$ *is called a spatial curve if and only if it does not lie in a plane.*

In the Euclidean space $\mathbb{R}^3$, a curve is a planar curve if and only if its torsion is identically equal to zero. Analogously, we may ask which curves in $\mathbb{R}^{2,1}$ have torsion identically equal to zero.

The answer to this question is not the same as in Euclidean case. In fact, $\tau \equiv 0$ is a necessary – but not sufficient – condition for a curve to be planar in Minkowski space.

Proposition 4 (Walrave, 1995) *A curve* $\mathbf{c}(t) \in \mathbb{R}^{2,1}$ *has vanishing torsion if and only if* $\mathbf{c}(t)$ *is a planar curve or a curve similar to the so–called W–null–cubic*

$$\mathbf{w}(s) = \frac{1}{6\sqrt{2}}(6s - s^3, 3\sqrt{2}s^2, 6s + s^3)^\top. \tag{54}$$

Proof: (Sketch, see Walrave (1995) for details) Consider a curve $\mathbf{c}(s) \in \mathbb{R}^{2,1}$ such that $\tau \equiv 0$, $\kappa \neq 0$. When $\mathbf{c}(s)$ is space–like or time–like, one can easily verify that the third derivative $\mathbf{c}'''(s)$ of $\mathbf{c}(s)$ is a linear combination of $\mathbf{c}'(s)$ and $\mathbf{c}''(s)$, which implies that $\mathbf{c}(s)$ is a planar curve. When $\mathbf{c}(s)$ is light–like, $\tau \equiv 0$ yields $\mathbf{c}(s) = \frac{1}{6\sqrt{2}}(6s - s^3, 3\sqrt{2}s^2, 6s + s^3)^\top$.

Therefore, the only spatial curve in $\mathbb{R}^{2,1}$ (up to Minkowski similarities) with torsion identically equal to zero is the light–like curve (54), which we will refer to as the *W*–null–cubic. Note that $\mathbf{w}(s)$ is parameterized by its pseudo arc length. □

Remark 5 The W–null–cubic is also an MPH curve, since any polynomial light–like curve is an MPH curve.

2.9 Helices in Minkowski space

We start with a brief summary of some basic results from Euclidean space.

A helix in $\mathbb{R}^3$ is a spatial curve for which the tangent includes a constant angle with a fixed line. Any such a line is called the axis of the helix. The well known Lancret's theorem states that a necessary and sufficient condition for a spatial curve to be a helix in $\mathbb{R}^3$ is that the ratio of its curvature to torsion is constant. The proof of this theorem uses Frenet formulas and can be found in many textbooks on differential geometry, e.g. Kreyszig (1991).

In the Euclidean version of the Lancret's theorem the restriction to spatial curves rules out curves with vanishing torsion. However, as shown in Section 2.8, this is generally not the case in Minkowski space.

Definition 2 *A curve* $\mathbf{c}(t) \in \mathbb{R}^{2,1}$ *is called a helix if and only if there exists a constant vector* $\mathbf{v} \neq (0,0,0)^\top$ *such that* $\langle \mathbf{T}(t), \mathbf{v} \rangle$ *is constant, where* $\mathbf{T}(t)$ *is the unit tangent vector of* $\mathbf{c}(t)$*. Any line, which is parallel to the vector* $\mathbf{v}$*, is called the axis of the helix* $\mathbf{c}(t)$*.*

Proposition 5 (Lancret's theorem in $\mathbb{R}^{2,1}$) *A spatial curve* $\mathbf{c}(t) \in \mathbb{R}^{2,1}$ *is a helix if and only if* $\tau = \alpha\kappa$*, where* α *is a real constant and* κ*,* τ *are the Minkowski curvature and torsion of* $\mathbf{c}(t)$*.*

Proof: Recall that $\alpha = 0$ (i.e. $\tau \equiv 0$) corresponds to the W–null–cubic as shown in Proposition 4. From the Frenet formulas for light–like curves

follows that the binormal vector $\mathbf{B}$ of the W–null–cubic is a constant vector and $\langle \mathbf{T}, \mathbf{B} \rangle = 1$. This implies that the W–null–cubic is a helix in $\mathbb{R}^{2,1}$.

Now, let us suppose that $\alpha \neq 0$. As the proof is analogous for all five different cases of curves and corresponding Frenet formulas, we provide the proof of Lancret's theorem for two of the cases only.

Let $\mathbf{c}'(t)$ be space–like and $\mathbf{c}''(t)$ not light–like and let $\mathbf{c}(t)$ be a helix in $\mathbb{R}^{2,1}$. Then there exists a constant vector $\mathbf{v} \neq (0,0,0)^\top$ such that $\langle \mathbf{T}, \mathbf{v} \rangle = \beta$, $\beta \in \mathbb{R}$. By differentiating this equation with respect to t and using Frenet formulas we obtain $\langle \mathbf{N}, \mathbf{v} \rangle = 0$ and thus $\mathbf{v} = a\mathbf{T} + b\mathbf{B}$, where $a, b \in \mathbb{R}$. Again, by differentiating we get $\mathbf{N}(a\kappa + b\tau) = 0$, which gives $\tau = -\frac{a}{b}\kappa$ ($b = 0$ implies that $\mathbf{c}(t)$ is a straight line).

Conversely, let $\tau = \alpha\kappa$. Then we choose the vector $\mathbf{v} = \mathbf{T} - \frac{1}{\alpha}\mathbf{B}$. By differentiating this equation with respect to t one obtains that $\mathbf{v}' = (0,0,0)^\top$, i.e. $\mathbf{v}$ is a constant vector. Moreover, $\langle \mathbf{T}, \mathbf{v} \rangle = \langle \mathbf{T}, \mathbf{T} - \frac{1}{\alpha}\mathbf{B} \rangle = 1$, which proves that $\mathbf{c}(t)$ is a helix in $\mathbb{R}^{2,1}$. □

Remark 6 For the remainder of the thesis we restrict ourselves to space–like and light–like helices only. In order to avoid confusion, we will call these curves SL–helices.

Proposition 6 *Any polynomial SL–helix in Minkowski space is an MPH curve.*

Proof: Let $\mathbf{c}(t)$ be a polynomial light–like helix. Clearly, any polynomial light–like curve is an MPH curve.

Now, let $\mathbf{c}(t)$ be a polynomial space–like helix. Then there exists a constant vector $\mathbf{v}$ such that

$$\langle \mathbf{T}, \mathbf{v} \rangle = \alpha, \tag{55}$$

where α is a real constant. One can easily verify that $\alpha = 0$ leads to a contradiction with $\mathbf{c}(t)$ being a helix, since the torsion of $\mathbf{c}(t)$ would be identically equal to zero (cf. Proposition 4). Therefore $\alpha \neq 0$.

The unit tangent vector of $\mathbf{c}(t)$ can be obtained from $\mathbf{T} = \frac{\mathbf{c}'(t)}{\sqrt{\langle \mathbf{c}'(t), \mathbf{c}'(t) \rangle}}$. By substituting $\mathbf{T}$ in (55) we obtain

$$\frac{\langle \mathbf{c}'(t), \mathbf{v} \rangle}{\alpha} = \sqrt{\langle \mathbf{c}'(t), \mathbf{c}'(t) \rangle}. \tag{56}$$

As the curve $\mathbf{c}(t)$ is a polynomial curve, the left–hand side of (56) is a polynomial. Consequently, the right–hand side of (56) is a polynomial as well and hence $\mathbf{c}(t)$ is an MPH curve. $\square$

3 Minkowski Pythagorean hodograph cubics

The aim of this section is to take a closer look at Minkowski Pythagorean hodograph cubic curves, their properties and classification both in planar and spatial case.

3.1 MPH cubics and cubic helices

In this section we present a correspondence between polynomial helices in Minkowski space and MPH curves.

3.1.1 Space–like MPH cubics

Proposition 7 *The ratio of curvature to torsion of a spatial space–like MPH cubic is constant. Consequently, spatial space–like MPH cubics are helices in* $\mathbb{R}^{2,1}$.

Proof: We will prove the proposition by a direct computation. Let $\mathbf{c}(t) = (x(t), y(t), r(t))^\top \in \mathbb{R}^{2,1}$ be a spatial space–like MPH cubic. Then there exist four linear polynomials (cf. Moon (1999))

$$\begin{aligned} u(t) &= u_0(1-t) + u_1 t,\ v(t) = v_0(1-t) + v_1 t, \\ p(t) &= p_0(1-t) + p_1 t,\ q(t) = q_0(1-t) + q_1 t, \end{aligned} \tag{57}$$

such that

$$\begin{aligned} x'(t) &= u(t)^2 - v(t)^2 - p(t)^2 + q(t)^2, \\ y'(t) &= -2(u(t)v(t) + p(t)q(t)), \\ r'(t) &= 2(u(t)q(t) + v(t)p(t)), \\ \sigma(t) &= u(t)^2 + v(t)^2 - p(t)^2 - q(t)^2. \end{aligned} \tag{58}$$

Since $\mathbf{c}(t)$ is a space–like curve, we may (without loss of generality) assume that $\mathbf{c}'(0) = (1,0,0)^\top$, which implies $u_0 = 0$, $p_0 = 0$ and $q_0^2 - v_0^2 = 1$. Expressing the curve $\mathbf{c}(t)$ in Bézier form and computing the following scalar triple product yield that $\mathbf{c}(s)$ is a planar curve if

$$[\mathbf{c}'(0), \mathbf{c}'(1), \mathbf{c}(1) - \mathbf{c}(0)] = (u_1 - p_1)(u_1 + p_1)(v_1 q_0 - q_1 v_0) = 0. \tag{59}$$

According to Proposition 2, $\mathbf{c}(t)$ has an inflection point if

$$(u_1 - p_1)(u_1 + p_1)\sigma(t) = 0. \tag{60}$$

One can observe from (59) and (60) that $\mathbf{c}(t)$ has an inflection if it has a light–like tangent (or it is a planar curve). Thus spatial space–like MPH cubics have no inflections.

Applying the formulas (40) and (41) to the curve $\mathbf{c}(t)$ gives that the curvature and torsion of $\mathbf{c}(t)$ are given by

$$\kappa(t) = \frac{2\sqrt{|(u_1 - p_1)(u_1 + p_1)|}}{\sigma^2(t)}, \quad \tau(t) = \frac{2(v_1 q_0 - q_1 v_0)}{\sigma^2(t)}. \tag{61}$$

Consequently, the ratio of $\kappa(t)$ to $\tau(t)$ does not depend on t. □

3.1.2 Light–like MPH cubics

Proposition 8 *Any spatial light–like cubic is similar to the W–null–cubic.*

Proof: Let us consider a spatial light–like polynomial curve $\mathbf{c}(t)$ of degree 3. Let $t = t(s)$ be a reparameterization of $\mathbf{c}(t)$ such that $\mathbf{c}(t(s))$ is parameterized by the pseudo arc length and let $\mathbf{T}(s)$, $\mathbf{N}(s)$ and $\mathbf{B}(s)$ be the tangent, normal and binormal vector and $\tau(s)$ the torsion of $\mathbf{c}(t)$. We denote by $\mathbf{c}'$ and $\dot{\mathbf{c}}$ the first derivative of $\mathbf{c}$ with respect to t and s, respectively. For the sake of brevity we omit the dependence on s. Then we have

$$\mathbf{T} = \mathbf{c}'(t)\frac{\mathrm{d}t}{\mathrm{d}s}. \tag{62}$$

Three consecutive differentiations of (62) with respect to s and simplifications using Frenet formulas yield

$$\begin{aligned} \mathbf{N} &= \mathbf{c}''(t)\left(\frac{\mathrm{d}t}{\mathrm{d}s}\right)^2 + \mathbf{c}'(t)\frac{\mathrm{d}^2t}{\mathrm{d}s^2}, \\ \tau\mathbf{T} - \mathbf{B} &= \mathbf{c}'''(t)\left(\frac{\mathrm{d}t}{\mathrm{d}s}\right)^3 + 3\mathbf{c}''(t)\frac{\mathrm{d}t}{\mathrm{d}s}\frac{\mathrm{d}^2t}{\mathrm{d}s^2} + \mathbf{c}'(t)\frac{\mathrm{d}^3t}{\mathrm{d}s^3}, \\ \dot{\tau}\mathbf{c}'(t)\frac{\mathrm{d}t}{\mathrm{d}s} = \dot{\tau}\mathbf{T} &= \mathbf{c}''''(t)\left(\frac{\mathrm{d}t}{\mathrm{d}s}\right)^4 + a_3(s)\mathbf{c}'''(t) + a_2(s)\mathbf{c}''(t) + \mathbf{c}'(t)\frac{\mathrm{d}^4t}{\mathrm{d}s^4}, \end{aligned} \tag{63}$$

where $a_3(s) = \left(\frac{\mathrm{d}t}{\mathrm{d}s}\right)^2 \frac{\mathrm{d}^2t}{\mathrm{d}s^2} = (\dot{t})^2\ddot{t}$ and $a_2(s)$ is a function of s.

Let us consider the scalar triple product $[\mathbf{T}, \mathbf{N}, \tau\mathbf{T} - \mathbf{B}]$. Using (62) and (63) one obtains

$$[\mathbf{T}, \mathbf{N}, \tau\mathbf{T} - \mathbf{B}] = [\mathbf{T}, \mathbf{N}, -\mathbf{B}] = [\mathbf{c}'(t), \mathbf{c}''(t), \mathbf{c}'''(t)]\left(\frac{\mathrm{d}t}{\mathrm{d}s}\right)^6. \tag{64}$$

Since the vectors $\mathbf{T}(s)$, $\mathbf{N}(s)$ and $\mathbf{B}(s)$ are linearly independent, the vectors $\mathbf{c}'(t)$, $\mathbf{c}''(t)$ and $\mathbf{c}'''(t)$ are linearly independent as well. Consequently, by comparing coefficients and due to the fact that $\mathbf{c}''''(t) = (0, 0, 0)^\top$, the third equation of (63) implies

$$a_3(s) = 0, \quad a_2(s) = 0, \quad \dot{\tau}\frac{\mathrm{d}t}{\mathrm{d}s} = \frac{\mathrm{d}^4t}{\mathrm{d}s^4}. \tag{65}$$

From $a_3(s) = 0$ one may conclude that $t = \alpha s + \beta$ and therefore the last equation of (65) implies that τ is constant.

Finally, we express the binormal vector $\mathbf{B}$ using the second equation of (63):

$$\begin{aligned} \mathbf{B} &= \tau\mathbf{T} - \alpha^3\mathbf{c}'''(t), \\ \dot{\mathbf{B}} &= \dot{\tau}\mathbf{T} + \tau\dot{\mathbf{T}} - \alpha^4\mathbf{c}''''(t) = \tau\mathbf{N}. \end{aligned} \tag{66}$$

On the other hand, from the Frenet formulas we have that $\dot{\mathbf{B}} = -\tau\mathbf{N}$. Therefore, the torsion τ is identically equal to zero. Proposition 4 concludes the proof. □

3.1.3 Summary

In this section we will summarize the previously obtained results (see the scheme in Fig. 19).

Theorem 1 *A spatial curve in Minkowski space is an MPH cubic if and only if it is a space-like or light–like cubic helix.*

Proof: From Propositions 7 and 8 follows that any spatial MPH cubic satisfies the assumptions of the Lancret's theorem 5 and therefore any such curve is a helix in Minkowski space. On the other hand, we have proved (cf. Proposition 6) that any polynomial SL–helix is an MPH curve. □

3.2 Classification of planar MPH cubics

In order to prepare the discussion of spatial helices, we present a classification of planar MPH cubics.

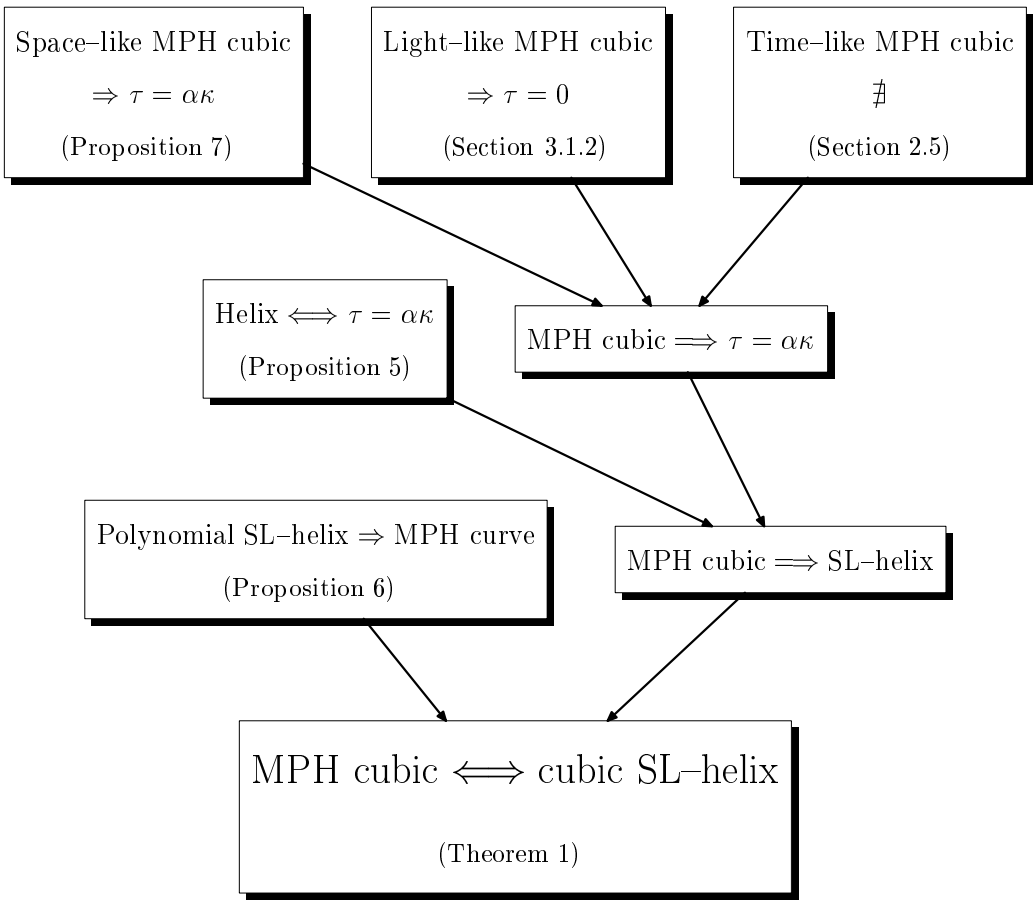

Figure 19: Summary of obtained results concerning spatial MPH cubics.

3.2.1 MPH cubics in space–like and light–like planes

A thorough discussion of planar MPH cubics in space–like planes was given in Farouki & Sakkalis (1990), as these curves are in fact planar PH cubics. It turns out that any planar PH cubic (which is not a straight line) is similar to the so–called Tschirnhausen cubic (see Fig. 20) given by $\mathbf{T}(t) = (3t^2, t-3t^3)^\top$.

Let us consider a polynomial planar curve $\mathbf{c}(t) = (x(t), y(t))^\top$. The MPH condition in a light–like plane degenerates to $x'^2(t) = \sigma^2(t)$ and hence any polynomial curve in a light–like plane is an MPH curve. Therefore the only case remaining to consider is the case of a time–like plane.

3.2.2 MPH cubics in time–like planes

An MPH curve $\mathbf{c}(t) = (x(t), y(t))^\top$ lying in a time–like plane is nothing else but a curve in Minkowski plane $\mathbb{R}^{1,1}$ whose hodograph satisfies $x'^2(t) - y'^2(t) = \sigma^2(t)$, where $\sigma(t)$ is a polynomial in t.

Proposition 9 *Any MPH cubic in Minkowski plane $\mathbb{R}^{1,1}$ with exactly one point with a light–like tangent is similar (in Minkowski sense) to the curve $\mathbf{q}_1(t) = (t^3 + 3t, t^3 - 3t)^\top$ (see Fig. 21).*

Any MPH cubic in Minkowski plane $\mathbb{R}^{1,1}$ with exactly two different points with light–like tangents is similar (in Minkowski sense) to the curve $\mathbf{q}_2(t) = (t^3 + 3t, 3t^2)^\top$ (see Fig. 22).

There are no MPH cubics in $\mathbb{R}^{1,1}$ except for the curves $\mathbf{q}_1(t)$, $\mathbf{q}_2(t)$ and straight lines.

Proof: Let us suppose that $\mathbf{c}(t) = (x(t), y(t))^\top$ is an MPH cubic in $\mathbb{R}^{1,1}$. Then there exist two linear polynomials $u(t) = u_0(1-t) + u_1 t$, $v(t) = v_0(1-$

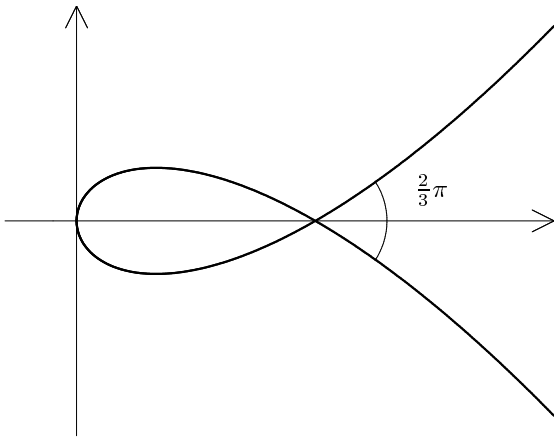

Figure 20: The Tschirnhausen cubic.

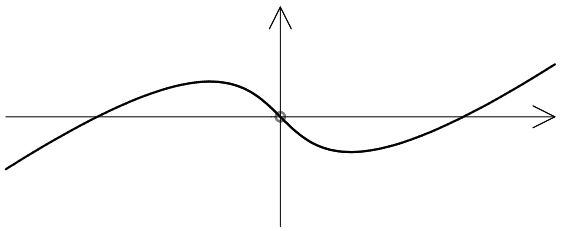

Figure 21: MPH cubic in $\mathbb{R}^{1,1}$ with exactly one point with a light–like tangent (marked by the grey circle).

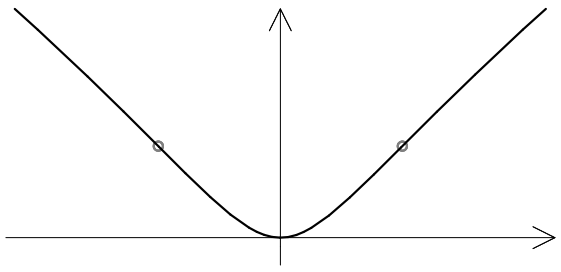

Figure 22: MPH cubic in $\mathbb{R}^{1,1}$ with exactly two different points with light–like tangents (marked by the grey circles).

$t) + v_1 t$ (cf. Kubota (1972)) such that

$$\begin{aligned} x'(t) &= u^2(t) + v^2(t), \\ y'(t) &= 2u(t)v(t), \\ \sigma(t) &= u^2(t) - v^2(t), \end{aligned} \tag{67}$$

where σ is the parametric speed

$$\begin{aligned} &\sigma = (at - u_0 - v_0)(bt - u_0 + v_0), \text{ where} \\ &a = u_0 - u_1 + v_0 - v_1,\ b = u_0 - u_1 - v_0 + v_1. \end{aligned} \tag{68}$$

Depending on the number of light–like tangents of $\mathbf{c}(t)$ we will distinguish the following four cases.

Case 1: The curve $\mathbf{c}(t)$ has infinitely many light–like tangents. This case occurs when $\sigma(t) \equiv 0$, which implies that $\mathbf{c}(t)$ is a part of a light–like straight line.

Case 2: The curve $\mathbf{c}(t)$ has no light–like tangents. This means that $\sigma(t)$ has no roots, i.e. $a = 0$ and $b = 0$ (see 68). One can easily verify that $\mathbf{c}(t)$ is a part of a straight line.

Case 3: The curve $\mathbf{c}(t)$ has exactly one light–like tangent. The limit case, when the two roots of σ degenerate into one, gives again straight lines only. Let us (without loss of generality) suppose that $a \neq 0$ and $b = 0$. Then $\mathbf{c}(t)$ has the light–like tangent corresponding to $t_0 = \frac{u_0+v_0}{a}$. We may assume that $t_0 = 0$ (otherwise we would reparameterize $\mathbf{c}(t)$) and therefore $u_0 + v_0 = 0$. A simple calculation reveals that

$$\mathbf{c}(t) = (\alpha t^3 + \beta t, \alpha t^3 - \beta t)^\top;\ \alpha = \frac{2}{3}(u_0 + v_1)^2,\ \beta = 2u_0^2. \tag{69}$$

By a reparameterization $t = t\sqrt{\frac{\beta}{3\alpha}}$ of $\mathbf{c}(t)$ given in (69) (the equality $\alpha = 0$ yields a straight line) and a scaling by factor $\sqrt{\frac{27\alpha}{\beta^3}}$ we obtain the curve $\mathbf{q}_1(t)$.

Case 4: The curve $\mathbf{c}(t)$ has exactly two different light–like tangents corresponding to $t_1 = \frac{u_0+v_0}{a}$ and $t_2 = \frac{v_0-u_0}{b}$, $a \neq 0$, $b \neq 0$ and $t_1 \neq t_2$. Let us consider the following transformation of the curve $\mathbf{c}(t) = (x(t), y(t))^\top$ consisting of a reparameterization $t = t + \delta$, a scaling by factor λ, a hyperbolic rotation with a hyperbolic angle φ and a translation given by the vector $(\varrho_1, \varrho_2)^\top$:

$$\mathbf{p}(t) = \lambda \begin{pmatrix} \cosh\varphi & \sinh\varphi \\ \sinh\varphi & \cosh\varphi \end{pmatrix} \mathbf{c}(t+\delta) + \begin{pmatrix} \varrho_1 \\ \varrho_2 \end{pmatrix}. \tag{70}$$

A straightforward but long computation gives that for the values

$$\varphi = \frac{1}{2}\ln\frac{b^2}{a^2},\ \delta = \frac{u_0^2 - u_0u_1 + v_0v_1 - v_0^2}{ab},\ \lambda = 3a^2\sqrt{\frac{b^2}{a^2}} \tag{71}$$

and ϱ_1, ϱ_2 such that $\mathbf{p}(0) = (0,0)^\top$, the curve becomes

$$\mathbf{p}(t) = (a^2b^2t^3 + 3c^2t, 3abct^2)^\top;\ c = u_1v_0 - v_1u_0. \tag{72}$$

A reparameterization $t = t\sqrt{\frac{c^2}{a^2b^2}}$ of $\mathbf{p}(t)$ given in (72) and a scaling by factor $\frac{1}{c^2}\sqrt{\frac{a^2b^2}{c^2}}$ gives the curve $\mathbf{q}_2(t)$. The equality $c = 0$ obviously leads to a straight line. □

3.3 Classification of spatial space–like MPH cubics

The following classification of spatial space–like MPH cubics is based on the notion of tangent indicatrix, the curve on the unit hyperboloid describing the variation of the unit tangent vector, cf. Fig. 23.

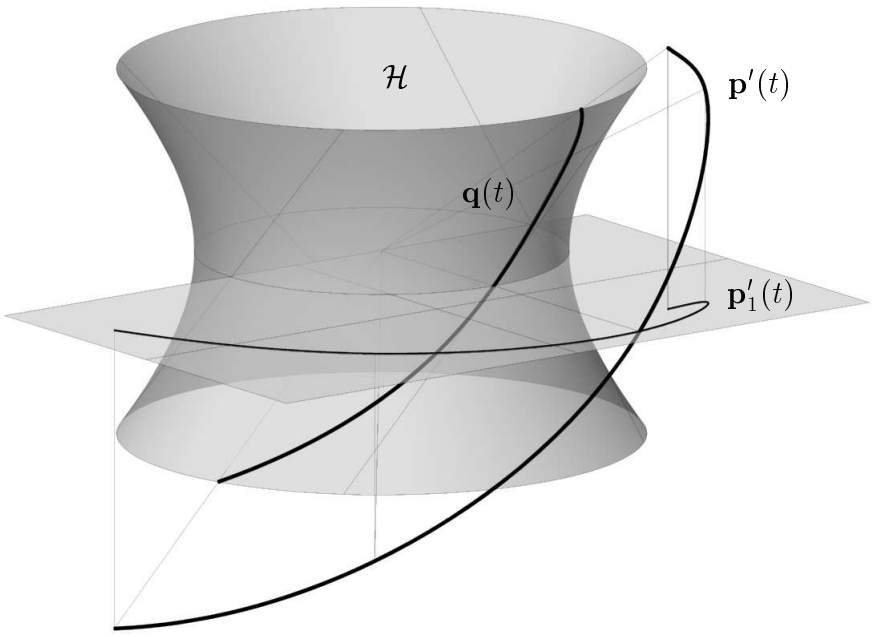

Figure 23: Hodograph $\mathbf{p}'(t)$ of a space–like curve $\mathbf{p}(t)$ along with its projection $\mathbf{p}_1'(t)$ to the xy plane and the corresponding tangent indicatrix $\mathbf{q}(t) = \frac{\mathbf{p}'(t)}{||\mathbf{p}'(t)||}$ lying on the unit hyperboloid $\mathcal{H}$.

3.3.1 Orthogonal projections into planes perpendicular to the axis

Let $\mathbf{c}(t)$ be a space–like MPH cubic with curvature $\kappa \neq 0$ and torsion $\tau \neq 0$ and let $\mathbf{T}$ and $\mathbf{B}$ be the unit tangent and binormal vector of $\mathbf{c}(t)$. From the proof of Lancret's theorem (cf. Proposition 5) follows that the direction of the axis of $\mathbf{c}(t)$ (considered as a helix in $\mathbb{R}^{2,1}$) is given by the vector $\mathbf{v} = \mathbf{T} - \frac{\kappa}{\tau}\mathbf{B}$.

One can easily verify that $\langle \mathbf{T}, \mathbf{v} \rangle = 1$ and $||\mathbf{v}||^2 = 1 + \frac{\kappa^2}{\tau^2}||\mathbf{B}||^2$. Therefore, when $\mathbf{B}$ is space–like, the vector $\mathbf{v}$ is space–like as well. In the case when $\mathbf{B}$ is time–like, the causal character of $\mathbf{v}$ may be arbitrary, e.g. the axis of $\mathbf{c}(t)$

is light–like if and only if $||\mathbf{B}||^2 = -1$ and $\tau = \pm\kappa$.

In Euclidean space one can use the following approach for constructing spatial PH cubics (cubic helices). It is obvious that an orthogonal projection of a PH cubic to a plane perpendicular to its axis is a planar PH cubic (since the length of the tangent vector of the projection is a constant multiple of the length of the tangent vector of the original curve), i.e. the Tschirnhausen cubic. Therefore all PH cubics can be obtained as helices "above" the Tschirnhausen cubic by choosing its slope (or equivalently the constant ratio of its curvature to torsion), see Fig. 24. Consequently, there exists only one spatial PH cubic up to orthogonal transforms and 1D scalings in $\mathbb{R}^3$, see Farouki and Sakkalis (1994). Unfortunately, in Minkowski space, this approach does not include the case of light–like axes.

Remark 7 Let $\mathbf{c}(t) = (x(t), y(t), r(t))^\top$ be a spatial space–like MPH cubic whose axis is space–like. We can suppose without loss of generality that its axis is the y axis. Then its hodograph satisfies $x'^2(t) + y'^2(t) - r'^2(t) = \sigma^2(t)$ for some polynomial $\sigma(t)$ and the orthogonal projection of $\mathbf{c}(t)$ to the xr plane is the curve $\mathbf{c}_0(t) = (x(t), 0, r(t))^\top$. As

$$|\sigma(t)| = \sqrt{x'^2(t) + y'^2(t) - r'^2(t)} = \lambda\sqrt{|x'^2(t) - r'^2(t)|} \tag{73}$$

for some constant $\lambda \neq 0$, there exists a polynomial $\sigma_0(t)$ such that $x'^2(t) - r'^2(t) = \pm\sigma_0^2(t)$. Therefore, the orthogonal projection of a spatial space–like MPH cubic in the direction of its axis is either a planar MPH cubic or a planar *time–like* MPH cubic satisfying $x'^2(t) - r'^2(t) = -\sigma_0^2(t)$. The notion of time–like MPH curve can be generalized to space, however, there is no application for it so far. In the planar case, one can think of time–like MPH curves as of space–like MPH curves, but with swapped space and time axis. Consequently, for the remainder of the thesis we include planar time–like MPH curves into planar MPH curves, as no confusion is likely to arise.

In the case of a time–like axis (the r axis) of a spatial space–like MPH cubic

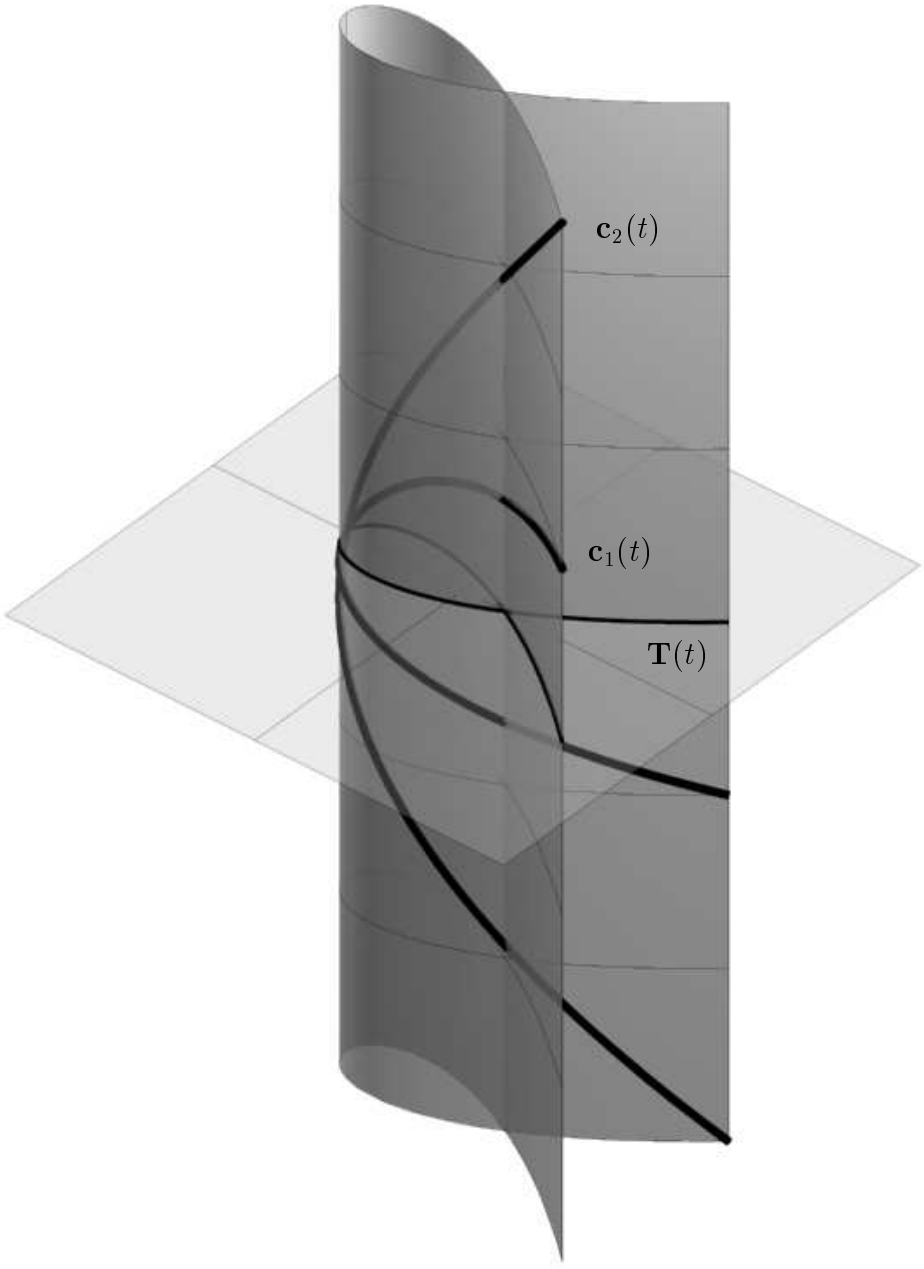

Figure 24: Two PH cubics $\mathbf{c}_1(t)$ and $\mathbf{c}_2(t)$ "above" the Tschirnhausen cubic $\mathbf{T}(t)$.

the orthogonal projection in the direction of its axis is a planar PH cubic, i.e. the Tschirnhausen cubic.

3.3.2 Characterization of MPH curves by their tangent indicatrix

As observed by Farouki and Han (2005), the tangent indicatrix uniquely determines PH curves. Namely, if two PH curves in $\mathbb{R}^3$ have hodographs with relatively prime components and posses the same tangent indicatrix, they differ by a Euclidean similarity. It follows that any rational curve on the unit sphere

$$\mathbf{c}(t) = (a(t), b(t), c(t))^\top, \quad \gcd\{a(t), b(t), c(t)\} = \text{const.} \tag{74}$$

uniquely determines (up to similarities) a PH curve. Now, we reformulate these results for the Minkowski case.

Proposition 10 *Let $\mathbf{p}(t)$, $\tilde{\mathbf{p}}(t)$ be space–like MPH curves of degree d with possibly up to $d-1$ points with light–like tangents whose hodographs have relatively prime components. If $\mathbf{p}(t)$ and $\tilde{\mathbf{p}}(t)$ share the same tangent indicatrix, then they are similar (in Minkowski sense).*

Proof: Let $\mathbf{p}(t) = (x(t), y(t), r(t))^\top$, $\tilde{\mathbf{p}}(t) = (\tilde{x}(t), \tilde{y}(t), \tilde{r}(t))^\top$ be space–like MPH curves and let $x'^2(t)+y'^2(t)-r'^2(t) = \sigma(t)^2$, $\tilde{x}'^2(t)+\tilde{y}'^2(t)-\tilde{r}'^2(t) = \tilde{\sigma}(t)^2$ for some polynomials $\sigma(t) \not\equiv 0$, $\tilde{\sigma}(t) \not\equiv 0$. As $\deg(\mathbf{p}(t)) = \deg(\tilde{\mathbf{p}}(t)) = d$, $\deg(\sigma(t)) = \deg(\tilde{\sigma}(t)) = d-1$ and light–like tangents of $\mathbf{p}(t)$, $\tilde{\mathbf{p}}(t)$ correspond to roots of $\sigma(t)$, $\tilde{\sigma}(t)$, respectively.

We can assume that

$$\begin{aligned} \sigma(t) &= (t-\alpha_1)^{k_1}(t-\alpha_2)^{k_2}\cdots(t-\alpha_m)^{k_m}\varepsilon(t), \\ \tilde{\sigma}(t) &= (t-\tilde{\alpha}_1)^{l_1}(t-\tilde{\alpha}_2)^{l_2}\cdots(t-\tilde{\alpha}_n)^{l_n}\tilde{\varepsilon}(t), \end{aligned} \tag{75}$$

where $\varepsilon(t) \neq 0$, $\tilde{\varepsilon}(t) \neq 0$ are polynomials such that $\deg(\varepsilon(t)) + \sum_{c=1}^{m} k_c = d-1$, $\deg(\tilde{\varepsilon}(t)) + \sum_{c=1}^{n} l_c = d-1$, and α_i, α_j are all real roots of $\sigma(t)$, $\tilde{\sigma}(t)$, respectively.

Since the curves $\mathbf{p}(t)$, $\tilde{\mathbf{p}}(t)$ have the same tangent indicatrix $\mathbf{p}'(t)/\sigma(t) = \tilde{\mathbf{p}}'(t)/\tilde{\sigma}(t)$, we obtain

$$\begin{aligned} x'(t)(t-\alpha_1)^{k_1}\cdots(t-\alpha_m)^{k_m}\varepsilon(t) &= \tilde{x}'(t)(t-\tilde{\alpha}_1)^{l_1}\cdots(t-\tilde{\alpha}_n)^{l_n}\tilde{\varepsilon}(t), \\ y'(t)(t-\alpha_1)^{k_1}\cdots(t-\alpha_m)^{k_m}\varepsilon(t) &= \tilde{y}'(t)(t-\tilde{\alpha}_1)^{l_1}\cdots(t-\tilde{\alpha}_n)^{l_n}\tilde{\varepsilon}(t), \\ r'(t)(t-\alpha_1)^{k_1}\cdots(t-\alpha_m)^{k_m}\varepsilon(t) &= \tilde{r}'(t)(t-\tilde{\alpha}_1)^{l_1}\cdots(t-\tilde{\alpha}_n)^{l_n}\tilde{\varepsilon}(t). \end{aligned} \tag{76}$$

As $x'(t)$, $y'(t)$, $r'(t)$ and $\tilde{x}'(t)$, $\tilde{y}'(t)$, $\tilde{r}'(t)$ are relatively prime polynomials and $\tilde{\varepsilon}(t)$, $\varepsilon(t)$ have no real roots, it follows that (after a suitable rearrangement) $n = m$, $k_c = l_c$ and $\alpha_c = \tilde{\alpha}_c$ for $c = 1 \ldots n$. Moreover, $\varepsilon(t)$ and $\tilde{\varepsilon}(t)$ have to divide each other and therefore $\varepsilon(t) = \gamma\tilde{\varepsilon}(t)$ for some scalar factor $\gamma \neq 0$. □

Corollary 2 *Let* $\mathbf{q}(t) = (a(t), b(t), c(t))^{\top}/\sigma(t)$ *be a rational curve on the unit hyperboloid and* $gcd\{a(t), b(t), c(t)\} = const$. *Then there exists a unique (up to Minkowski similarities) MPH curve, whose tangent indicatrix is* $\mathbf{q}(t)$.

Proof: As $\mathbf{p}(t)$ lies on the unit hyperboloid, we have $a^2(t) + b^2(t) - c^2(t) = \sigma^2(t)$. The curve

$$\mathbf{p}(t) = \gamma \int \mathbf{q}(t)\sigma(t)\,\mathrm{d}t + \mathbf{p}_0, \tag{77}$$

where $\gamma \neq 0$ is a scalar factor and $\mathbf{p}_0$ represents a translation, has the desired tangent indicatrix. The proof then follows from Proposition 10. □

3.3.3 Classification and normal forms

In particular, the results concerning the tangent indicatrices apply to space–like MPH cubics (with up to two points with light–like tangents). However,

π	Condition	Hyperbolic angle	Canonical position	Conic section (Euclid. classif.)
sl.	$k < -l$	$\frac{1}{2}\ln(-\frac{k+l}{k-l})$	π_s: $r = r_0$	'circle'
tl.	$k > -l, k^2 - l^2 \neq k^2$	$\frac{1}{2}\ln(\frac{k+l}{k-l})$	π_t: $y = y_0 \neq \pm 1$	'hyperbola'
	$k > -l, k^2 - l^2 = k^2$	$\frac{1}{2}\ln(\frac{k+l}{k-l})$	$\tilde{\pi}_t$: $y = \pm 1$	2 int. lines
ll.	$k = -l, m \neq 0$	$\ln \frac{m}{k}$	π_l: $y - r + 1 = 0$	'parabola'
	$k = -l, m = 0$	0	$\tilde{\pi}_l$: $y - r = 0$	2 par. lines

Table 2: Canonical positions of a plane π, see Figure 25. The abbreviations sl., tl., and ll. stand for space–, time– and light–like, respectively.

in this special case of MPH curves of degree 3, more can be achieved. As (space–like) MPH cubics are curves of a constant slope (see Proposition 5), their tangent indicatrix is a planar (conic) section of the unit hyperboloid.

Lemma 1 *Any plane π can be mapped using Lorentz transforms to one of the canonical positions shown in Table 2.*

Proof: Let us consider a plane π given by $ky + lr + m = 0$, $k \geq 0$, $l \leq 0$, $(k, l) \neq (0, 0)$, $m > 0$ (otherwise we rotate it about the time–axis and/or mirror it with respect to the xy plane). Depending on its causal character we transform π using hyperbolic rotations introduced in Table 2, cf. Figure 25. □

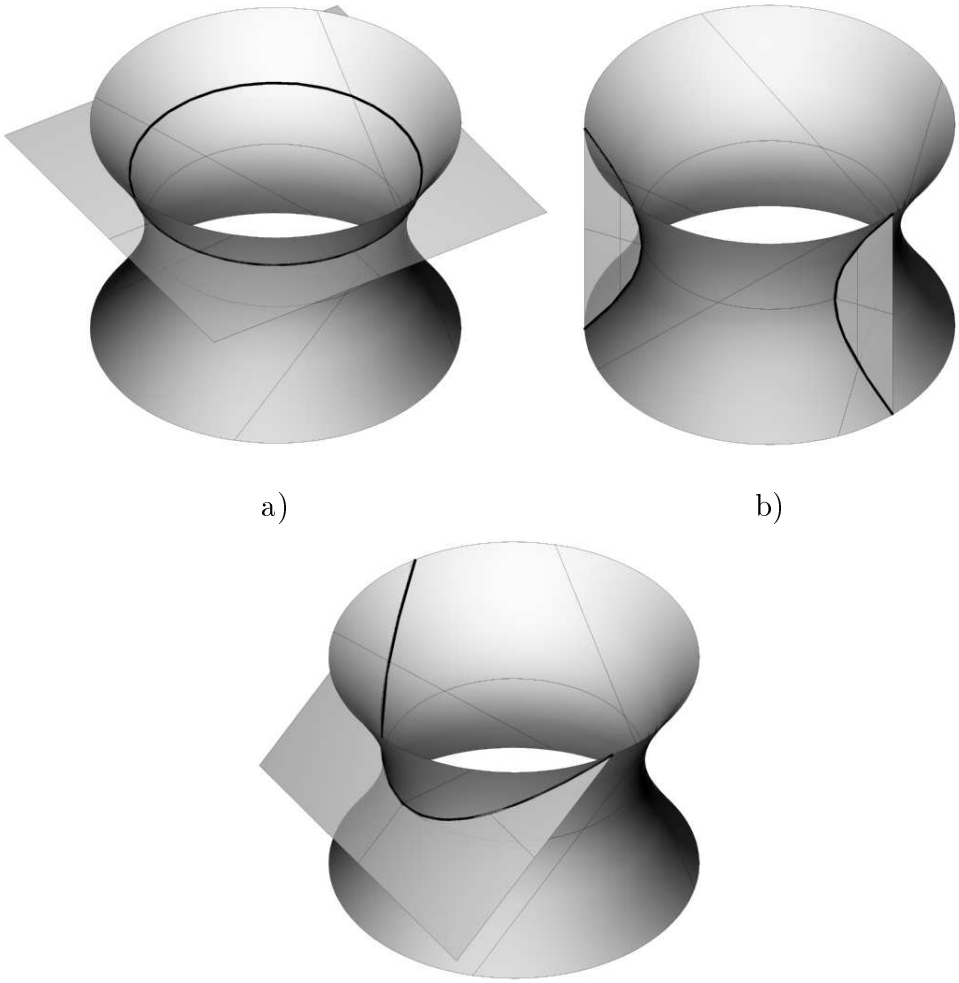

a) b)

c)

Figure 25: The unit hyperboloid $\mathcal{H}$, canonical positions of a plane π and corresponding conic sections (Euclidean classification): a) space–like plane π_s and a 'circle' $\mathcal{K}_s$ b) time–like plane π_t and a 'hyperbola' $\mathcal{K}_t$ c) light–like plane π_l and a 'parabola' $\mathcal{K}_l$.

Theorem 2 *Any spatial space–like MPH cubic is similar (in Minkowski sense) to one of the curves listed in Table 3.*

Proof: We distinguish two cases depending on whether the axis of the MPH cubic is light–like or not.

Case 1: Let $\mathbf{p}(t)$ be a spatial space–like MPH cubic whose axis is not light–like. Its orthogonal projection in the direction of its axis is a planar MPH cubic (cf. Remark 7). Now, we make use of the classification of planar MPH cubics described in Section 3.2. As the construction of $\mathbf{p}(t)$ is analogous in the case of space–like and time–like axis, we present the computation for MPH cubics "above" the Tschirnhausen cubic $\mathbf{T}(t) = (3t^2, t - 3t^3)^\top$ only.

Let $\mathbf{p}(t) = (3t^2, t - 3t^3, r(t))^\top$, where $r(t) = at^3 + bt^2 + ct$. Then we have $\mathbf{p}'(t) = (6t, 1 - 9t^2, 3at^2 + 2bt + c)^\top$ and

$$||\mathbf{p}'(t)||^2 = (\alpha t^2 + \beta t + \gamma)^2 \tag{78}$$

must hold for some constants α, β and γ. Comparing the coefficients in (78) gives the following system of equations:

$$\begin{aligned} \alpha^2 + 9a^2 - 81 &= 0, \\ \alpha\beta + 6ab &= 0, \\ \beta^2 + 2\alpha\gamma + 4b^2 + 6ac - 18 &= 0, \\ \beta\gamma + 2bc &= 0, \\ \gamma^2 + c^2 - 1 &= 0. \end{aligned} \tag{79}$$

All solutions of the form (a, b, c) of (79) are found to be $(-3\lambda, 3\sqrt{1-\lambda^2}, \lambda)$ and $(3\lambda, 0, \lambda)$, $|\lambda| < 1$. However, as the first family of solutions gives only planar cubics, the only spatial space–like MPH cubics with time–like axis are

Axis	Canonical position	1D scaling factor	κ, τ
Space–like	$(t^3+3t, \lambda(t^3-3t), 3t^2)^\top$	$\lambda \neq 0$	$\tau = -\lambda\kappa$
	$(3t^2, \lambda(t^3-3t), t^3+3t)^\top$	$\lvert\lambda\rvert > 1$	$\tau = -\lambda\kappa$
Time–like	$(3t^2, t-3t^3, \lambda(3t^3+t))^\top$	$\lvert\lambda\rvert < 1,\ \lambda \neq 0$	$\tau = \lambda\kappa$
Light–like	$\frac{1}{6}(3t^2, t^3-6t, t^3)^\top$		$\kappa = -\tau = 1$
	$(3t^2, t^3-6t, 6t)^\top$		$\tau = -\kappa$

Table 3: Canonical positions of spatial space–like MPH cubics.

given by

$$\mathbf{p}(t) = (3t^2, t-3t^3, \lambda(3t^3+t))^\top, \quad |\lambda| < 1, \quad \lambda \neq 0. \tag{80}$$

Note that there exists only one spatial space–like MPH cubic with time–like axis up to Minkowski similarities and 1D scalings given by the factor λ. For $\lambda = 0$ one obviously obtains a planar MPH cubic and the limit cases $\lambda = \pm 1$ give the W–null–cubic. All spatial space–like MPH cubics with space–like axes can be found analogously with the help of the planar MPH cubics presented in Proposition 9.

Case 2: On the other hand, let $\mathbf{q}(t)$ be a spatial space–like MPH cubic whose axis is light–like. As the above construction (based on Remark 7) cannot be used in this case, we turn our attention to the tangent indicatrix $\mathbf{r}(t)$ of $\mathbf{q}(t)$. Since $\mathbf{r}(t)$ lies in a light–like plane, according to Lemma 1 we consider the plane π_l: $y - r + 1 = 0$, cf. Table 2, Fig. 25c. The 'parabola' $\mathcal{K}_l = \pi_l \cap \mathcal{H}$ has the equation $\mathbf{r}(t) = (t, \frac{t^2}{2} - 1, t^2)^\top$ and the corresponding MPH cubic (scaled by 6) is given by $\mathbf{q}(t) = (3t^2, t^3 - 6t, t^3)^\top$. All other rational biquadratic parameterizations of the 'parabola' $\mathcal{K}_l$ are given by the reparameterizations

$t = (a\tau + b)/(c\tau + d)$, $ad - bc \neq 0$ (refer to Farin (1987)) of $\mathbf{r}(t)$:

$$\tilde{\mathbf{r}}(\tau) = \left(\frac{a\tau + b}{c\tau + d}, \frac{(a\tau + b)^2 - 2(c\tau + d)^2}{2(c\tau + d)^2}, \frac{(a\tau + b)^2}{2(c\tau + d)^2} \right)^\top . \tag{81}$$

The MPH cubic (again scaled by 6) corresponding to $\mathbf{r}(\tau)$ is then given by

$$\tilde{\mathbf{q}}(\tau) = \begin{pmatrix} \tau(2ca\tau^2 + 3\tau da + 3\tau cb + 6db) \\ \tau(a^2\tau^2 + 3a\tau b + 3b^2 - 2c^2\tau^2 - 6c\tau d - 6d^2) \\ \frac{1}{a}(a\tau + b)^3 \end{pmatrix}^\top . \tag{82}$$

A straightforward computation shows that for $c \neq 0$ we have

$$\frac{4c^4}{(bc - ad)^3} L\tilde{\mathbf{q}} \left(\frac{ad - bc}{2c^2} t - \frac{d}{c} \right) + (\tau_1, \tau_2, \tau_3)^\top = (3t^2, t^3 - 6t, 6t)^\top, \tag{83}$$

where L is the Lorentz transform

$$L = \frac{1}{2c^2} \begin{pmatrix} 2c^2 & 2ca & -2ca \\ -2ca & 2c^2 - a^2 & a^2 \\ 2ca & a^2 & -2c^2 - a^2 \end{pmatrix} \tag{84}$$

and $(\tau_1, \tau_2, \tau_3)^\top$ is a translation vector computed from $\mathbf{q}(0) = (0, 0, 0)^\top$. When $c = 0$ one obtains that

$$\frac{a}{d^3} \mathbf{q} \left(\frac{d}{a} t - \frac{b}{a} \right) + (\tilde{\tau}_1, \tilde{\tau}_2, \tilde{\tau}_3)^\top = (3t^2, t^3 - 6t, t^3)^\top. \tag{85}$$

The results are summarized in Table 3. The ratios of curvature to torsion of the spatial space–like MPH cubics are also shown. □

3.4 Spatial light–like MPH cubics: The W–null–cubic

We have already shown that the only spatial light–like MPH cubic is the W–null–cubic $\mathbf{w}(t) = (3t^2, t - 3t^3, t + 3t^3)^\top$, compare with (1) and (54).

According to Wunderlich (1973), it is the normal form of the only cubic helix (for constant slope $\alpha = \pi/4$) in Euclidean space. Moreover, as shown by Wagner and Ravani (1997), it is also the only so–called cubic RF curve, i.e. a polynomial cubic with rational Frenet–Serret motion (of degree 5).

The orthogonal projections of the W–null–cubic into the xy, yr and xr planes are again PH or (time–like) MPH curves (see Fig. 26). The projections are similar to the Tschirnhausen cubic $\mathbf{T}(t) \in \mathbb{R}^2$ (see Section 3.2, Fig. 20), to the curve with one light–like tangent $\mathbf{q}_1(t) \in \mathbb{R}^{1,1}$ (cf. Proposition 9, Fig. 21) and to the curve with two light–like tangents $\mathbf{q}_2(t) \in \mathbb{R}^{1,1}$ (cf. Proposition 9, Fig. 22), respectively.

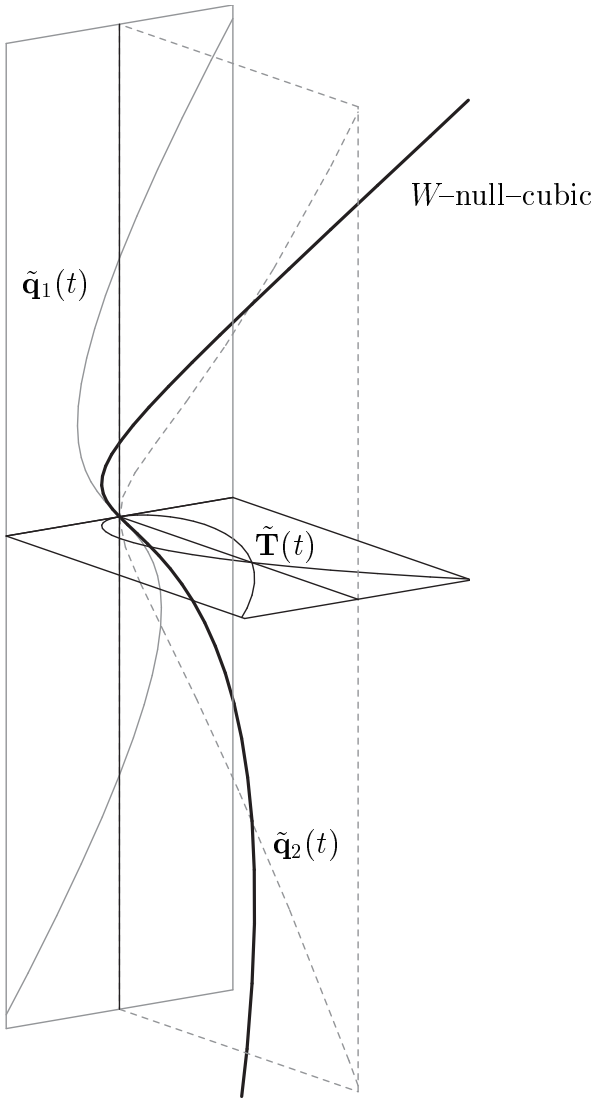

Figure 26: The W–null–cubic and its projections to coordinate planes.

4 Interpolation of G^1 Hermite boundary data

Consider an MPH cubic in Bézier form

$$\mathbf{g}(t) = \mathbf{p}_0\,(1-t)^3 + \mathbf{p}_1\,3t(1-t)^2 + \mathbf{p}_2\,3t^2(1-t) + \mathbf{p}_3\,t^3,\ t \in [0,1], \quad (86)$$

which is to interpolate the two given points $\mathbf{q}_0 = \mathbf{p}_0$ and $\mathbf{q}_1 = \mathbf{p}_3$, and the associated space-like unit tangent directions $\mathbf{t}_0$ and $\mathbf{t}_1$, see Fig. 27. More precisely, we have to find constants a and b such that the inner control points satisfy

$$\mathbf{p}_1 = \mathbf{p}_0 + a\mathbf{t}_0, \text{ and } \mathbf{p}_2 = \mathbf{p}_3 - b\mathbf{t}_1, \quad (87)$$

and the cubic is MPH. Since the degree of the hodograph $\mathbf{g}'(t)$ is two, this implies that there exists a quadratic polynomial

$$\sigma(t) = \sigma_0\,(1-t)^2 + \sigma_1\,2t(1-t) + \sigma_2\,t^2 \quad (88)$$

such that $||\mathbf{g}'(t)||^2 = 9\sigma(t)^2$. Let

$$\mathbf{l}_0 = a\mathbf{t}_0,\ \mathbf{l}_1 = (\mathbf{p}_3 - \mathbf{p}_0) - a\mathbf{t}_0 - b\mathbf{t}_1,\ \mathbf{l}_2 = b\mathbf{t}_1, \quad (89)$$

be the legs of the control polygon of the cubic. The MPH condition leads to the five equations (cf. Choi et al., 1999)

$$\sigma_0^2 = \langle \mathbf{l}_0, \mathbf{l}_0 \rangle, \qquad \sigma_2^2 = \langle \mathbf{l}_2, \mathbf{l}_2 \rangle, \quad (90)$$

$$\sigma_0\sigma_1 = \langle \mathbf{l}_0, \mathbf{l}_1 \rangle, \qquad \sigma_1\sigma_2 = \langle \mathbf{l}_1, \mathbf{l}_2 \rangle \quad \text{and} \quad (91)$$

$$\sigma_0\sigma_2 + 2\sigma_1^2 = \langle \mathbf{l}_0, \mathbf{l}_2 \rangle + 2\langle \mathbf{l}_1, \mathbf{l}_1 \rangle. \quad (92)$$

The first two equations (90) are equivalent to $\sigma_0 = \pm a$ and $\sigma_2 = \pm b$. As $\sigma(t)$ and $-\sigma(t)$ yield the same hodograph $\mathbf{g}'(t)$, it suffices to consider only two of the four possible sign combinations,

$$\sigma_0 = a, \quad \sigma_2 = \pm b, \quad (93)$$

since the other two give the same results.

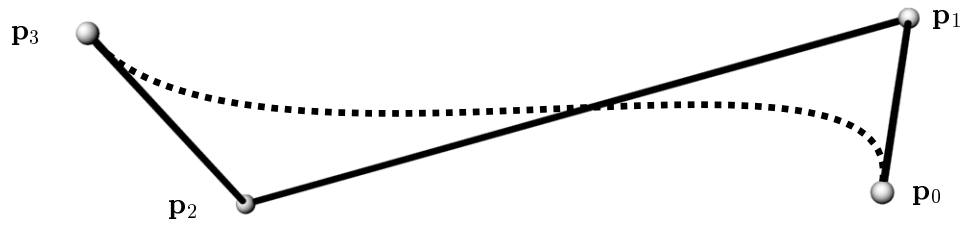

Figure 27: MPH cubic interpolant in Bézier form.

The first equation in (91) leads to

$$\sigma_1 = \langle \mathbf{t}_0, \mathbf{l}_1 \rangle. \tag{94}$$

After eliminating σ_1 from the two equations (91), and using (89) and (93), we arrive at one of the two equations

$$\langle \mathbf{l}_1, \mathbf{t}_0 \mp \mathbf{t}_1 \rangle = 0, \tag{95}$$

depending on the choice of the sign in $\sigma_2 = \pm b$.

These equations form necessary conditions for the existence of a solution. From a geometric point of view, the leg $\mathbf{l}_1$ of the control polygon must be parallel to a plane with the normal vector $\mathbf{t}_0 \mp \mathbf{t}_1$ (with respect to Minkowski inner product). It is well known that all lines which are parallel to a given plane and intersect two skew lines form a hyperbolic paraboloid. Consequently, in the case of non–planar input data we get such a hyperbolic paraboloid from each of the two cases in (95). The control polygons of the MPH cubics lie completely on these surfaces, see Fig. 28.

By substituting (93) and (94) into (92) we get one of the two equations

$$\pm ab + 2\langle \mathbf{t}_0, \mathbf{l}_1 \rangle^2 = ab\langle \mathbf{t}_0, \mathbf{t}_1 \rangle + 2\langle \mathbf{l}_1, \mathbf{l}_1 \rangle, \tag{96}$$

depending on the choice of sign in (93).

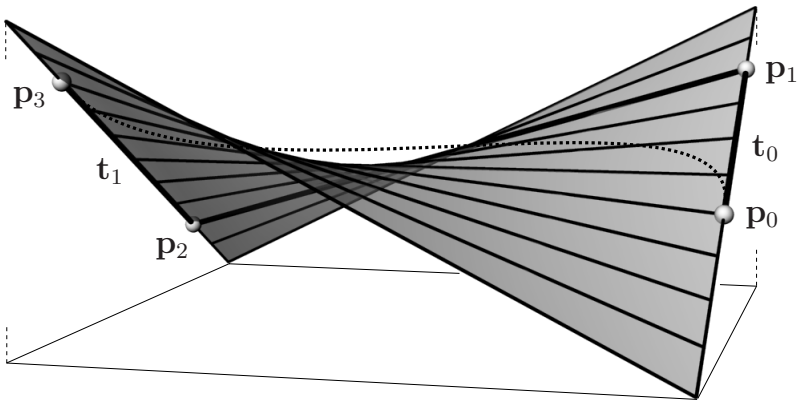

Figure 28: Necessary condition: The control polygon of the interpolating MPH cubic lies on a certain hyperbolic paraboloid.

Finally we solve (95) for a and substitute the result into the corresponding equation (96). For each of the two cases, this leads to a quadratic equation $E_{1/2}(b) = 0$. Consequently, we may obtain up to four real solutions to the interpolation problem. The two equations $E_{1/2}(b) = 0$ are rather long, and we do not include them in a general expanded form. See Section 4.3 for canonical cases of these equations.

Let $E_i(b) = \phi_i b^2 + \xi_i b + \psi_i$, $\phi_1\phi_2 \neq 0$, $\xi_i^2 - 4\phi_i\psi_i > 0$, where $i \in \{1, 2\}$. Then we denote the solutions as

$$b_{i,1} = \frac{-\xi_i + \sqrt{\xi_i^2 - 4\phi_i\psi_i}}{2\phi_i},\ b_{i,2} = \frac{-\xi_i - \sqrt{\xi_i^2 - 4\phi_i\psi_i}}{2\phi_i}. \tag{97}$$

The ordering of the solutions $b_{i,j}$ is important in the following discussions. Note that multiplying equations (96) by negative constants is not allowed, since it changes the labeling.

GIVEN: End points $\mathbf{q}_0$, $\mathbf{q}_1$ with assoc. space–like tangent vectors $\mathbf{t}_0$, $\mathbf{t}_1$.
1. Solve the equation $E_i(b)$ for b $(i = 1, 2) \implies b_{i,1},\ b_{i,2}$.
2. Compute $a_{i,1}$, $a_{i,2}$ from $\langle \mathbf{l}_1, \mathbf{t}_0 \mp \mathbf{t}_1 \rangle = 0$ corresponding to $b_{i,1}$, $b_{i,2}$.
OUTPUT: Four MPH cubic interpolants given by (86) and (87).

Table 4: G^1 interpolation by MPH cubics.

The algorithm for computing the interpolants is summarized in Table 4. An example will be presented later (see Section 4.6).

Remark 8 The two solutions obtained by choosing the plus signs in (93) corresponding to the plus sign in (96) and the minus sign in (95), which are found by solving $E_1(b) = 0$, will be called the *solutions of the first kind*. The other two solutions will be called the *solutions of the second kind*.

4.1 Canonical positions of the boundary tangents

The following sections study the number of solutions for given G^1 input data. In order to analyze the solvability, we simplify the given input data without loss of generality as far as possible. First, we move the starting point $\mathbf{g}(0)$ of the curve $\mathbf{g}(t)$ to the origin, while the endpoint $\mathbf{g}(1)$ remains arbitrary, i.e.

$$\mathbf{p}_0 = (0, 0, 0)^\top, \quad \mathbf{p}_3 = (x, y, r)^\top. \tag{98}$$

Then we apply Lorentz transforms in order to obtain one among five canonical positions, as described in the following proposition.

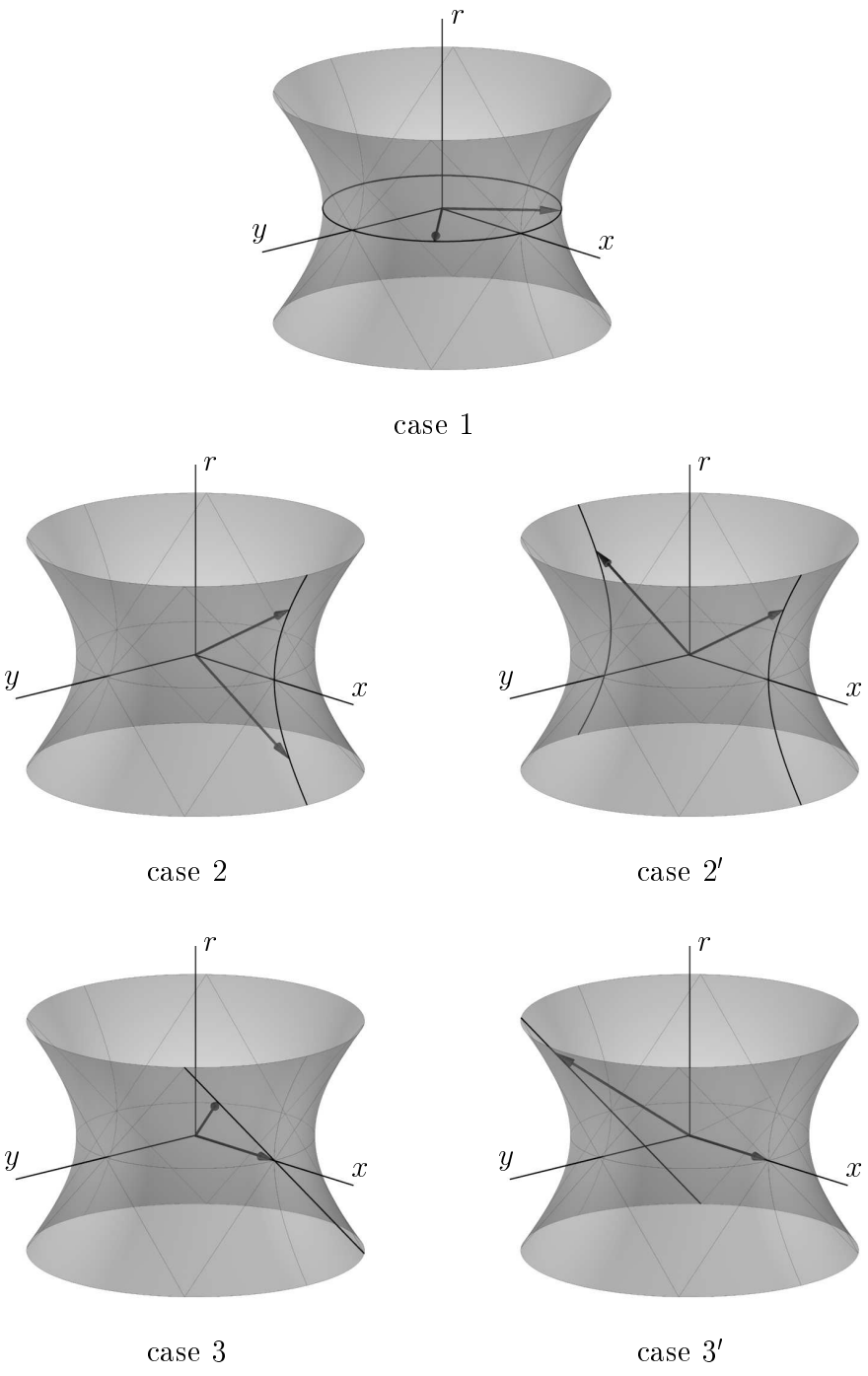

Figure 29: Five canonical positions of two unit space–like vectors $\mathbf{t}_0$, $\mathbf{t}_1$ (depicted as arrows). See Fig. 30 for 2D views.

			canonical position		
no.	**s**	**d**	$\mathbf{t}_0$	$\mathbf{t}_1$	$f \in$
1	*sl.*	*sl.*	$(\cos f, \sin f, 0)^\top$	$(\cos f, -\sin f, 0)^\top$	$(-\frac{\pi}{2}, \frac{\pi}{2}]$
2	*sl.*	*tl.*	$(\cosh f, 0, \sinh f)^\top$	$(\cosh f, 0, -\sinh f)^\top$	$(-\infty, \infty)$
$2'$	*tl.*	*sl.*	$(\cosh f, 0, \sinh f)^\top$	$(-\cosh f, 0, \sinh f)^\top$	$(-\infty, \infty)$
3	*sl.*	*ll.*	$(1, 0, 0)^\top$	$(1, f, f)^\top$	$(0, \infty)$
$3'$	*ll.*	*sl.*	$(1, 0, 0)^\top$	$(-1, f, f)^\top$	$(0, \infty)$

Table 5: Canonical positions of two space–like unit vectors $\mathbf{t}_0, \mathbf{t}_1$. The abbreviations sl., tl., and ll. stand for space–, time– and light–like, respectively.

Proposition 11 *Any pair of space–like unit vectors* $\mathbf{t}_0$, $\mathbf{t}_1$ *in three dimensional Minkowski space can be mapped by a Lorentz transform to one of the canonical positions described in Table 5, depending on the causal characters of their sum and difference vectors* $\mathbf{s} = \mathbf{t}_0 + \mathbf{t}_1$ *and* $\mathbf{d} = \mathbf{t}_1 - \mathbf{t}_0$.

Proof: The plane spanned by $\mathbf{t}_0$ and $\mathbf{t}_1$ can be space–like (case 1), time–like (cases 2 and $2'$) or light–like (cases 3 and $3'$), depending on whether the restriction of the quadratic form $\mathbf{v} \mapsto \langle \mathbf{v}, \mathbf{v} \rangle$ to the plane is positive definite, indefinite or semi–definite, respectively. Using a suitable Lorentz transform we map it into one of the planes $r = 0$, $y = 0$ or $y - r = 0$, respectively. Within these planes, the unit vectors (characterized by $x^2 + y^2 - r^2 = 1$) form a circle, a hyperbola or a pair of parallel lines (in the Euclidean sense), see Figure 30. Using another Lorentz transform one may map them to one

of the canonical configurations listed in Table 5. □

Remark 9 The remainder of this section studies the number of solutions for given G^1 input data. Later, in Section 4.4, we will analyze the behavior of piecewise G^1 Hermite interpolation of data taken from a space–like C^∞ curve by MPH cubic splines. In this context, cases $2'$ and $3'$ from Proposition 11 cannot occur, provided that sufficiently close endpoints are chosen (see Section 4.4). Consequently, the solvability in these cases will not be analyzed now.
Moreover, since the interpolation procedure does not distinguish between the different possible orientations of the boundary tangents, cases 2 and $2'$ are equivalent, and the cases 3 and $3'$ are equivalent. Therefore, only the cases 1,2 and 3 have to be addressed, which are distinguished by the causal character of $\mathbf{d} = \mathbf{t}_1 - \mathbf{t}_0$.

4.2 Computation of hyperbolic rotations

In this section we analyze the canonical positions given in Proposition 11 in more detail and compute the hyperbolic angles, which can be used to transform the unit space–like boundary vectors into such positions. The reader may skip this section altogether without losing the continuity of the text.

Due to

$$||\mathbf{t}_0 \pm \mathbf{t}_1||^2 = ||\mathbf{t}_0||^2 \pm 2\langle \mathbf{t}_0, \mathbf{t}_1 \rangle + ||\mathbf{t}_1||^2 = 2 \pm 2\langle \mathbf{t}_0, \mathbf{t}_1 \rangle, \tag{99}$$

at least one of the two vectors $\mathbf{s}$ and $\mathbf{d}$ is space–like, and the five cases of the Proposition 11 therefore cover all possible situations. Let

$$\mathbf{t}_0 = (\cos(\alpha_0)\cosh(\beta_0), \sin(\alpha_0)\cosh(\beta_0), \sinh(\beta_0))^\top. \tag{100}$$

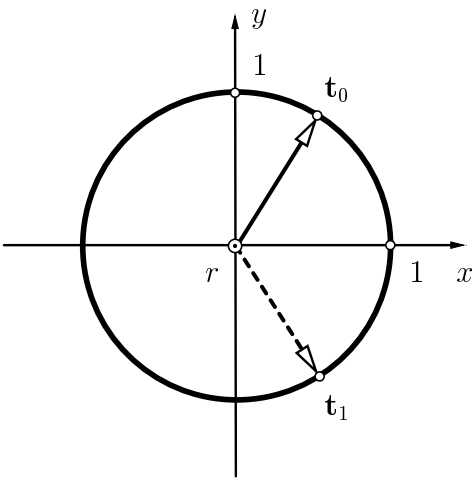

case 1: $r = 0$

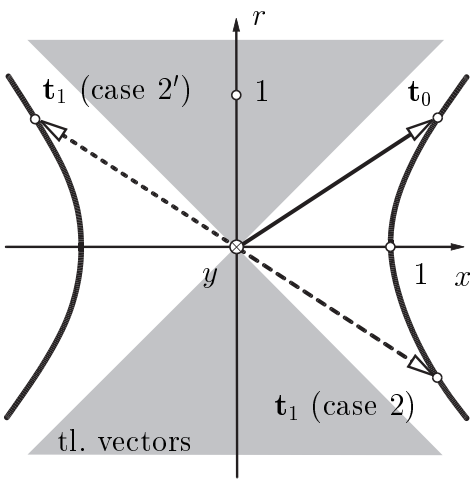

cases $2, 2'$: $y = 0$

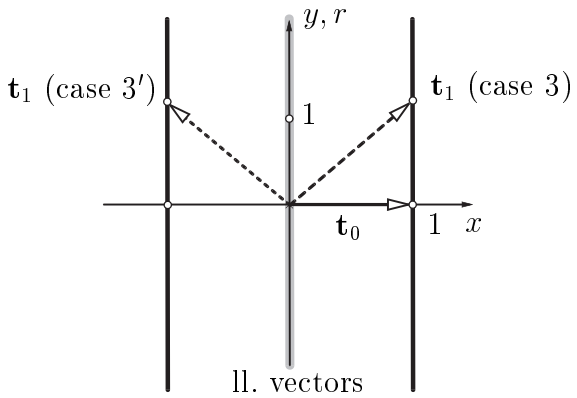

cases $3, 3'$: $y - r = 0$

Figure 30: The canonical positions of the plane spanned by the two vectors $\mathbf{t}_0, \mathbf{t}_1$, the curves formed by the unit vectors (bold) and the time–like resp. light–like vectors (interior and boundary of the grey regions in cases 2,2′ and 3,3′). See Fig. 29 for 3D views.

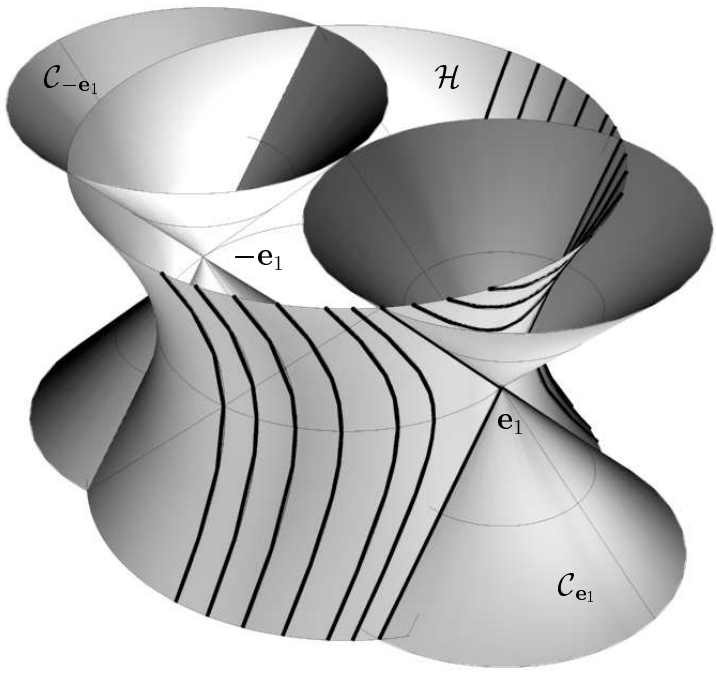

Figure 31: Trajectories of hyperbolic rotations.

The Lorentz transform

$$L = R(\frac{-\pi}{2})H(-\beta_0)R(\frac{\pi}{2} - \alpha_0) \tag{101}$$

maps $\mathbf{t}_0$ to $\mathbf{e}_1 = (1, 0, 0)^\top$, and $\mathbf{t}_1$ to

$$\mathbf{t}_1^L = L\mathbf{t}_1 = (\cos(\alpha_1)\cosh(\beta_1), \sin(\alpha_1)\cosh(\beta_1), \sinh(\beta_1))^\top. \tag{102}$$

Since $L\mathbf{t}_0 = (1, 0, 0)^\top$ is invariant under hyperbolic rotations, we may map the vector $\mathbf{t}_1^L$ to $H(\gamma)\mathbf{t}_1^L$, without changing $L\mathbf{t}_0$.

Let us analyze these hyperbolic rotations from a geometric point of view. Fig. 31 shows several hyperbolic rotation trajectories of points (end points

of space–like unit vectors with starting point at the origin) lying on the unit hyperboloid $\mathcal{H} : x^2 + y^2 - r^2 = 1$ along with the light cones $\mathcal{C}_{\mathbf{e}_1}$ of the point $(1,0,0)^\top$ and $\mathcal{C}_{-\mathbf{e}_1}$ of the point $(-1,0,0)^\top$. The trajectories of the endpoint of the vector $\mathbf{t}_1^L$ are hyperbolas or two straight lines which are the intersection curves of the unit hyperboloid and planes $P_{x_0} : x = x_0$ parallel to the yr plane. Depending on the causal character of $\mathbf{s}$ and $\mathbf{d}$ we arrive at one of the following five cases (cf. Proposition 11.

Case 1: Both $\mathbf{s}$ and $\mathbf{d}$ are space–like. Then $x_0 \in (-1,1)$ and $P_{x_0} \cap \mathcal{H}$ is a hyperbola intersecting the xy plane. Thus there exists a hyperbolic angle γ_1 and an angle f_1, for which we have $H(\gamma_1)\mathbf{t}_1^L = (\cos f_1, \sin f_1, 0)^\top$. Applying the rotation $R(\frac{-f_1}{2})$ we can map $H(\gamma_1)\mathbf{t}_1^L$ and $\mathbf{e}_1$ into the first canonical position.

Case 2: $\mathbf{s}$ is space–like and $\mathbf{d}$ is time–like. In this case $x_0 \in (1,\infty)$ and $P_{x_0} \cap \mathcal{H}$ is a hyperbola intersecting the xr plane. This proves the existence of hyperbolic angles γ_2 and f_2, for which we have $H(\gamma_2)\mathbf{t}_1^L = (\cosh f_2, 0, \sinh f_2)^\top$. In order to map the vectors to the proposed symmetric position one can apply the transform $R(\frac{-\pi}{2})H(-\frac{f_2}{2})R(\frac{\pi}{2})$.

Case 2': $\mathbf{s}$ is time–like. In this case $x_0 \in (-\infty,-1)$ and $P_{x_0} \cap \mathcal{H}$ is a hyperbola intersecting the xr plane. Therefore there exist hyperbolic angles γ_2' and f_2', for which we have $H(\gamma_2')\mathbf{t}_1^L = (-\cosh f_2', 0, \sinh f_2')^\top$. In order to map the vectors to the proposed symmetric position we apply the transform $R(\frac{\pi}{2})H(-\frac{f_2'}{2})R(\frac{-\pi}{2})$.

Case 3: $\mathbf{s}$ is space–like and $\mathbf{d}$ is light–like. Then $x_0 = 1$ and $P_{x_0} \cap \mathcal{H}$ are two straight lines, the intersection lines of the hyperboloid $\mathcal{H}$ and the cone $\mathcal{C}_{\mathbf{e}_1}$. Obviously there exists γ_3 such that $\mathbf{t}_1^L$ is mapped onto one of the four vectors: $H(\gamma_3)\mathbf{t}_1^L = (1, \pm f_3, \pm f_3)^\top$. According to the signs of the coordinates of $H(\gamma_3)\mathbf{t}_1^L$ we apply one of the maps given by matrices T_1, T_2 or T_1T_2 to get the desired result.

Case 3': $\mathbf{s}$ is light–like. Then $x_0 = -1$ and $P_{x_0} \cap \mathcal{H}$ are two straight lines, the intersection lines of the hyperboloid $\mathcal{H}$ and the cone $\mathcal{C}_{-e_1}$. Then there exists γ_3' such that $\mathbf{t}_1^L$ is mapped onto one of the four vectors: $H(\gamma_3')\mathbf{t}_1^L = (-1, \pm f_3', \pm f_3')^\top$. As in the previous case, by applying a map given by matrices T_1, T_2 or T_1T_2 we arrive at the desired result. □

For future use we discuss the computation of the hyperbolic rotations (introduced in Proposition 11) mapping any pair of space–like unit vectors to one of the canonical positions described in Table 5.

Let us assume we have two space–like unit vectors

$$\mathbf{r} = (\cos(\alpha)\cosh(\beta), \sin(\alpha)\cosh(\beta), \sinh(\beta))^\top, \quad \mathbf{e}_1 = (1,0,0)^\top. \tag{103}$$

The Minkowski square norm of their sum and difference $\mathbf{s} = \mathbf{r}+\mathbf{e}_1$, $\mathbf{d} = \mathbf{r}-\mathbf{e}_1$ equals

$$||\mathbf{s}||^2 = 2 - 2\cos\alpha\cosh\beta, \tag{104}$$

$$||\mathbf{d}||^2 = 2 + 2\cos\alpha\cosh\beta. \tag{105}$$

An arbitrary hyperbolic rotation can be represented by the matrix

$$H_\gamma = \begin{pmatrix} 1 & 0 & 0 \\ 0 & \cosh\gamma & \sinh\gamma \\ 0 & \sinh\gamma & \cosh\gamma \end{pmatrix}. \tag{106}$$

Applying this matrix to the vector $\mathbf{r}$ gives

$$H_\gamma\mathbf{r} = \begin{pmatrix} \cos\alpha\cosh\beta \\ \cosh\gamma\sin\alpha\cosh\beta + \sinh\gamma\sinh\beta \\ \sinh\gamma\sin\alpha\cosh\beta + \cosh\gamma\sinh\beta \end{pmatrix} = \begin{pmatrix} \tilde{\mathbf{r}}_1 \\ \tilde{\mathbf{r}}_2 \\ \tilde{\mathbf{r}}_3 \end{pmatrix}. \tag{107}$$

Now we will compute the hyperbolic angle γ such that H_γ maps the vector $\mathbf{r}$ into one of the following planes:

Case 1: $H_\gamma \mathbf{r}$ lies in the plane $r = 0$. Then $\mathbf{d}$ and $\mathbf{s}$ are space-like and γ can be computed from the equation $\tilde{\mathbf{r}}_3 = 0$.

Case 2: $H_\gamma \mathbf{r}$ lies in the plane $y = 0$. Then $\mathbf{d}$ or $\mathbf{s}$ is time-like and γ can be computed from the equation $\tilde{\mathbf{r}}_2 = 0$.

Case 3: $H_\gamma \mathbf{r}$ lies in the plane $x = \pm 1$. Then $\tilde{\mathbf{r}}_1 = \pm 1$, which is clearly equivalent to the condition for $\mathbf{s}$ or $\mathbf{d}$ to be light–like. No computation of γ is needed in this case.

In the first two cases we arrive at the following formula for $\gamma_\pm$:

$$\gamma_\pm = \frac{1}{2} \ln(\pm \frac{R_1}{R_2}), \tag{108}$$

where

$$R_1 = \sin\alpha \cosh\beta - \sinh\beta, \; R_2 = \sin\alpha \cosh\beta + \sinh\beta. \tag{109}$$

Using goniometric identities we can see that $R_1 = 0$ or $R_2 = 0$ if and only if $||\mathbf{s}||^2 = 0$ or $||\mathbf{d}||^2 = 0$. Therefore, due to the $\pm$ sign in (108), there exists a solution $\gamma_\pm$ for any given space–like unit vector $\mathbf{r}$. This is in complete agreement with the results derived in Proposition 11.

Remark 10 The first tangent vector could always be mapped to $\mathbf{e}_1 = (1, 0, 0)^\top$. We use additional Lorentz transforms mapping the two vectors into a symmetric positions in order to simplify the equations in the following chapters.

4.3 Solvability analysis

We study the solvability for the cases 1, 2 and 3 of the given input data, and for the (degenerate) case of linearly dependent boundary tangents. While cases 1 and 2 are regular ("generic"), case 3 and the degenerate case of linearly dependent boundary occur for singular data.

4.3.1 Regular cases

Case 1: Space–like difference d. We consider G^1 Hermite data, as specified in case 1 of Proposition 11. Recall that $\mathbf{p}_0 = (0,0,0)^\top$ and $\mathbf{p}_3 = (x,y,r)^\top$, see (98). The two equations (95) lead to

$$a = \frac{y+bs}{s} \quad \text{resp.} \quad a = \frac{x-bc}{c}, \tag{110}$$

depending on the choice of the sign, where $s = \sin f$ and $c = \cos f$. After using them to eliminate a from (96), we get the two quadratic equations

$$\begin{aligned} E_1 &= (8c^4-10c^2+2)b^2+(-8sc^2y+8s^2cx+2sy)b-2(sx-cy)^2+2r^2 = 0, \\ E_2 &= (8c^4-6c^2)b^2+(-8sc^2y-8c^3x+6cx)b-2(sx-cy)^2+2r^2 = 0. \end{aligned}$$

The roots of $E_1(b)$ (resp. $E_2(b)$), along with the a values obtained from the first (resp. second) equation (110), give the solutions of the first kind, resp. of the second kind. Clearly, these roots may be conjugate complex. Moreover, if $f \in \{0, \pm\frac{\pi}{6}, \pm\frac{\pi}{3}, \frac{\pi}{2}\}$, then one of the two quadratic equations degenerates into a linear one.

In the general case ($f \notin \{0, \pm\frac{\pi}{6}, \pm\frac{\pi}{3}, \frac{\pi}{2}\}$), the number of real solutions of the first or second kind depends on the signs of the discriminants D_1, D_2 with respect to the parameter b,

$$\begin{aligned} D_1 &= 4s^2(4s^2x^2 + (1-4c^2)y^2 + (16c^2-4)r^2), \\ D_2 &= 4c^2((1-4s^2)x^2 + 4c^2y^2 + (16s^2-4)r^2). \end{aligned} \tag{111}$$

Consider a quadratic cone $C: \ \alpha x^2 + \beta y^2 + \gamma r^2 = 0$, where $\alpha\beta\gamma \neq 0$. A given point $\tilde{\mathbf{p}} = (\tilde{x}, \tilde{y}, \tilde{r})^\top$ is said to lie

$$\left.\begin{array}{c}\text{inside}\\ \text{on}\\ \text{outside}\end{array}\right\} \text{ the cone } C \text{ if } \quad \alpha\tilde{x}^2 + \beta\tilde{y}^2 + \gamma\tilde{r}^2 \left\{\begin{array}{l} < 0\\ = 0\\ > 0\end{array}\right. . \tag{112}$$

Fig. 32 visualizes the two families of quadratic cones D_1 resp. D_2. Note that the x– resp. y–axis is always outside. The cones D_1 share the two common lines $(0, \pm 2t, t)^\top$, $t \in \mathbb{R}$ and two tangent planes $y^2 = 4r^2$ along them. Analogously, the cones D_2 share the two common lines $(\pm 2t, 0, t)^\top$, $t \in \mathbb{R}$ and the associated tangent planes $x^2 = 4r^2$.

Proposition 12 *For any given value of* $f \in (-\frac{\pi}{2}, \frac{\pi}{2}) \setminus \{0, \pm\frac{\pi}{6}, \pm\frac{\pi}{3}\}$, *the number of real solutions of the* G^1 *interpolation problem by MPH cubics with a space–like difference vector* $\mathbf{d}$ *depends on the mutual position of the end point* $\mathbf{p}_3 = (x, y, r)^\top \neq (0, 0, 0)^\top$ *and the quadratic cones* D_1, D_2. *If* $\mathbf{p}_3 = (x, y, r)$ *lies outside, on, or inside* D_i, *then the number of solutions of the* i*–kind equals two, one, or zero, respectively. In any case one obtains at least two real solutions.*

Proof: The last part remains to be shown. By inspecting the two families of cones, one can verify that the interior parts of the cones do not intersect. Indeed, if $f \approx 0$, then the y-axis is inside D_1 and the r–axis is inside D_2. If $f \to \pm\frac{\pi}{2}$, then the r–axis is inside D_1 and the x-axis is inside D_2. □

We conclude this section with a short discussion of singular cases.

- If $f = \frac{\pi}{3}$, then E_1 is linear in b and yields one solution when $x \neq 0$. If $x = 0$ then we obtain infinitely many or no solutions of the first kind,

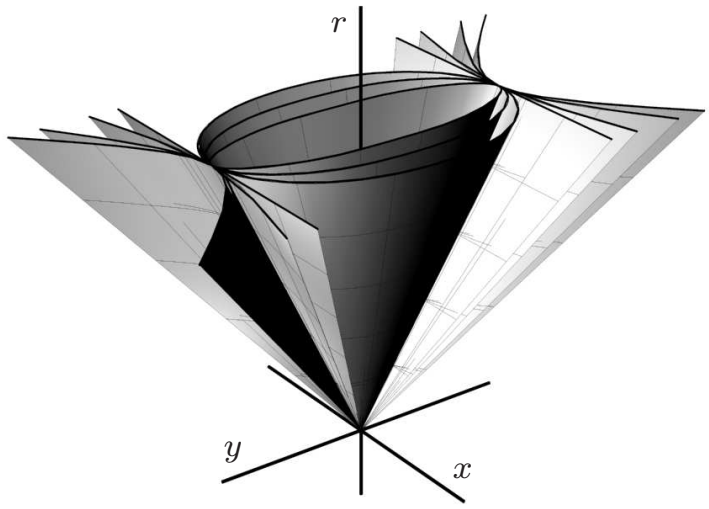

a)

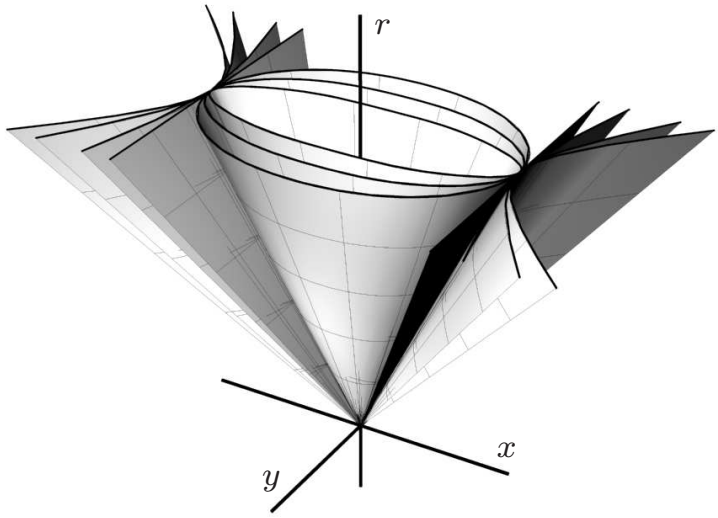

b)

Figure 32: Space–like difference vector **d**: a) The family D_1, and b) the family D_2 of quadratic cones for various values of the parameter f.

depending on whether $8r^2 - 2y^2 = 0$ or not. The second equation E_2 can be dealt with as in the regular case.

- If $f = \frac{\pi}{6}$, then E_2 is linear in b. The discussion of the number of solutions is analogous to the previous case.
- Coinciding endpoints, $\mathbf{p}_0 = \mathbf{p}_3 = (0,0,0)^\top$. The first equation (110) gives $a = b$, and $E_1 = 0$ implies $f = \pm\frac{\pi}{3}$. This is in perfect agreement with the fact that any planar PH curve of degree three is similar to the Tschirnhausen cubic (see Farouki & Sakkalis (1990)) as the angle between the tangents at the double point of the Tschirnhausen cubic equals $\frac{\pi}{3}$. The second case gives an equivalent result.
- The case of linearly dependent boundary tangents $f \in \{0, \frac{\pi}{2}\}$ will be analyzed in the last paragraph of Section 4.3.2.

Remark 11 Some solutions may have the wrong orientation ($a < 0$ or $b > 0$) or singular end points ($a = 0$ or $b = 0$). While this could be characterized by certain nonlinear inequalities for the components of $\mathbf{p}_3$, we will present another approach in Section 4.4.

Case 2: Time–like difference d. The analysis in the case of a time-like difference vector $\mathbf{d}$ is similar, but reveals a different behaviour. We consider G^1 Hermite data, as specified in case 2 of Proposition 11. The two equations (95) lead to

$$a = \frac{r + bS}{S} \quad \text{resp.} \quad a = \frac{x - bC}{C}, \tag{113}$$

depending on the choice of the sign, where $S = \sinh f$ and $C = \cosh f$. After using them to eliminate a from (96), we get the two quadratic equations

$$\begin{aligned} E_1 &= (8C^4{-}10C^2{+}2)b^2{+}(8C^2r{-}8SCx{-}2r)Sb{+}2(Sx - Cr)^2{-}2y^2{=}0, \\ E_2 &= (8C^4{-}6C^2)b^2{+}(6Cx{-}8C^3x{+}8C^2Sr)b{+}2(Sx - Cr)^2{-}2y^2{=}0. \end{aligned}$$

Their roots, along with the a values obtained from the first (resp. second) equation (113), give the solutions of the first kind, resp. of the second kind.

If $f = 0$, then the first equation degenerates into a linear equation. Otherwise, the number of real solutions of the first or second kind depends on the signs of the discriminants $D1$, D_2 with respect to the parameter b,

$$\begin{aligned} D_1 &= 4S^2(4S^2x^2 + (16C^2 - 4)y^2 + (1 - 4C^2)r^2), \\ D_2 &= 4C^2((4S^2 + 1)x^2 + (16S^2 + 4)y^2 - 4C^2r^2). \end{aligned} \tag{114}$$

Similarly to the previous case, we obtain two families of quadratic cones with apex at the origin, see Fig. 33. The r–axis is always inside both cones.

Proposition 13 *For any given value of $f \in \mathbb{R} \setminus \{0\}$, the number of real solutions of the G^1 interpolation problem by MPH cubics with a time–like difference vector $\mathbf{d}$ depends on the mutual position of the end point $\mathbf{p}_3 = (x, y, r)^\top \neq (0, 0, 0)^\top$ and the quadratic cones D_1, D_2. If $\mathbf{p}_3 = (x, y, r)$ lies outside, on, or inside D_i, then the number of solutions of the i–kind equals two, one, or zero, respectively. As a sufficient condition, if $4y^2 - r^2 > 0$, then we get two solutions of the first kind, and if $\frac{1}{4}x^2 + y^2 - r^2 > 0$, then we obtain two solutions of the second kind.*

Proof. The second part of the proposition can again be shown by analyzing the distribution of the cones. For $f \to \pm\infty$, both cones converge to the same limit cone $x^2 + 4y^2 - r^2 = 0$. For $f \to 0$, the cone D_1 converges to the two planes $4y^2 - r^2 = 0$, and D_2 converges to the limit cone $\frac{1}{4}x^2 + y^2 - r^2 = 0$. □

The only singular case concerns coinciding endpoints, $\mathbf{p}_3 = (0, 0, 0)^\top$. This case does not have any solutions, except for $f = 0$. When $\mathbf{d}$ is time–like, no planar MPH curve with a double point exists.

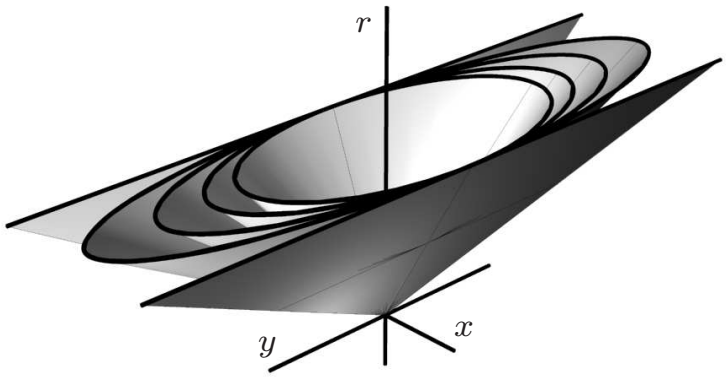

a)

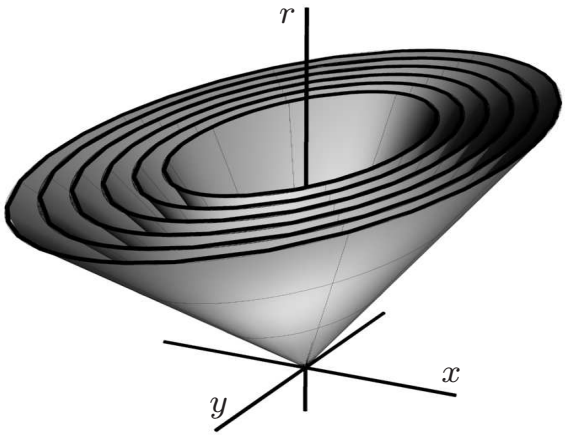

b)

Figure 33: Time–like difference **d**: The family a) D_1 and b) D_2 of quadratic cones for various values of the parameter f.

Remark 11 is again valid, but with possibly different signs for a and b, since cases 2 and $2'$ of Proposition 11 have been identified.

4.3.2 Singular cases

Case 3: Light–like difference d. We consider G^1 Hermite data, as specified in case 3 of Proposition 11. The first of the two equations (95) implies $f = 0$ (which will be analyzed in the next section) or $y = r$. Consequently, for a general difference vector $\mathbf{p}_3 = (x, y, r)^\top$ with $y \neq r$ we do not obtain any solutions of the first kind. If $y = r$, then any choice of a, b gives an MPH cubic.

On the other hand, the second equation (95) leads to

$$a = x - b + \frac{1}{2} f(y - r). \tag{115}$$

After eliminating a from the second equation (96), we get

$$E_2 = 3bf(y - r) - 2(bx + y^2 - r^2 - b^2). \tag{116}$$

The discriminant of the quadratic equation E_2 has the form

$$D_2 = 4x^2 + (y - r)(16y + 16r + 9f^2 y - 9f^2 r - 12fx). \tag{117}$$

Similarly to the regular cases, this equation defines a family of cones, see Fig. 34. For any given f and $\mathbf{p}_3$, the number of solutions can be decided with the help of the corresponding cone in this family.

Degenerate case: Linearly dependent tangent vectors. We may assume that $\mathbf{t}_0 = \mathbf{t}_1 = (1, 0, 0)^\top$. Solutions of the first kind exist if and only if $y^2 = r^2$, and any choice of a, b then gives a solution. Solutions of the second kind exist if the discriminant $D_2 = 4x^2 + 16y^2 - 16r^2$ of E_2 is non–negative.

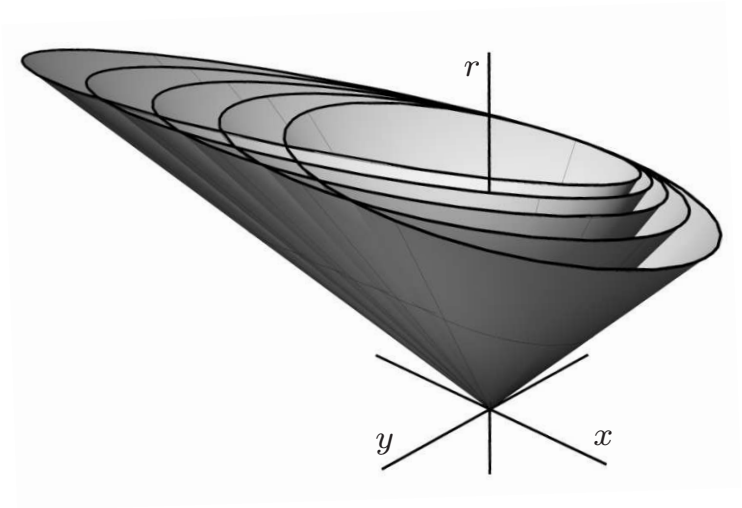

Figure 34: Light–like difference **d**: family $D_2 = 0$ of quadratic cones for various values of the parameter f.

4.4 Asymptotic analysis

As shown in the previous sections, the solvability of the G^1 Hermite interpolation problem depends heavily on the given data. In the remainder of the thesis we take a different approach, as follows. We consider a curve segment $\mathbf{p} = \mathbf{p}(s)$ with $s \in [0, S_{max}]$ in Minkowski space, which is assumed to be space–like. The coordinate function are assumed to be C^∞, and the parameter s is assumed to be the Minkowski arc length, i.e. $\langle \mathbf{p}', \mathbf{p}' \rangle = 1$.

For a given step–size h, we generate points and tangents at the points $s = ih$, $i = 0, 1, 2, \ldots$ and apply the G^1 Hermite interpolation procedure by MPH cubics to the pairs of adjacent points and tangents. We analyze the existence and the behaviour of the solutions for decreasing step–size $h \to 0$.

4.4.1 Regular cases

Using the Frenet formulas (see Section 2.6) we generate a Taylor expansion of the given curve. The derivatives at $s = 0$ evaluate to

$$\begin{aligned} &\mathbf{p}'(0) = \mathbf{T}_0, \mathbf{p}''(0) = \mathbf{T}'(0) = \kappa_0 \mathbf{N}_0, \\ &\mathbf{p}'''(0) = \kappa_1 \mathbf{N}_0 + \kappa_0 \mathbf{N}'(0) = \kappa_1 \mathbf{N}_0 \mp (\kappa_0^2 \mathbf{T}_0 + \kappa_0 \tau_0 \mathbf{B}_0), \end{aligned} \tag{118}$$

etc., where $\mathbf{T}_0 = \mathbf{T}(0)$, $\mathbf{N}_0 = \mathbf{N}(0)$, $\mathbf{B}_0 = \mathbf{B}(0)$, $\kappa_0 = \kappa(0)$, $\kappa_1 = \kappa'(0)$, $\tau_0 = \tau(0)$, etc.. The choice of the sign in $\mathbf{p}'''(0)$ (and all further derivatives) depends on the causal character of the normal vector $\mathbf{N}_0$. In the generic case, the normal vector $\mathbf{N}$ is either space–like or time–like.

Note that the equations (118) are not valid at Minkowski inflections, where $\mathbf{N}_0$ is light–like. These cases have to be studied separately.

Using suitable initial conditions, we generate a Taylor expansion of the given curve,

$$\mathbf{p}(s) = \mathbf{p}(0) + s\mathbf{p}'(0) + \frac{s^2}{2}\mathbf{p}''(0) + \frac{s^3}{6}\mathbf{p}'''(0) + \dots . \tag{119}$$

Without loss of generality, we choose $\mathbf{p}(0) = (0,0,0)^\top$, $\mathbf{T}_0 = (1,0,0)^\top$, and $\{\mathbf{N}_0, \mathbf{B}_0\} = \{(0,1,0)^\top, (0,0,1)^\top\}$, depending on the causal character of $\mathbf{N}_0$.

We analyze the interpolants to the G^1 Hermite data sampled at s_0 and $s_1 = s_0 + h$. In the limit case $h \to 0$, the normal vector $\mathbf{N}(0)$ plays the role of the difference vector $\mathbf{d}$ of the end tangent vectors.

Proposition 14 *Let $\mathbf{p}(s)$ be a space–like C^∞ curve with a space–like or time–like principal normal vector at $\mathbf{p}(s_0)$. Consequently, the Minkowski curvature satisfies $\kappa \neq 0$ at $\mathbf{p}(s_0)$. Then the G^1 Hermite interpolation of $\mathbf{p}(s)$ in $[s_0, s_0 + h]$ by MPH cubics has four solutions, provided that the step–size $h > 0$ is sufficiently small. Exactly one among them matches the shape of the given curve segment and possesses the approximation order four.*

Proof: Let $s_0 = 0$. If $\mathbf{N}(0)$ is space–like, then this remains valid for $s \in [0, h]$, provided that h is sufficiently small. The given curve has the Taylor expansion[1]

$$\mathbf{p}(s) = \begin{pmatrix} s - \frac{1}{6}\kappa_0^2 s^3 - \frac{1}{8}\kappa_0\kappa_1 s^4 + \mathcal{O}(s^5) \\ \frac{1}{2}\kappa_0 s^2 + \frac{1}{6}\kappa_1 s^3 + \frac{1}{24}(\kappa_2 + \kappa_0(\tau_0^2 - \kappa_0^2))s^4 + \mathcal{O}(s^5) \\ \frac{1}{6}\kappa_0\tau_0 s^3 + \frac{1}{24}(2\kappa_1\tau_0 + \kappa_0\tau_0)s^4 + \mathcal{O}(s^5) \end{pmatrix}. \tag{120}$$

After sampling the Hermite boundary data at $s_0 = 0$ and $s_1 = h$, we generate Taylor expansions of the two quadratic equations $E_i(b) = 0$ and their discriminants,

$$\begin{aligned} D_1 &= \kappa_0^4 h^8 + 2\kappa_0^3\kappa_1 h^9 + \mathcal{O}(h^{10}), \\ D_2 &= 4h^4 - \tfrac{16}{3}\kappa_0^2 h^6 - \tfrac{16}{3}\kappa_0\kappa_1 h^7 + \mathcal{O}(h^8). \end{aligned} \tag{121}$$

If h is sufficiently small, then the discriminants are positive and we obtain four real solutions.

The first solution of the first kind will be analyzed in more detail. The corresponding parameters a, b have the expansions

$$a_{1,1} = \frac{1}{3} + \frac{\kappa_1}{12\kappa_0}h + \mathcal{O}(h^2), \quad b_{1,1} = \frac{1}{3} - \frac{\kappa_1}{12\kappa_0}h + \mathcal{O}(h^2). \tag{122}$$

Hence, if h is sufficiently small, then the interpolant matches the orientations of the given tangent vectors. These parameters lead to the solution $\mathbf{q}(t) =$

[1] We used the computer algebra system Maple 9.

$(\bar{x}(t), \bar{y}(t), \bar{r}(t))^\top$, where

$$\begin{aligned} \bar{x}(t) &= th + \frac{\kappa_1 t(1-t)}{4\kappa_0} h^2 + \mathcal{O}(h^3), \\ \bar{y}(t) &= \frac{1}{2}\kappa_0 t^2 h^2 + \frac{1}{12}\kappa_1 t^2(3-t)h^3 + \mathcal{O}(h^4), \\ \bar{r}(t) &= \frac{1}{6}\kappa_0\tau_0 t^3 h^3 - \frac{1}{24}\tau_0(\kappa_0(1-2t) - \kappa_1(1+t))h^4 + \mathcal{O}(h^5). \end{aligned} \tag{123}$$

This solution approximates the given C^∞ curve with the (geometric) approximation order 4, i.e.

$$\mathbf{q}(t(\tau)) - \mathbf{p}(h\tau) = \mathcal{O}(h^4) \tag{124}$$

holds for all $\tau \in [0,1]$ where $t(\tau)$ is a reparameterization $[0,1] \to [0,1]$,

$$t(\tau) = \tau + h\tau(\tau-1)\frac{\kappa_1}{4\kappa_0} + h^2\tau(\tau-1)\frac{L_1\tau + L_2}{96\kappa_0^2}, \tag{125}$$

where

$$\begin{aligned} L_1 &= 10\kappa_1^2 + 8\kappa_0^2\tau_0^2 - 8\kappa_0^4, \\ L_2 &= 4\kappa_0^4 - 4\kappa_0^2\tau_0^2 - 17\kappa_1^2 + 12\kappa_0\kappa_2. \end{aligned} \tag{126}$$

The remaining three solutions can be analyzed in a similar way. It can be shown that the solutions of the second kind do not preserve the orientation of the boundary tangents, while the second solution of the first kind exhibits an 'overshooting' behaviour. Figure 38 a) (page 94) visualizes the typical shape. These solutions do not match the shape of the given curve, and they do not possess the approximation order 4.

An analogous discussion can be given when the normal vector of $\mathbf{p}$ at the origin is time–like. We obtain similar results, but by choosing the solution corresponding to the parameters $a_{1,2}$ and $b_{1,2}$ as the 'best' one. □

Remark 12 In order to obtain the expansion (123) of the solution $\mathbf{q}(t)$ one has to guarantee that all quantities used to compute it (such as D_1, $a_{1,1}, b_{1,1}$,

etc.) are C^∞ with respect to h and that all operations involved yield C^∞ results. Additions and multiplications preserve continuity and modify the expansions in a straightforward way. The only square roots involved in our interpolation algorithm are $\sqrt{D_1}$ and $\sqrt{D_2}$. However, a closer look at the leading terms of the expansions of D_1 and D_2 (see (121)) reveals that the expansions of $\sqrt{D_1}$ and $\sqrt{D_2}$ are well defined.

The last technical difficulty is related to divisions. One can verify that all the divisions involved in the above proof do not introduce any essential singularities. However, some divisions may introduce removable singularities for $h = 0$. In those cases we extend the resulting ratios continuously to $h = 0$.

In fact, it suffices to guarantee that the given curve $\mathbf{p}(s)$ is C^{12} (instead of C^∞). In this case one has to check that all quantities involved in the proof of Proposition 14 have the desired level of differentiability. In case of C^∞ input data all the expressions are in fact C^∞.

4.4.2 Singular cases

Minkowski inflections correspond to points where the normal vector $\mathbf{N}$ is light–like. This occurs at an isolated point or within an entire interval.

Case 1: Isolated Minkowski inflection. We suppose that the normal vector of $\mathbf{p}(s)$ at the origin is light–like and the canonical Taylor expansion of $\mathbf{p}(s)$ at the origin has the form

$$\mathbf{p}(s) = s \begin{pmatrix} 1 \\ 0 \\ 0 \end{pmatrix} + \frac{s^2}{2} \begin{pmatrix} x_2 \\ y_2 \\ r_2 \end{pmatrix} + \frac{s^3}{6} \begin{pmatrix} x_3 \\ y_3 \\ r_3 \end{pmatrix} + \frac{s^4}{24} \begin{pmatrix} x_4 \\ y_4 \\ r_4 \end{pmatrix} + \begin{pmatrix} \mathcal{O}(s^5) \\ \mathcal{O}(s^5) \\ \mathcal{O}(s^5) \end{pmatrix}.$$

j	y_j, r_j	$(-h_0, 0)$	0	$(0, h_0)$
odd	$y_j > r_j$	time–like $\mathbf{N}$	light–like $\mathbf{N}$	space–like $\mathbf{N}$
odd	$y_j < r_j$	space–like $\mathbf{N}$	light–like $\mathbf{N}$	time–like $\mathbf{N}$
even	$y_j > r_j$	space–like $\mathbf{N}$	light–like $\mathbf{N}$	space–like $\mathbf{N}$
even	$y_j < r_j$	time–like $\mathbf{N}$	light–like $\mathbf{N}$	time–like $\mathbf{N}$

Table 6: Causal character of normal vector $\mathbf{N}$.

From equation $\langle \mathbf{p}'(s), \mathbf{p}'(s) \rangle = 1$, which holds for all s from some neighborhood of $s_0 = 0$, we obtain without loss of generality that $x_2 = 0$, $y_2 = \kappa$, $r_2 = \kappa$, $x_3 = 0$, $x_4 = \kappa(r_3 - y_3)$ etc. Therefore the expansion of $\mathbf{p}''(s)$ takes the form

$$\mathbf{p}''(s) = \kappa\mathbf{N} = \begin{pmatrix} 0 \\ \kappa \\ \kappa \end{pmatrix} + s \begin{pmatrix} 0 \\ y_3 \\ r_3 \end{pmatrix} + \frac{s^2}{2} \begin{pmatrix} 3\kappa(r_3 - y_3) \\ y_4 \\ r_4 \end{pmatrix} + \begin{pmatrix} \mathcal{O}(s^3) \\ \mathcal{O}(s^3) \\ \mathcal{O}(s^3) \end{pmatrix}.$$

Let j be the least index such that $y_j \neq r_j$, $j \geq 3$ (the case when j does not exist is considered in the paragraph addressing inflected segments). Then there exists an $h_0 > 0$ for which the normal vector $\mathbf{N}$ of $\mathbf{p}(s)$ at the interval $(-h_0, 0)$, at the origin and at the interval $(0, h_0)$ has the causal character as specified in Table 6.

This classification follows directly from the expansion of $\mathbf{p}''(s)$ and from the fact that $x_i = 0$ for every $2 \leq i \leq j$, $i \in \mathbb{N}$.

The discriminants D_1, D_2 of the two quadratic equations for b have the

expansions

$$\begin{aligned} D_1 &= k_j \kappa (r_j - y_j)^2 h^{2j+4} + \mathcal{O}(h^{2j+5}), \\ D_2 &= 4h^4 + \mathcal{O}(h^{4+j}), \end{aligned} \tag{129}$$

where k_j is a nonzero constant. Thus, all four solutions are real if $\kappa \neq 0$, provided that the stepsize h is sufficiently small. The case when $\kappa = 0$ yields an analogous result.

Similar to the previous section, we may identify the best solution. However, the geometric approximation order of this solution is only two. Consequently, *isolated Minkowski inflections reduce the approximation order.*

Case 2: Curve with inflected segments. This section analyzes a case which would not be present in the Euclidean world: a non–straight curve segment, where all points are inflection points.

More precisely, the normal vector is assumed to be light–like within an entire interval. This property characterizes curves which are contained in light–like planes. One boundary curve of the associated planar domain is a straight line (the intersection of the light–like plane with the plane $r = 0$).

Proposition 15 *Let $\mathbf{p}(s)$ be a space–like C^∞ curve with a light–like normal vector for $s \in [s_0, s_0 + h]$, where $h > 0$. Then the G^1 Hermite interpolation of $\mathbf{p}(s)$ in $[s_0, s_0 + h]$ by MPH cubics has infinitely many solutions. For one of them the orientations of the tangent vectors are preserved and the approximation of $\mathbf{p}(s)$ is of order four.*

Proof: Following (37), we may suppose (without loss of generality) that $\mathbf{N}(0) = (0, \frac{\sqrt{2}}{2}, \frac{\sqrt{2}}{2})^\top$, $\mathbf{B}(0) = (0, \frac{\sqrt{2}}{2}, -\frac{\sqrt{2}}{2})^\top$. Then the canonical Taylor

expansion takes the form

$$\mathbf{p}(s) = \begin{pmatrix} s \\ \frac{\sqrt{2}}{4}s^2 + \frac{\sqrt{2}}{12}(\kappa_1 + \tau_0)s^3 + \mathcal{O}(s^4) \\ \frac{\sqrt{2}}{4}s^2 + \frac{\sqrt{2}}{12}(\kappa_1 + \tau_0)s^3 + \mathcal{O}(s^4) \end{pmatrix}. \tag{130}$$

In this case, the first equations of (95), (96) are automatically satisfied. We obtain a two–parameter family of interpolants of the first kind, since the parameters a_1 and b_1 can be chosen arbitrarily. The coordinates of the interpolants $(\bar{x}(t), \bar{y}(t), \bar{r}(t))^\top$ have the expansions

$$\begin{aligned} \bar{x}(t) &= ((3a_1 + 3b_1 - 2)t^3 + (-6a_1 - 3b_1 + 3)t^2 + (3a_1)t)h, \\ \bar{y}(t) &= \bar{r}(t) = \frac{\sqrt{2}}{4}((6b_1 - 2)t^3 + (3 - 6b_1)t^2)h^2 + \mathcal{O}(h^3). \end{aligned}$$

By choosing $a_1 = b_1 = \frac{1}{3}$, the approximation order becomes four again and the interpolant matches the orientations of the boundary tangent vectors.

On the other hand, from the second set of equations (95), (96) we get $a_2 = 1 - b_2$, $E_2(b_2) = -2a_2b_2$ and therefore $a_{2,1} = b_{2,2} = 0$, $a_{2,2} = b_{2,1} = 1$. The interpolants of the second kind have a singular point at one of the segment boundaries. □

4.5 Bounding the Hausdorff distance of planar domains

The Hausdorff distance of two sets $A, B \subset \mathbb{R}^n$ is defined as

$$\mathrm{HD}(A, B) = \max\{\max_{\mathbf{a}\in A}\{\min_{\mathbf{b}\in B}\{||\mathbf{a} - \mathbf{b}||_E\}\}, \max_{\mathbf{b}\in B}\{\min_{\mathbf{a}\in A}\{||\mathbf{a} - \mathbf{b}||_E\}\}\}, \tag{132}$$

where $||.||_E$ denotes Euclidean norm.

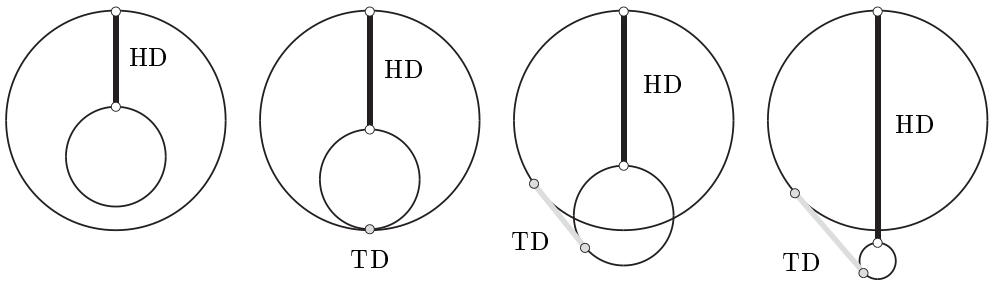

Figure 35: Tangential distances (TD) vs. Hausdorff distances (HD) of two circles; the radii are assumed to be positive. In the first (resp. second) example, the tangential distance is imaginary (zero), since the difference vector between the points in Minkowski space describing the two circles is time–like (light–like).

Obviously, the Hausdorff distance of two circles with non–negative radii r_1, r_2 in the plane equals $\Delta r + \Delta c$, where $\Delta r = |r_1 - r_2|$ is the difference of the radii, and Δc is the distance between the centers. Consequently, the bound on the Euclidean distance between two curves in Minkowski space $\mathbf{p}(s)$, $\mathbf{q}(s)$ implies an upper bound on the Hausdorff distance between the associated planar domains,

$$\mathrm{HD}(\Omega_{\mathbf{p}}, \Omega_{\mathbf{q}}) \leq \sqrt{2} \max_{s \in I} ||\mathbf{p}(s) - \mathbf{q}(s)||_E. \tag{133}$$

Therefore, the results on the approximation order of the MAT imply analogous results for the Hausdorff distance of the associated planar domains.

Note that the Lorentz metric is not suitable for bounding the Hausdorff distance; it represents the so–called tangential distance between two circles, see Figure 35.

4.6 Examples

In this section we present numerical results obtained by applying the previously designed MPH approximation scheme.

Example 1: Let us apply the G^1 Hermite interpolation scheme to the curve segment $\mathbf{c}(t) = (0.7e^t, 2.7\ln(1+t), \sin t)^\top$, $t \in [0,1]$. We consider the curve segment as the medial axis transform of a planar domain Ω. All four interpolants are shown in Fig. 36 along with the rational approximations of the original domain boundary $\partial\Omega$. In this case, the second interpolant is the best one.

Example 2: We consider the space–like cubic arc (the MAT of a planar domain Ω, cf. Fig. 37) $\mathbf{h}(t) = (t, t^2, \frac{t^3}{2})^\top$ with the parameter domain $t \in [0,1]$. We apply the G^1 Hermite interpolation scheme to the curve segment obtained for $t \in [0, \frac{1}{2}]$, i.e. to the left half of the curve shown in Fig. 37.

The G^1 Hermite data are $\mathbf{h}(0) = (0,0,0)^\top$, $\mathbf{h}(\frac{1}{2}) = (\frac{1}{2}, \frac{1}{4}, \frac{1}{16})^\top$ and $\mathbf{h}'(0) = \mathbf{e}_1$, $\mathbf{h}'(\frac{1}{2}) = (1, 1, \frac{3}{8})^\top$. The algorithm described in Table 4 gives four solutions for parameters a and b:

$$\begin{aligned}
&\text{a)} \quad a_{1,1} = 0.128036, \qquad b_{1,1} = 0.184193,\\
&\text{b)} \quad a_{1,2} = 0.586249, \qquad b_{1,2} = 0.520228,\\
&\text{c)} \quad a_{2,1} = 0.811725, \qquad b_{2,1} = -0.158310,\\
&\text{d)} \quad a_{2,2} = -0.175181, \qquad b_{2,2} = 0.492110.
\end{aligned} \tag{134}$$

The four interpolants in Minkowski space are shown in Fig. 38 (top), along with the rational approximations to the original domain boundary $\partial\Omega$ (bottom). The first interpolant (black curve in the top figure) is obviously the

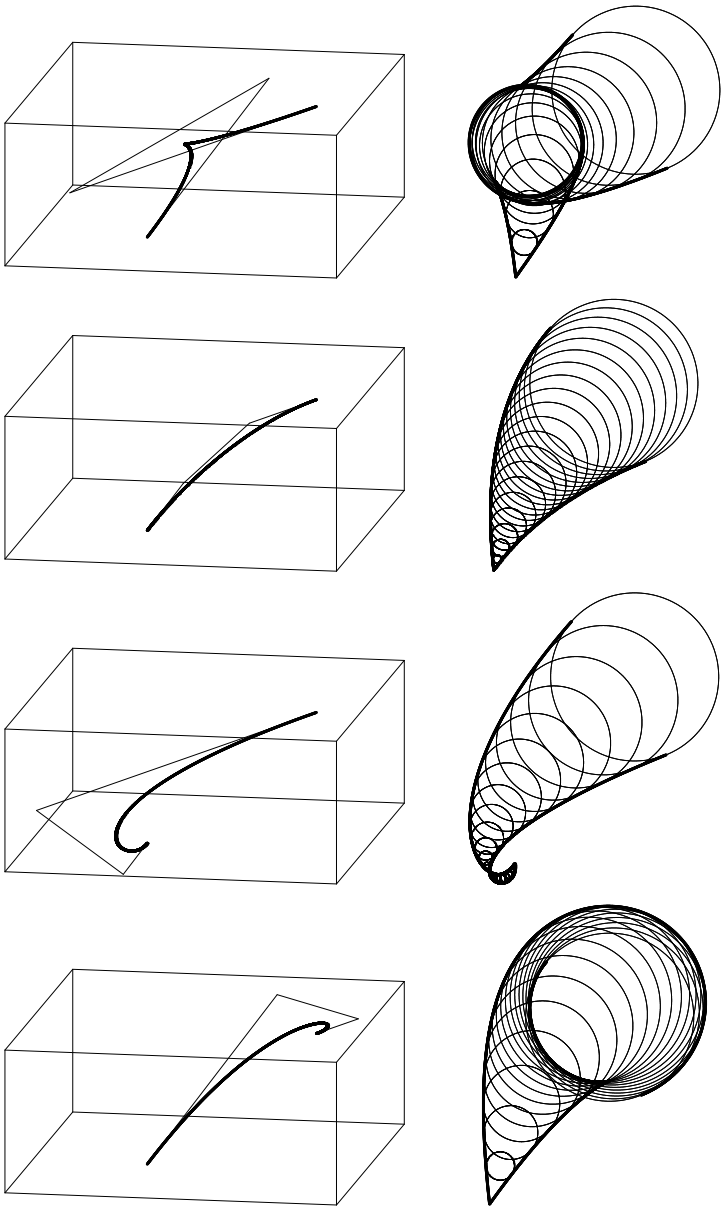

a) b)

Figure 36: a) Four interpolants to the given medial axis transform, b) corresponding circles and their rational envelopes.

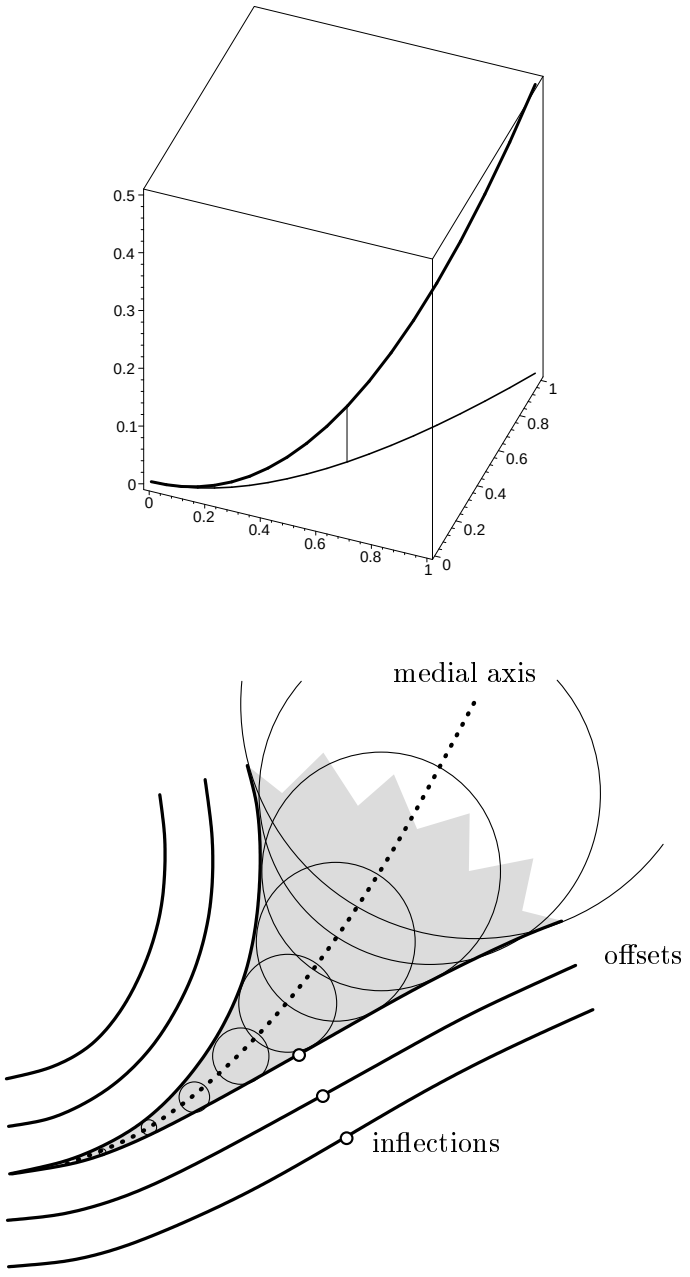

Figure 37: Top: Curve in $\mathbb{R}^{2,1}$ with a Minkowski inflection point. Bottom: associated planar domain, its offsets and the inflections of the boundary.

i	$m_{i,1}$	$m^{\rho}_{i,1}$	$M_{i,1}$	$M^{\rho}_{i,1}$	$H_{i,1}$	$H^{\rho}_{i,1}$
0	$2.253 \cdot 10^{-2}$	–	$3.575 \cdot 10^{-3}$	–	$3.286 \cdot 10^{-3}$	–
1	$2.985 \cdot 10^{-3}$	7.548	$2.389 \cdot 10^{-4}$	14.967	$2.322 \cdot 10^{-4}$	14.151
2	$3.861 \cdot 10^{-4}$	7.731	$1.560 \cdot 10^{-5}$	15.307	$1.549 \cdot 10^{-5}$	14.996
3	$4.877 \cdot 10^{-5}$	7.918	$9.887 \cdot 10^{-7}$	15.784	$9.867 \cdot 10^{-7}$	15.694
4	$6.112 \cdot 10^{-6}$	7.978	$6.201 \cdot 10^{-8}$	15.943	$6.198 \cdot 10^{-8}$	15.920
5	$7.646 \cdot 10^{-7}$	7.995	$3.879 \cdot 10^{-9}$	15.985	$3.879 \cdot 10^{-9}$	15.980
6	$9.559 \cdot 10^{-8}$	7.999	$2.425 \cdot 10^{-10}$	15.996	$2.425 \cdot 10^{-10}$	15.995

Table 7: Numerical results obtained by G^1 MPH interpolation and refinement via subdivision.

best one, and the given MAT cannot be visually distinguished from this curve. This fact was to be expected, since the normal vector of $\mathbf{h}(t)$ is space–like for every $t \in [0, \frac{1}{2}]$ (see Section 4.4.1).

Example 3: Consider again the cubic arc of Example 2. We will interpolate $\mathbf{h}(t)$ using the G^1 MPH interpolation scheme and a binary subdivision. For the i–th level of subdivision ($i = 0, 1, 2, \ldots$) and the n–th interval span $[\frac{n-1}{2^{i+1}}, \frac{n}{2^{i+1}}]$ we have the first order Hermite data $\mathbf{p}_{i,n-1} = \mathbf{h}(\frac{n-1}{2^{i+1}})$, $\mathbf{p}_{i,n} = \mathbf{h}(\frac{n}{2^{i+1}})$ and $\mathbf{t}_{i,n-1} = \mathbf{h}'(\frac{n-1}{2^{i+1}})$, $\mathbf{t}_{i,n} = \mathbf{h}'(\frac{n}{2^{i+1}})$, where $n = 1, \ldots, 2^i$.

Following the results from Section 4.4.1 and Example 2 we consider the interpolant corresponding to $a_{1,1}$, $b_{1,1}$ only. We denote this interpolant $\mathbf{q}_{i,n}(s)$ and linearly reparameterize it to $s \in [\frac{n-1}{2^{i+1}}, \frac{n}{2^{i+1}}]$.

The numerical results are presented in Table 7. The values $m_{i,n}$, $M_{i,n}$ and

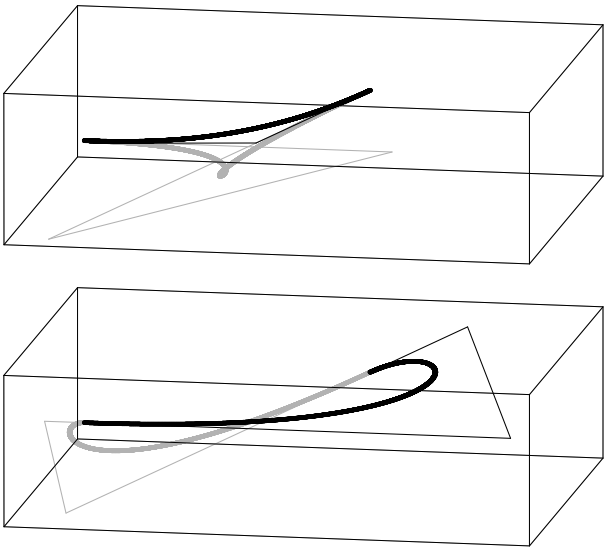

a)

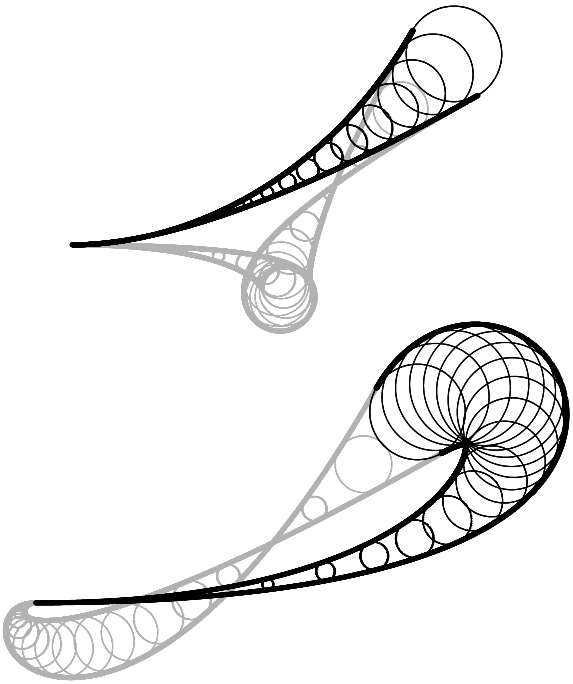

b)

Figure 38: a) Four interpolants to the given medial axis transform, b) corresponding circles and their rational envelopes. Top – solutions of the first kind, bottom – solutions of the second kind.

$H_{i,n}$ are sampling–based estimates of various distances between the original curve $\mathbf{h}(t)$ and its interpolants. More precisely, we study the parametric distance

$$m_{i,n} = \max_t\{||\mathbf{q}_{i,n}(t) - \mathbf{h}(t)||_E\}, \tag{135}$$

the parametric distance after the reparameterization (125)

$$M_{i,n} = \max_t\{||\mathbf{q}_{i,n}(\tau(t)) - \mathbf{h}(t)||_E\} \tag{136}$$

and the Hausdorff distance

$$H_{i,n} = \max\{\max_t\{\min_s\{||\mathbf{h}(t) - \mathbf{q}_{i,n}(s)||_E\}\}, \max_s\{\min_t\{||\mathbf{h}(t) - \mathbf{q}_{i,n}(s)||_E\}\}\},$$

where $s, t \in [\frac{n-1}{2^{i+1}}, \frac{n}{2^{i+1}}]$ and $||.||_E$ denotes Euclidean norm. For each level of subdivision, only the distances obtained for the first segment ($n = 1$) are reported. Moreover, the ratios of two adjacent values for $i = 1, 2, \ldots$ are shown, i.e. $m^\rho_{i,1} = \frac{m_{i,1}}{m_{i-1,1}}$, $M^\rho_{i,1} = \frac{M_{i,1}}{M_{i-1,1}}$ and $H^\rho_{i,1} = \frac{H_{i,1}}{H_{i-1,1}}$.

The numerically computed ratios confirm that the approximation order of the best solution is three resp. four before resp. after the reparameterization.

Example 4: The curve $\mathbf{h}(t) = (t, t^2, \frac{t^3}{2})^\top$ has Minkowski inflections for $t = \pm\frac{\sqrt{3}}{3}$ and $t = \pm\sqrt{2}$. Let us now take a closer look at the inflection $t = \frac{\sqrt{3}}{3}$. Figure 37 (top) depicts the curve $\mathbf{h}(t)$ for $t \in [0, 1]$ along with its projection to the xy plane. The parameter value $t = \frac{\sqrt{3}}{3}$ is marked by the thin line. Figure 37 (bottom) shows the associated planar domain and the inflections of the boundaries, see Proposition 3.

The numerical data obtained from the subdivision scheme analogous to the one in Example 3 for the parameter interval $[\frac{\sqrt{3}}{3}, 1]$ are summarized in Table 8. Again, compare the values with the results of Section 4.4.2: the approximation order – after the reparameterization – is equal to two.

i	$m_{i,1}$	$m_{i,1}^{\rho}$	$M_{i,1}$	$M_{i,1}^{\rho}$	$H_{i,1}$	$H_{i,1}^{\rho}$
0	$1.845 \cdot 10^{-1}$	–	$1.438 \cdot 10^{-1}$	–	$7.735 \cdot 10^{-2}$	–
1	$8.404 \cdot 10^{-2}$	2.195	$3.333 \cdot 10^{-2}$	4.098	$1.981 \cdot 10^{-2}$	3.905
2	$4.141 \cdot 10^{-2}$	2.029	$7.948 \cdot 10^{-3}$	4.048	$4.995 \cdot 10^{-3}$	3.966
3	$2.049 \cdot 10^{-2}$	2.021	$1.940 \cdot 10^{-3}$	4.024	$1.254 \cdot 10^{-3}$	3.983
4	$1.019 \cdot 10^{-2}$	2.012	$4.791 \cdot 10^{-4}$	4.012	$3.142 \cdot 10^{-4}$	3.991
5	$5.078 \cdot 10^{-3}$	2.006	$1.191 \cdot 10^{-4}$	4.006	$7.864 \cdot 10^{-5}$	3.996
6	$2.535 \cdot 10^{-3}$	2.003	$2.968 \cdot 10^{-5}$	4.003	$1.967 \cdot 10^{-5}$	3.998

Table 8: Numerical results obtained by G^1 MPH interpolation and refinement via subdivision at an inflection point.

Remark 13 So far, curves with light–like tangents have been excluded. Still, such points may be present in applications, e.g. in the case of boundaries with vertices. If a point on the Minkowski space curve approaches a point with a light–like tangent, then the curvature goes to infinity. The interpolation procedure can be adapted to this case, and the analysis of the number of solutions can be carried over. As observed in our numerical experiments, a 'nice' solution exists always, provided that the stepsize is sufficiently small. The approximation order of this solution is again equal to two, similar to the case of inflections.

5 Conclusion

In this thesis we thoroughly investigated a relation between MPH cubics and cubic helices in Minkowski space. Among other results we proved that any polynomial space–like or light–like helix in $\mathbb{R}^{2,1}$ is an MPH curve. The converse result holds for cubic MPH curves, i.e. spatial MPH cubics are helices in $\mathbb{R}^{2,1}$. Based on these results and properties of tangent indicatrices of MPH curves we presented a complete classification of planar and spatial MPH cubics.

As demonstrated in this thesis, MPH curves can be used for approximating the medial axis transform of a planar domain. As an advantage, they admit a rational parameterization of the offset curves of the domain boundary. We have presented a general method for converting a space–like C^∞ curve (MAT) into a G^1 spline via MPH cubics.

Based on the mutual position of the given first order Hermite data we derived the conditions for the existence and the number of interpolants. Using Taylor expansions we studied the approximation order, which is generally equal to four, but it reduces to two at isolated Minkowski inflections. Moreover, our theoretical results were demonstrated by several numerical examples.

List of Figures

List of Tables

References

Blaschke, W. (1929), Vorlesungen über Differentialgeometrie III, Springer, Berlin.

Cho H. Ch., Choi, H. I., Kwon S.–H., Lee D. S., and Wee N.–S. (2004), Clifford algebra, Lorentzian geometry and rational parametrization of canal surfaces, Computer Aided Geometric Design, 21, 327–339.

Choi, H. I., Choi, S. W., and Moon, H. P. (1997), Mathematical theory of medial axis transform, Pacific J. Math., 181(1), 57–88.

Choi, H. I., Han, Ch. Y., Moon, H. P., Roh, K. H., and Wee, N. S. (1999), Medial axis transform and offset curves by Minkowski Pythagorean hodograph curves, Computer Aided Design, 31, 59–72.

Choi, H. I., Lee, D. S., and Moon, H. P. (2002), Clifford algebra, spin representation and rational parameterization of curves and surfaces, Adv. Comput. Math., 17, 5–48.

Degen, W. L. F. (2004), Exploiting curvatures to compute the medial axis for domains with smooth boundary, Computer Aided Geometric Design, 21, 641–660.

Dietz, R., Hoschek, J., and Jüttler, B. (1993), An algebraic approach to curves and surfaces on the sphere and other quadrics, Computer Aided Geometric Design, 10, 211–229.

Ekmekci, N., and Ilarslan, K. (1998), Higher curvatures of a regular curve in Lorentzian space, J. Inst. Math. & Comp. Sci., 11(2), 97–102.

Farin, G. (1987), Curves and Surfaces for Computer Aided Geometric Design, Morgan-Kaufmann, San Francisco.

Farouki, R. T. (2002), Pythagorean–hodograph curves, Handbook of Computer Aided Geometric Design (J. Hoschek, G. Farin & M.-S. Kim, eds.), Elsevier, 405–427.

Farouki, R. T., and Han, C. Y. (2005), Algorithms for spatial Pythagorean-hodograph curves, 2005, to appear.

Farouki, R. T., and Sakkalis T. (1990), Pythagorean hodographs, IBM J. of Research and Development, 34, 736–752.

Farouki, R. T., and Sakkalis, T. (1994) , Pythagorean–hodograph space curves, Adv. Comput. Math 2, 41–66.

Kim, G.–I., and Ahn M.–H. (2003), C^1 Hermite interpolation using MPH quartic, 2003, Computer Aided Geometric Design, 20, 469–492.

Kosinka, J., and Jüttler, B. (2006), G^1 Hermite Interpolation by Minkowski Pythagorean Hodograph Cubics, Computer Aided Geometric Design, to appear.

Kosinka, J., and Jüttler, B. (2006), Cubic Helices in Minkowski space, Sitzungsber. Österr. Akad. Wiss., Math.-Nat. Kl., to appear.

Kreyszig, E. (1991), Differential Geometry, Dover.

Kriele, M. (1999), Spacetime: foundations of general relativity and differential geometry, Springer, Berlin.

Kubota, K. K. (1972), Pythagorean triples in unique factorization domains, American mathematical monthly, 79, 503–505.

Moon, H. P. (1999), Minkowski Pythagorean hodographs, Computer Aided Geometric Design, 16, 739–753.

Piegl, L., and Tiller, W. (1995), The NURBS Book, Springer, London.

Pottmann, H., and Peternell, M. (1998), Applications of Laguerre geometry in CAGD, Computer Aided Geometric Design 15, 165–186

Wagner, M. G., and Ravani B. (1997), Curves with rational Frenet-Serret motion, Computer Aided Geometric Design, 15, 79–101.

Walrave, J. (1995), Curves and surfaces in Minkowski space, Doctoral thesis, K. U. Leuven, Fac. of Science, Leuven.

Wunderlich, W. (1973), Algebraische Böschungslinien dritter und vierter Ordnung, Sitzungsber., Abt. II, Österr. Akad. Wiss., Math.–Naturw. Kl., 181, 353–376.